(2)

Defense Nuclear Agency
Alexandria, VA 22310-3398

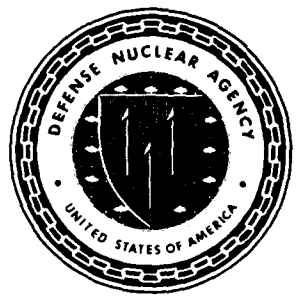

DNA-TR-87-162-V2

PRPSIM—A FORTRAN Code to Calculate Properties of Radio Wave Propagation in a Structured Ionized Medium

Volume II—Theory and Models

R. E. Dodson
D. J. Krueger
F. W. Guigliano
Mission Research Corporation
P.O. Drawer 719
San Diego, CA 93102-0719

December 1989

Technical Report

CONTRACT No. DNA 001-85-C-0067

DISTRIBUTION LIST UPDATE

This mailer is provided to enable DNA to maintain current distribution lists for reports. We would appreciate your providing the requested information.

☐ Add the individual listed to your distribution list.

☐ Delete the cited organization/individual.

☐ Change of address.

NAME: _____

ORGANIZATION: _____

OLD ADDRESS	CURRENT ADDRESS

TELEPHONE NUMBER: ( ) _____

SUBJECT AREA(s) OF INTEREST:

_____

_____

_____

DNA OR OTHER GOVERNMENT CONTRACT NUMBER: _____

CERTIFICATION OF NEED-TO-KNOW BY GOVERNMENT SPONSOR (if other than DNA):

SPONSORING ORGANIZATION: _____

CONTRACTING OFFICER OR REPRESENTATIVE

SIGNATURE

CUT HERE AND RETURN

Director
Defense Nuclear Agency
ATTN: TITL
Washington, DC 20305-1000

Director
Defense Nuclear Agency
ATTN: TITL
Washington, DC 20305-1000

UNCLASSIFIED

SECURITY CLASSIFICATION OF THIS PAGE

REPORT DOCUMENTATION PAGE

1a REPORT SECURITY CLASSIFICATION UNCLASSIFIED	1b RESTRICTIVE MARKINGS
2a SECURITY CLASSIFICATION AUTHORITY N/A since Unclassified	3 DISTRIBUTION/AVAILABILITY OF REPORT Approved for public release; distribution is unlimited.
2b DECLASSIFICATION/DOWNGRADING SCHEDULE N/A since Unclassified	
4 PERFORMING ORGANIZATION REPORT NUMBER(S) MRC-R-1011	5 MONITORING ORGANIZATION REPORT NUMBER(S) DNA-TR-87-162-V2
6a NAME OF PERFORMING ORGANIZATION Mission Research Corporation 6b OFFICE SYMBOL (If applicable)	7a NAME OF MONITORING ORGANIZATION Defense Nuclear Agency
6c ADDRESS (City, State, and ZIP Code) P.O. Drawer 719 Santa Barbara, CA 93102-0719	7b ADDRESS (City, State, and ZIP Code) 6801 Telegraph Road Alexandria, VA 22310-3398
8a NAME OF FUNDING/SPONSORING ORGANIZATION 8b OFFICE SYMBOL (If applicable) RAAE/Wittwer	9 PROCUREMENT INSTRUMENT IDENTIFICATION NUMBER DNA 001-85-C-0067
8c ADDRESS (City, State, and ZIP Code)	10 SOURCE OF FUNDING NUMBERS PROGRAM ELEMENT NO: 62715H; PROJECT NO: B; TASK NO: B; WORK UNIT ACCESSION NO: DH008719

11 TITLE (Include Security Classification)
PRPSIM—A FORTRAN Code to Calculate Properties of Radio Wave Propagation in a Structured Ionized Medium, Volume II—Theory and Models

12 PERSONAL AUTHOR(S)
Dodson, R.E.; Krueger, D.J.; Guigliano, F.W.

13a TYPE OF REPORT	13b TIME COVERED	14 DATE OF REPORT (Year, Month, Day)	15 PAGE COUNT
Technical	FROM 871031 TO 890331	891201	124

16 SUPPLEMENTARY NOTATION
This work was sponsored by the Defense Nuclear Agency RDT&E RMC Code 3220 85469 B B 00007 25904D.

17 COSATI CODES			18 SUBJECT TERMS (Continue on reverse if necessary and identify by block number)		
FIELD	GROUP	SUB-GROUP	Satellite Communications	Propagation Effects	SCENARIO
12	5		Nuclear Weapons Effects	Computer Code	
20	14		Signal Scintillation	Radar	

19 ABSTRACT (Continue on reverse if necessary and identify by block number)

This report describes the PRPSIM (Properties of Radio Wave Propagation in a Structured Ionized Medium) code; a FORTRAN computer program for use in evaluating electromagnetic propagation effects resulting from detonation of nuclear weapons on satellite communications and radar systems. The code uses nuclear environment data files created by the SCENARIO high altitude, multiburst nuclear phenomenology code. PRPSIM calculates propagation effects due to enhanced mean ionization levels (e.g. absorption, noise, refraction, phase shift, Doppler and time delay variations, etc). and scintillation effects due to ionization structure (e.g. amplitude and phase scintillation, fading, angular scattering, frequency selective scintillation, etc.). The code is written in ANSI FORTRAN-77 and has been installed and run on VAX, CDC/CYBER, ELXSI/EMBOS, and CRAY-1 computer systems. Volume I of the report is a user's guide which describes code installation, input, output, structure, and application. Volume II describes the underlying propagation effects theory and computational models.

20 DISTRIBUTION/AVAILABILITY OF ABSTRACT	21 ABSTRACT SECURITY CLASSIFICATION	
☐ UNCLASSIFIED/UNLIMITED ☒ SAME AS RPT ☐ DTIC USERS	UNCLASSIFIED	
22a NAME OF RESPONSIBLE INDIVIDUAL Bennie F. Maddox	22b TELEPHONE (Include Area Code) (703) 325-7042	22c OFFICE SYMBOL DNA/CSTI

DD FORM 1473, 84 MAR — 83 APR edition may be used until exhausted. All other editions are obsolete.

SECURITY CLASSIFICATION OF THIS PAGE
UNCLASSIFIED

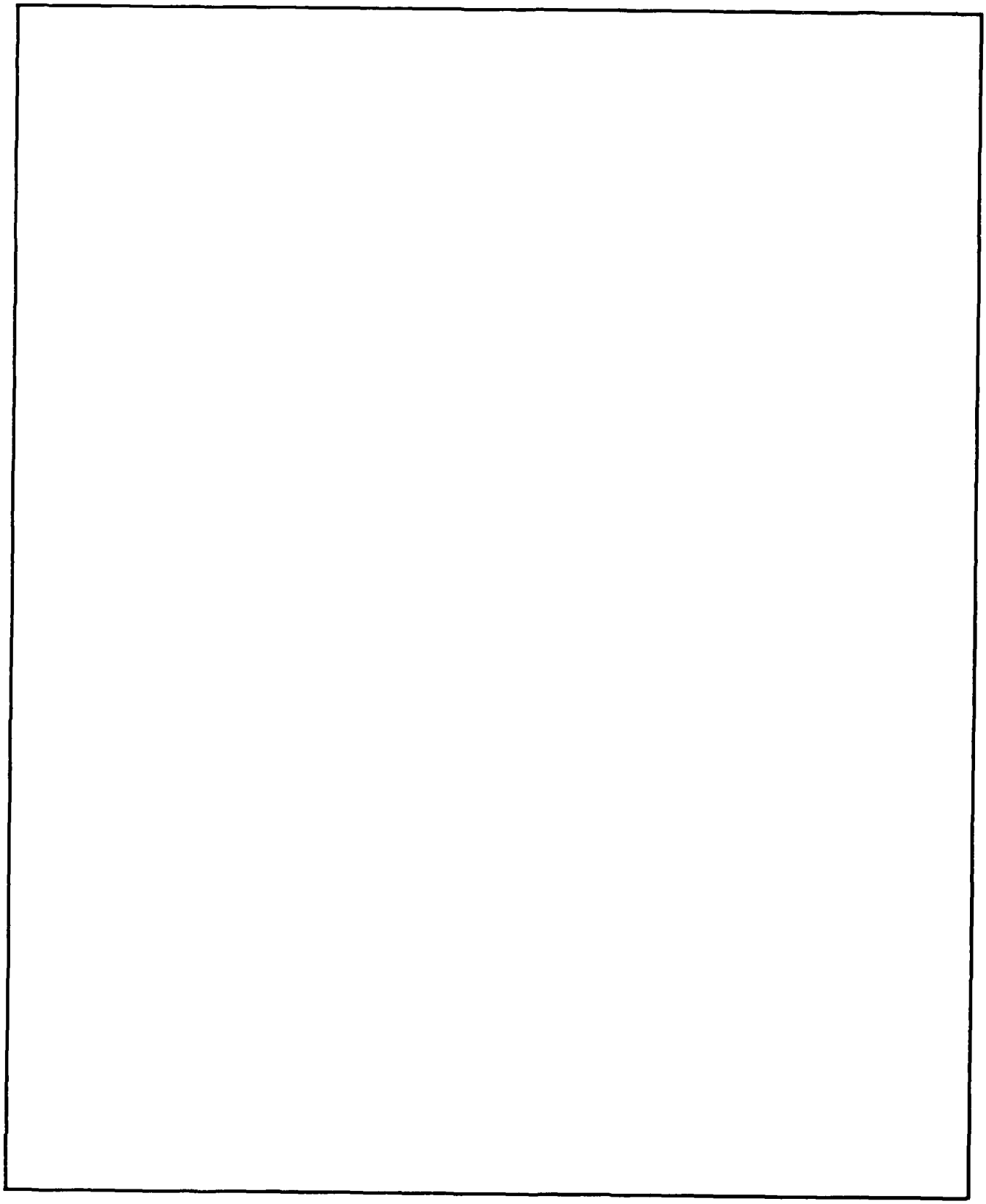

CONVERSION TABLE

Conversion factors for U.S. Customary to metric (SI) units of measurement

MULTIPLY TO GET	BY	TO GET DIVIDE
angstrom	1.000 000 X E -10	meters (m)
atmosphere (normal)	1.013 25 X E +2	kilo pascal (kPa)
bar	1.000 000 X E + 2	kilo pascal (kPa)
barn	1.000 000 X E -28	meter^2 (m^2)
British thermal unit (thermochemical)	1.054 350 X E + 3	joule (J)
calorie (thermochemical)	4.184 000	joule (J)
cal (thermochemical)/cm^2	4.184 000 X E -2	mega joule/m^2 (MJ/m^2)
curie	3.700 000 X E +1	*giga becquerel (GBq)
degree (angle)	1.745 329 X E -2	radian (rad)
degree Fahrenheit	t_k = (t°F + 459.67)/1.8	degree kelvin (K)
electron volt	1.602 19 X E -19	joule (J)
erg	1.000 000 X E -7	joule (J)
erg/second	1.000 000 X E -7	watt (W)
foot	3.048 000 X E -1	meter (m)
foot-pound-force	1.355 818	joule (J)
gallon (U.S. liquid)	3.785 412 X E -3	meter^3 (m^3)
inch	2.540 000 X E -2	meter (m)
jerk	1.000 000 X E +9	joule (J)
joule/kilogram (J/kg)(radiation dose absorbed)	1.000 000	Gray (Gy)
kilotons	4.183	terajoules
kip (1000 lbf)	4.448 222 X E +3	newton (N)
kip/inch^2 (ksi)	6.894 757 X E +3	kilo pascal (kPa)
ktap	1.000 000 X E +2	newton-second/m^2 ($N\text{-}s/m^2$)
micron	1.000 000 X E -6	meter (m)
mil	2.540 000 X E -5	meter (m)
mile (international)	1.609 344 X E +3	meter (m)
ounce	2.834 952 X E -2	kilogram (kg)
pound-force (lbs avoirdupois)	4.448 222	newton (N)
pound-force inch	1.129 848 X E -1	newton-meter (N • m)
pound-force/inch	1.751 268 X E +2	newton/meter (N/m)
pound-force/foot^2	4.788 026 X E -2	kilo pascal (kPa)
pound-force/inch^2 (psi)	6.894 757	kilo pascal (kPa)
pound-mass (lbm avoirdupois)	4.535 924 X E -1	kilogram (kg)
pound-mass-foot^2 (moment of inertia)	4.214 011 X E -2	kilogram-meter^2 ($kg \bullet m^2$)
pound-mass/foot^3	1.601 846 X E +1	kilogram/meter^3 (kg/m^3)
rad (radiation dose absorbed)	1.000 000 X E -2	**Gray (Gy)
roentgen	2.579 760 X E -4	coulomb/kilogram (C/kg)
shake	1.000 000 X E -8	second (s)
slug	1.459 390 X E +1	kilogram (kg)
torr (mm Hg, 0° C)	1.333 220 X E -1	kilo pascal (kPa)

*The becquerel (Bq) is the SI unit of radioactivity; 1 B_q = 1 event/s.
**The Gray (Gy) is the SI unit of absorbed radiation.

TABLE OF CONTRACTS

Section		Page
	Conversion Table	iii
	List of Illustrations	v
	List of Tables	vi
1	INTRODUCTION	1
2	RF SIGNAL PROPAGATION	6
	2.1 Introduction to the Models of Propagation Disturbances	6
	2.2 Scintillation, Absorption, and Mean Electron Density Effects	7
	2.2.1 Geometry of Propagation Path	11
	2.2.2 Point-wise Integration Along Propagation Path	19
	2.2.3 Calculation of Signal Parameters from Primitive Integrals	32
	2.3 Antenna Filtering	46
	2.4 Antenna Noise Temperature	47
	2.5 Refraction	56
	2.5.1 Primary Angle Bending and Multipath	56
	2.5.2 Focusing and Defocusing	67
	2.5.3 Refractive Effects on Phase and Time Delay	69
	2.5.4 Model Implementation Comments	71
3	INTERFACE WITH THE PROPAGATION ENVIRONMENT	75
	3.1 Introduction	75
	3.2 Retrieval and Storage of SCENARIO Data	76
	3.3 Propagation Path Intersection with the SCENARIO Grid	81
	3.4 Calculation of Primitive Data for Propagation Integrals	89
4	LIST OF REFERENCES	112

LIST OF ILLUSTRATIONS

Figure		Page
1	Propagation through a striated region	3
2	Geometric transformation from field oriented coordinates to line of sight coordinates	12
3	Geometric transformation from line of sight coordinates to antenna tangent plane coordinates	54
4	Multiple phase screen refraction geometry	59
5	Cross-sectional view of a phi-plane in the dipole aligned coordinate system of a uniform SCENARIO grid	83
6	Cross-sectional view of a phi-plane in the dipole aligned coordinate system of a "staggered" SCENARIO grid	84
7	Cartesian representation of the portion of the SCENARIO grid used for a DATAPT calculation at a single point	91

LIST OF TABLES

Table		Page
1	Summary of propagation disturbances calculated by PRPSIM	5
2	Summary of coordinate transformations for the four systems used by RFPROP module	14
3	Summary of equation numbers for major parameters calculated by RFPROP	45
4	SCENARIO cell quantities stored in mass storage by PROPEN module	80
5	Summary of parameters calculated or interpolated by DATAPT submodule	92

SECTION 1
INTRODUCTION

Transionospheric communications systems which rely on the propagation of radio frequency (RF) signals may suffer severe performance degradation when the ionosphere is disturbed by high altitude nuclear explosions. PRPSIM (Properties of Radio Wave Propagation in a Structured Ionized Medium) is a FORTRAN 77 computer program which has been designed to compute a set of parameters to enable the user to assess the severity of propagation effects for arbitrary link configurations in simulated nuclear environments. PRPSIM has been developed under the sponsorship of the Defense Nuclear Agency (DNA), and it uses the official DNA propagation algorithms to compute the signal parameters. These algorithms have been derived in a number of references. The purpose of this volume (Volume II) is to describe in detail, and in one source, all the computations performed by PRPSIM. For instruction in running the PRPSIM code, the reader should refer to the user's manual (Volume I).

The severity of the disruption of communications systems in nuclear environments depends on many factors, but these factors may be grouped into two general categories: (1) phenomenology parameters such as the number of bursts, weapon yields, altitudes, and magnetic locations of the bursts, and (2) link parameters such as signal carrier frequency, antenna characteristics, and link geometry and velocity relative to the nuclear environment. PRPSIM is a system propagation effects code which has been designed to provide the user with maximum flexibility in the specification of link parameters. It has no capability for providing phenomenology parameters, however. Instead, PRPSIM has been designed to operate in simulated nuclear environments generated by the MRC

phenomenology code SCENARIO. SCENARIO is a physics based code whose simulations of disturbed environments are obtained as the solutions of coupled, time-dependent equations which represent the dominant physical and chemical processes operating in the disturbed ionosphere. SCENARIO was developed under DNA sponsorship and was designed specifically to model nuclear environments generated by multiple, high altitude explosions above 100 km. The operation of the SCENARIO code is beyond the scope of this documentation, but detailed descriptions are available in several of the references listed at the end of this volume. Phenomenology data files are written by SCENARIO at discrete times after the initial explosion. PRPSIM may then interface with the SCENARIO environment at these specific times, or at any intermediate time by interpolating the phenomenology data between bracketing times.

The radiant energy generated by nuclear explosions produces very highly ionized regions in the atmosphere. The magnitude, location, spatial extent, and duration of the ionization are all sensitive functions of the weapon yield, altitude, and other phenomenology parameters. At relatively low altitudes (below about 50 km), most of the weapon energy is initially deposited in a relatively small region around the explosion, producing a compact but intensely ionized "fireball". At higher altitudes (above 100 km), the weapon energy is dispersed over a larger volume, producing a less intense but much larger and longer-lasting region of ionization. Another phenomenon which occurs for high altitude explosions and which has an adverse effect on RF signal propagation is the formation of structured ionization in the plasma. Typically, the plasma structure consists of long filaments of high electron density aligned along the geomagnetic field lines. These filaments (or "striations") may extend to very high altitudes and produce a scintillation of RF signals analogous to the scintillation of light waves propagating through a thermally turbulent atmosphere. Atmospheric disturbances typical of both low-altitude and high-altitude explosions are illustrated in Figure 1. The user should be

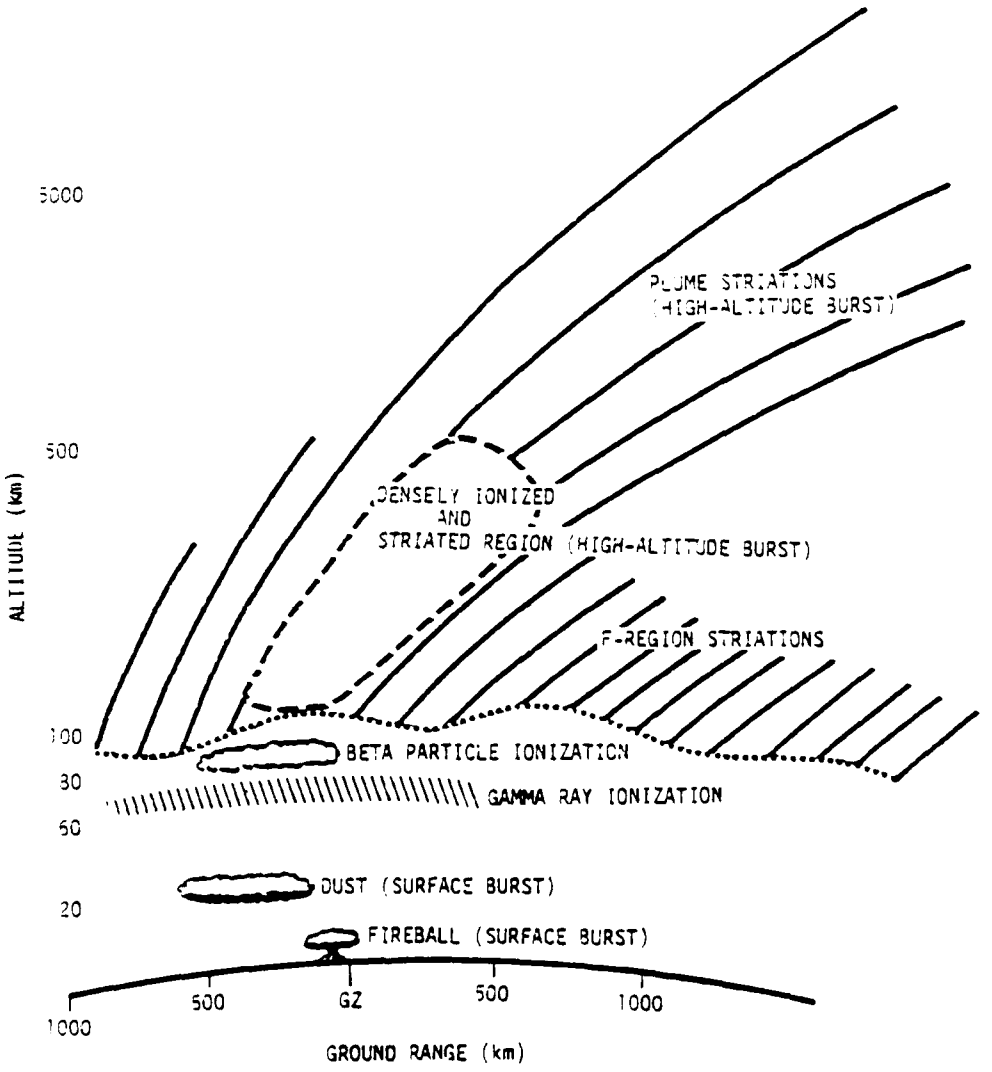

Figure 1. Propagation through a striated region.

aware that PRPSIM does not account for many of the effects typical of low-altitude and surface explosions.

The resulting signal degradation may be grouped into two classes of effects: (1) mean effects such as absorption, phase shift, time delay, etc. that are caused by the enhanced mean ionization, and (2) stochastic effects such as amplitude and phase scintillation, arrival angle scatter, and time delay jitter which are caused by the plasma structure and its motion relative to the propagation path. The various types of propagation disturbances and their overall effects are summarized in Table 1. The significance of each of these propagation effects on the performance of a particular system depends strongly on the link design (carrier frequency, data rate, type of modulation and coding, tracking loop configuration, etc.) and on the power margin and system requirements. Some degradation of the system performance, relative to that in an undisturbed environment, is inevitable in a nuclear disturbed environment. Careful attention to the nuclear propagation threat and application of practical engineering techniques can provide hardened link designs with acceptable levels of survivability in most nuclear environments. The purpose of PRPSIM is to provide the system engineer reliable data with which to assess system survivability in specific nuclear environments.

TABLE 1. Summary of various types of propagation disturbances and their overall effects.

PROPAGATION DISTURBANCE	EFFECTS ON PROPAGATED SIGNAL	EFFECTS ON SYSTEM OPERATION
Mean Ionization Propagation Disturbances calculated by PRPSIM.		
Absorption	Loss of RF energy due to electron-ion and electron-neutral collisions in ionized regions, causing signal attenuation.	Reduction of signal-to-noise ratio, causing possible loss of data and disruptions of signal acquisition and tracking.
Noise	Random RF energy emission from hot, ionized fireball regions.	Increased background noise, causing reduction of signal-to-noise ratio and possible loss of data.
Phase and Doppler Shift	Signal phase variation due to changes in TEC along propagation path.	Possible loss of phase/frequency lock and difficulty in signal acquisition and tracking.
Time Delay	Signal time-of-arrival variation due to changes in TEC along propagation path.	Possible loss of timing lock and difficulty in bit or PN code acquisition and tracking.
Faraday Rotation	Signal polarization rotation due to magnetoionic anisotropy.	Severe amplitude fading with linear polarization; no effect with circular polarization.
Striated Ionization Propagation Disturbances Calculated by PRPSIM.		
Amplitude Scintillation	Random fluctuations of signal amplitude due to scattering of signal energy by ionization irregularity structure.	Severe amplitude fading, causing increased data error rates and possible disruption of signal acquisition and tracking.
Phase Scintillation	Random fluctuations of signal phase due to TEC variation and scattering of signal energy by ionization irregularity structure.	Loss of signal coherence, causspossible loss of phase lock and catastrophic failure of demodulation.
Angular Scattering	Random fluctuations of signal angle-of-arrival due to scattering of signal energy by ionization irregularity structure.	Reduction of signal-to-noise ratio due to scattering loss in large antennas, causing possible loss of data.
Frequency Selective Scintillation	Random distortion of signal waveform and signal time delay due to frequency dependent angular scattering.	Degradation of signal detection, tracking, and demodulation; possible loss data due to intersymbol interface.

SECTION 2
RF SIGNAL PROPAGATION

2.1 INTRODUCTION TO THE MODELS OF PROPAGATION DISTURBANCES.

The primary task in any analysis of the propagation of an RF signal through a turbulent, ionized medium is a quantitative description of the variation of the ionization (or equivalently, of the index of refraction) as a function of time and location within the medium. All PRPSIM calculations are based on the assumption that the fluctuations at any particular time may be described by a spectral density function in three dimensions which decreases with increasing wave number according to an inverse power law. The power spectral density is parameterized by data generated by the SCENARIO environment simulation code at each point in the SCENARIO grid. The relevant parameters are transformed to a coordinate system which is invariant with respect to location within the grid, and the set of quantities which describe the scintillation of the RF signal are then calculated using the equations derived by Wittwer in the reports DNA-5304D[1] and DNA-IR-82-02[2].

PRPSIM is designed to operate in an anisotropic propagation environment. The scale lengths of the fluctuations in three directions are required: parallel to the magnetic field, and in two directions perpendicular to the field. The scale lengths are presumed to vary with location in the grid. The spectral index of the power law can have any value between 1.0 and 6.0. Currently, the value of the index is assumed to be invariant with respect to location, but in the future the code will be generalized to accommodate a variable index.

2.2 SCINTILLATION, ABSORPTION, AND MEAN ELECTRON DENSITY EFFECTS.

The set of parameters required to describe the propagation of a scintillated RF signal through a turbulent ionized medium is derived and discussed by Wittwer in DNA-5304D[1] and DNA-IR-82-02[2]. For completeness, we summarize here the equations used by PRPSIM to calculate these parameters. The reference numbers of the equations in Wittwer's documents are provided also, should the user have any questions regarding the derivations. All parameters are calculated by the module RFPROP. All the data required to define the propagation path and its end members (the transmitter and receiver) are passed directly to RFPROP by PRPSIM as arguments. These data consist of the transmitter and receiver location and velocity vectors, the number of carrier frequencies at which simulations are desired, the array containing those frequencies, and an array containing the effective antenna beamwidths at those frequencies.

The derivation of the parameters is based on the assumption that the fluctuation of the electron density and the index of refraction along the path can be represented by a power spectral density (PSD) function whose form is a simple power law:

$$PSD(K_r,K_s,K_t) = \begin{cases} \dfrac{8\pi^{3/2}\,\overline{\Delta n_i^2}\,L_r L_s L_t\,\Gamma(n)/\Gamma(n-3/2)}{(1 + L_r^2K_r^2 + L_s^2K_s^2 + L_t^2K_t^2)^n} & \text{if } (K_r^2+ K_s^2+ K_t^2)\,\ell^2 \leq 1 \\ 0 & \text{otherwise} \end{cases} \qquad (2\text{-}1)$$

where K_r and K_s are the spatial wave numbers of the fluctuations in two orthogonal directions perpendicular to the geomagnetic field vector, and K_t is the wave number in the direction parallel to the field; $\overline{\Delta n_i^2}$ is the variance of the index of refraction about its mean value; $\Gamma(n)$ is the gamma function of argument n; and n is proportional to the spectral index

$$n = \frac{1}{2} \text{ spectral index} + 1 \qquad (2\text{-}2)$$

(See Equation 1 of DNA-IR-82-02[2].) This form of the PSD is consistent with the observation of very sharply defined large scale structure in the ionosphere. The spectral index (or n) can be interpreted as a measure of the sharpness of the structure. We have assumed that the spectral index of the turbulence does not vary along the path. We have fixed its value at 2 because in situ measurements and theoretical analyses imply that this value best characterizes the local structure of the ionsophere. (See, for example, References 1 through 10 of DNA-IR-82-02[2].) The spectral index may be assigned any value within the range 1.0 to 6.0 ($1.5 < n \leq 4.0$), however.*

L_r, L_s, and L_t are the striation outer scale sizes as measured perpendicular and parallel to the field vector, and ℓ is the inner striation scale size. (These parameters are assigned by the data retrieval submodule DATAPT.) In the context of the PSD (Equation 2-1) used throughout this documentation, the scale size L is the distance (measured in a particular direction) over which the argument of the PSD (KL) changes by 1 radian in that direction. In general, the outer scale size L is not isotropic in direction because the large scale turbulence is strongly dependent on the geomagnetic field. The inner scale size ℓ is the smallest distance over which fluctuations can be detected. Its value is usually considered to be isotropic in direction because the small scale turbulence fluctuates rapidly and is not strongly influenced by the geomagnetic field. The structure of a plasma in a magnetic field is characterized by long striations aligned along the field lines. Because the striations are

* Wittwer's derivations are valid for the range $1.2 \leq n \leq 4.0$. The differential phase variance (equations 2-37 and 2-38) is undefined for $n \leq 1.5$, however. Until a valid expression for the phase variance is derived for $n \leq 1.5$, we shall restrict the value of n to be greater than 1.5.

long compared to their transverse dimensions, DATAPT assigns the longitudinal scale size L_t to a constant value of 150 km for all space throughout the sequence of the simulation. The characteristic transverse scale sizes are generated by the SCENARIO code. Typically, these are of the order of 10 km. DATAPT assigns the (isotropic) inner scale size a constant value of 10 meters.*

All the parameters required to parameterize the scintillated RF signal are functions of integrals which are integrated over the length of the path from the transmitter to the receiver. RFPROP utilizes a simple integration technique to evaluate each of these integrals -- with one exception which will be discussed in detail later. First, a set of path segments (Δz_i) is defined; second, a set of data describing the environment at the midpoint of the segment is retrieved for each of the segments; finally, the integrals are summed with the assumption that the value of the integrand at the center of the segment is a good estimate of the mean value of the integrand over the length of the segment; i.e., we compute the integral of each integrand f as

$$\int_0^{z_{end}} f(z)dz \simeq \sum_{i=0}^{N-1} f\left(\frac{z_{i+1}+z_i}{2}\right)(z_{i+1}-z_i) \simeq \sum_{i=1}^{N} f(\langle z_i \rangle)\Delta z_i \quad (2\text{-}3)$$

where N is the number of segments along the path. When we represent the integrands by functions which can be integrated analytically, it can be shown that the accuracy of this "mean-rectangular" technique is superior to the trapezoidal technique, and that it is comparable in accuracy to Simpson's technique.

---

* The values used for the longitudinal outer and the isotropic inner scale sizes were suggested in a private communication with L. A. Wittwer of DNA.

The set of path segments and the points at which the integrands are calculated are generated by the submodule PATHPT (described in Section 3.3). The set of points and line segments is such that each point corresponds to the midpoint of each line segment formed by the intersection of the path with the set of SCENARIO grid cells through which it passes. After initializing each integral register to zero, RFPROP begins to loop through the set of data points. At each point, the submodule DATAPT (described in Section 3.4) is called to retrieve the set of environmental data for the eight grid points surrounding the point and to interpolate these to the point. The environmental data set consists of the following: (1) the mean electron density [cm^{-3}], (2) the electron temperature [°K], (3) the electron density standard deviation about the mean [cm^{-3}], (4) the rms electron density [cm^{-3}], (5) the electron-neutral collision frequency [sec^{-1}], (6) the set of electron-ion collision frequencies [sec^{-1}] (the electron-ion collision frequency is a function of carrier frequency), (7) the three components of the ion velocity relative to the tangent plane of the point [cm sec^{-1}], (8) the partial time derivative of the mean electron density [$cm^{-3}sec^{-1}$], (9) the outer striation scale sizes in two directions perpendicular to the field [cm] (currently, these two values are equal), (10) the orientation angle of the major transverse striation dimension (currently zero), (11) the outer striation scale size parallel to the field [cm], (12) the isotropic inner striation scale size [cm], (13) the three components of the dipole magnetic field relative to the tangent plane of the point [Gauss], (14) the three components of the mean electron density gradient relative to the tangent plane [cm^{-4}], and (15) the six components of the second spatial derivative of the mean electron density relative to the tangent plane [cm^{-5}]. The components of the vectors and the second derivative are then transformed to a path oriented coordinate system as described later.

2.2.1 Geometry of Propagation Path.

All calculations are made in (or transformed to) the coordinate system aligned with the line of sight (LOS) along the path. The orientations of the coordinate axes of this system are as follows: the W-axis is oriented along the line of sight pointing away from the transmitter (the path origin) toward the receiver, the U-axis is perpendicular to the path and lies in the "vertical" plane containing the path and the center of the earth, and the V-axis is perpendicular to the path and perpendicular to the "vertical" plane. Note that the U-axis always points away from the center of the earth. The transformation from tangent plane coordinates to LOS coordinates is defined by a clockwise rotation of $(\pi/2+\lambda)$ about the Z (vertical) axis followed by a clockwise rotation of $(\pi/2-\varepsilon)$ about the Y-axis where ε is the elevation of the path measured from the transmitter (origin) to the receiver, and λ is the azimuth of the path.

In addition to the tangent plane (X-Y-Z) and LOS (U-V-W) coordinate systems, two other systems are used in RFPROP (see figure 2). These are the field aligned coordinate system (r-s-t) in which the power spectral density is expressed in Equation 2-1 and a system intermediate between the field aligned (r-s-t) system and the LOS (U-V-W) system which Wittwer designates as the (x-y-z) system. Note that this system must NOT be confused with the tangent plane (X-Y-Z) system. In the field aligned system the t-axis is parallel to the field vector and the r-axis is oriented in the plane perpendicular to the field vector along the direction in which the scale size is maximum. (The s-axis points in the direction along which the scale size is minimum.) Currently, the SCENARIO model provides only one scale size perpendicular to the field direction, and the choice of the r and s-axes is arbitrary. Until the orientation of the r-axis is specified explicitly by SCENARIO, we shall assume that the r-axis and the s-axis are equivalent. The x-axis of the (x-y-z) system is perpendicular to both the path and the field direction, that is

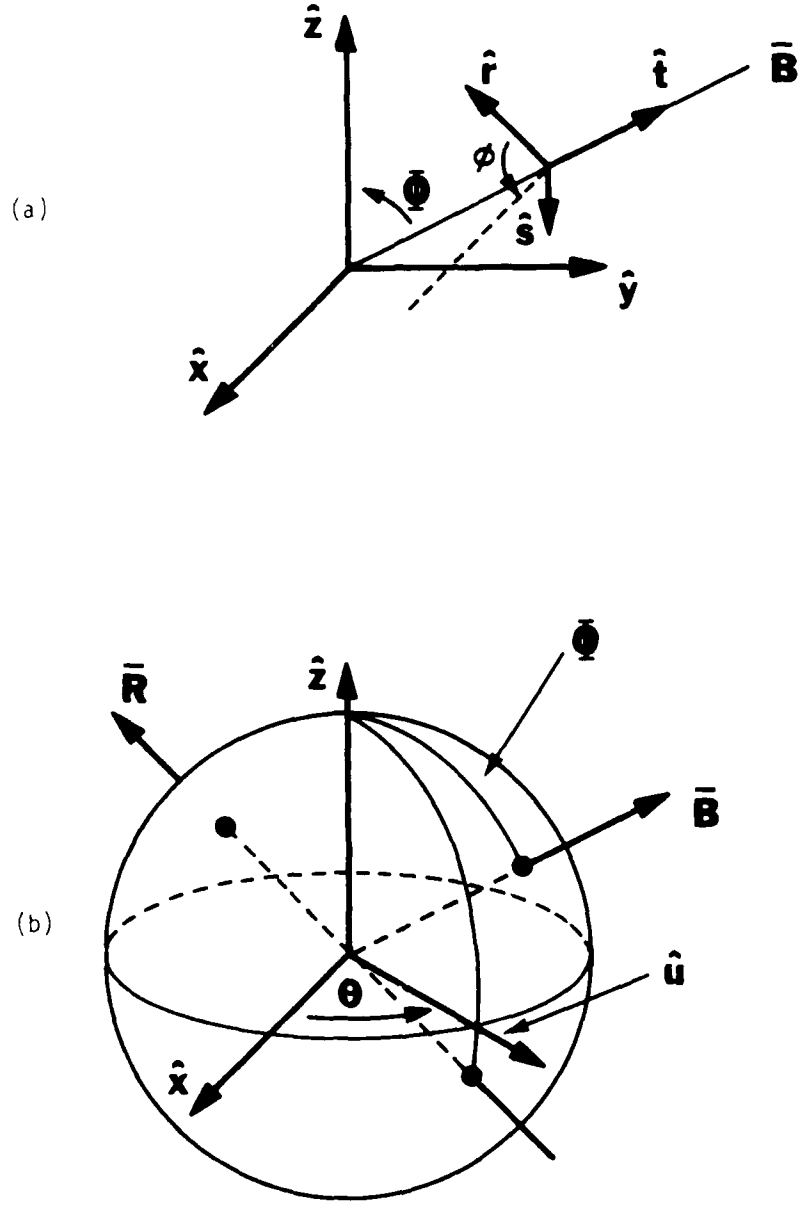

Figure 2. Geometric transformation from field oriented coordinates to line of sight (LOS) coordinates. In (a) the magnetic field is oriented along t, and the LOS lies along z. Rotations about two axes suffice to align t and z. In (b) R points toward the center of the earth, and together with z, it defines the "vertical" plane containing the LOS. The orientation of this plane is invariant along the LOS, and the components of all vectors transverse to the LOS are specified relative to it.

$$\hat{x} = \frac{\hat{t} \times \hat{z}}{\sin \Phi} \tag{2-4}$$

where Φ is the angle between the path and the field vector

$$\cos\Phi = \hat{t} \cdot \hat{z} = B_z / |\vec{B}| \tag{2-5}$$

and B_z is the field component along the path. More briefly, the y-axis is oriented along the field component in the plane perpendicular to the path.

The transformation from (r-s-t) coordinates to (x-y-z) is defined by two rotations: first, the (r-s-t) system is rotated counterclockwise about the t-axis through an angle ϕ to align the r-axis with the x-axis; next, the system is rotated counterclockwise about the x-axis through the angle Φ to align the t-axis with the z-axis. Note that if the plasma structure is isotropic in the r-s plane, we may set $\phi = 0$. One additional rotation is required to align the (x-y-z) system with the (U-V-W) system. To align the x-axis with the U-axis (in the vertical plane), rotate the (x-y-z) system counterclockwise about the z = W-axis through the angle θ, where

$$\tan\theta = B_u / B_v \tag{2-6}$$

Note that the W and z-axes coincide. Here, we often refer to Wittwer's z-axis as the W-axis. In contrast to the three other systems, the orientation of the (U-V-W) is fixed in space along the entire length of the path. All integrals are calculated in this fixed system.

Table 2. Summary of coordinate transformations for the four systems used by RFPROP module.

Tangent Plane to LOS.					
(X-Y-Z)	to	(U-V-W)	(1)	clockwise	$\pi/2 + \lambda$ about Z
			(2)	clockwise	$\pi/2 - \varepsilon$ about Y
Magnetic to Intermediate LOS					
(r-s-t)	to	(x-y-z)	(1)	counterclockwise	ϕ about t
			(2)	counterclockwise	Φ about x
Intermediate LOS to LOS.					
(x-y-z)	to	(U-V-W)	(1)	counterclockwise	θ about W = z

To simplify evaluation of the PSD and the signal parameters, define the "scale size operator" in magnetic coordinates as the diagonal matrix:

$$L = diag(L_r^2, L_s^2, L_t^2) \qquad [cm^2] \qquad (2\text{-}7)$$

To express the PSD function in the LOS coordinates, we transform the elements of the scale size operator by the second pair of rotations in Table 2:

$$L_x^2 = L_r^2 \cos^2\phi + L_s^2 \sin^2\phi \qquad [cm^2] \qquad (2\text{-}8)$$

$$L_y^2 = (L_r^2 \sin^2\phi + L_s^2 \cos^2\phi)\cos^2\Phi + L_t^2 \sin^2\Phi \qquad [cm^2] \qquad (2\text{-}9)$$

$$L_z^2 = (L_r^2 \sin^2\phi + L_s^2 \cos^2\phi)\sin^2\phi + L_t^2 \cos^2\phi \qquad [cm^2] \qquad (2\text{-}10)$$

$$L_{xy} = (L_s^2 - L_r^2)\cos\phi\cos\phi\sin\phi \qquad [cm^2] \qquad (2\text{-}11)$$

$$L_{xz} = (L_r^2 - L_s^2)\sin\phi\cos\phi\sin\phi \qquad [cm^2] \qquad (2\text{-}12)$$

$$L_{yz} = (L_t^2 - L_r^2 \sin^2\phi - L_s^2 \cos^2\phi)\cos\phi\sin\phi \qquad [cm^2] \qquad (2\text{-}13)$$

(See Equation 5-a through 5-f of DNA-IR-82-02[2].) And, finally, to express the transverse elements of the operator in the fixed (U-V-W) system:

$$L_u^2 = L_y^2 \cos^2\theta + L_x^2 \sin^2\theta - 2L_{xy}\cos\theta\sin\theta \qquad [cm^2] \qquad (2\text{-}14)$$

$$L_v^2 = L_x^2 \cos^2\theta + L_y^2 \sin^2\theta + 2L_{xy}\cos\theta\sin\theta \qquad [cm^2] \qquad (2\text{-}15)$$

$$L_{uv} = (L_y^2 - L_x^2)\cos\theta\sin\theta - L_{xy}(\sin^2\theta - \cos^2\theta) \qquad [cm^2] \qquad (2\text{-}16)$$

(See equations preceding Equation 18 of DNA-IR-82-02[2].) Note that Wittwer has switched the sense of the U and V-subscripts of the scale size operator in order to simplify the form of some of the equations which follow.

The "effective" structure scale size along the path (W-axis) is defined to be

$$\gamma_z = \frac{L_r L_s L_t}{\sqrt{\det(L)}} \qquad [cm] \qquad (2\text{-}17)$$

where

$$\det(L) = L_u^2 L_v^2 - (L_{uv})^2 = L_x^2 L_y^2 - (L_{xy})^2 \qquad [cm^4] \qquad (2\text{-}18)$$

is the determinant of the scale size operator on the U-V plane -- or on the x-y plane. (See Equation 10 of DNA-IR-82-02[2].)

The total time derivative of the mean electron density is computed as the sum of the partial time derivative (as computed by SCENARIO) and the scalar product of the density gradient and the velocity of the point on the path

$$\frac{dN_e}{dt} = \frac{\partial N_e}{\partial t} + \vec{V}_{pt} \cdot \text{grad}(N_e) \qquad [cm^{-3}sec^{-1}] \qquad (2\text{-}19)$$

where

$$\vec{V}_{pt} = \vec{V}_{org} + \left(\frac{z}{z_{end}}\right)(\vec{V}_{end} - \vec{V}_{org}) \qquad [cm\ sec^{-1}] \qquad (2\text{-}20)$$

and $\vec{V}_{org}$ and $\vec{V}_{end}$ are the velocities of the transmitter and receiver, respectively, and z and z_{end} are the distances to the point and to the receiver from the transmitter, respectively. The second and third time derivatives are estimated by assuming a power law function for the mean electron density:

$$N_e(t) = \alpha t^{-\beta} \qquad [cm^{-3}] \qquad (2\text{-}21)$$

Then

$$\frac{d^2N_e}{dt^2} = \frac{1}{N_e}\left(\frac{dN_e}{dt}\right)^2 - \frac{1}{t}\left(\frac{dN_e}{dt}\right) \qquad [cm^{-3}sec^{-2}] \qquad (2\text{-}22)$$

and

$$\frac{d^3N_e}{dt^3} = \frac{2}{N_e}\left(\frac{d^2N_e}{dt^2}\right)^2 - \frac{1}{N_e}\left(\frac{dN_e}{dt}\right)\left(\frac{d^2N_e}{dt^2}\right) \qquad [cm^{-3}sec^{-3}] \qquad (2\text{-}23)$$

Next, the components of the weighted effective plasma velocity at the point are calculated

$$\vec{V}_{eff} = \left(\frac{z_{end}}{z}\right)\left(\vec{V}_{ion} - \vec{V}_{pt}\right) \qquad [cm\ sec^{-1}] \qquad (2\text{-}24)$$

where $\vec{V}_{ion}$ is the local plasma velocity relative to a fixed coordinate system, and $\vec{V}_{pt}$ is the velocity of the point (Equation 2-20). (See equations following Equation 14 of DNA-IR-82-02[2].) This is used to compute the quantity ρ_v which in turn is used to compute the perpendicular signal decorrelation time:

$$\rho_v^2 = \frac{L_y^2 v_x^2 - 2L_{xy} v_x v_y + L_x^2 v_y^2}{\det(L)} \qquad [sec^{-2}] \qquad (2\text{-}25)$$

(See equation following Equation 14 of DNA-IR-82-02[2].) Although we have chosen to calculate it in the (x-y-z) system, it is a scalar quantity and may be calculated in any coordinate system.

Next, calculate Wittwer's B_n coefficient -- the coefficient of the first term in the Taylor series expansion of the differential decorrelation function. (See Equation B-1 of DNA-IR-82-02[2].)

$$\left(B_n(\rho^2)\right)^{m/2} = 1 - \frac{(\rho^2+\epsilon^2)^{(n-1)/2}\ K_{n-1}\left(\sqrt{\rho^2+\epsilon^2}\right)}{C_n 2^{n-2}\Gamma(n-1)} \qquad (2\text{-}26)$$

where ρ is a unitless quantity

$$\rho^2 = \frac{L_x^2 y^2 - 2L_{xy} xy + L_y^2 x^2}{\det(L)} \qquad (2\text{-}27)$$

and ϵ is the ratio of the inner to the (minimum) outer scale size, with Equation 2-26 valid in the range

$$3 \times 10^{-5} \leq \varepsilon \leq 0.1 \tag{2-28}$$

and

$$m = \text{minimum } (2, 2n-2) \tag{2-29}$$

$$c_n = \frac{\varepsilon^{n-1} K_{n-1}(\varepsilon)}{2^{n-2}\Gamma(n-1)} \tag{2-30}$$

where K_{n-1} is the modified Bessel function of order n-1. For the range of values of ε considered here, it is easy to show that c_n does not differ significantly from 1. (See Equation 9.6.9 and Table 9.8 of Abramowitz and Stegun[3].)

The coefficient β_n is then approximated as

$$\beta_n = \frac{\Gamma(n-1/2)}{c_n \sqrt{\pi}\,\Gamma(n-1)}\, f(n) h_n(\varepsilon) \tag{2-31}$$

where

$$f(n) = \begin{cases} (n-1)^{-1.10} & 1.2 \leq n \leq 2.0 \\ (n-1)^{-1.30} & 2.0 \leq n \leq 4.0 \end{cases} \tag{2-32}$$

and

$$h_n(\varepsilon) = \begin{cases} 1/3 + \dfrac{1}{4-2n}\left[1-\varepsilon^{4-2n}\right] & 1.2 \leq n < 2.0 \\ 1/3 - \ln(\varepsilon) & n = 2.0 \\ 1/3 + \dfrac{1}{2n-4}\left[1-\varepsilon^{2n-4}\right] & 2.0 < n \leq 4.0 \end{cases} \tag{2-33}$$

(See Appendix B of DNA-IR-82-02[2].) Note that both B_n and ρ are unitless and independent of the propagation frequency.

2.2.2 Point-Wise Integration Along Propagation Path.

RFPROP now begins to loop over the set of simulation frequencies, to calculate each integrand and sum that integrand into the appropriate primitive integral register. For these calculations, we need the frequency related parameters

$$\text{angular frequency:} \quad \omega = 2\pi f_c \quad [\text{rad sec}^{-1}] \tag{2-34}$$

$$\text{wavelength:} \quad \lambda = c/f_c \quad [\text{cm}] \tag{2-35}$$

$$\text{wave-number:} \quad K = 2\pi/\lambda \quad [\text{rad cm}^{-1}] \tag{2-36}$$

and the unitless variance of the index of refraction of the signal

$$\overline{\Delta n_i^2} = \frac{r_e^2 \, \sigma_{N_e}^2 \, \lambda^4}{4\pi^2} \tag{2-37}$$

where f_c is the signal carrier frequency (Hz), c is the speed of light (2.998E+10 cm sec^{-1}), r_e is the classical radius of the electron (2.8184E-13 cm), and $\sigma_{N_e}^2$ is the variance of the density at the point as calculated by SCENARIO. In order to eliminate unnecessary computuations, all calculations at a point are omitted if both the local mean electron density and its standard deviation fall below an arbitrary threshold value (currently set at 1 cm^{-3} for both parameters).

The differential phase variance at the point is

$$\frac{d\sigma^2}{dz} = \gamma K^2 \overline{\Delta n_i^2} \; \ell_z \qquad [\text{rad}^2\text{cm}^{-1}] \qquad (2\text{-}38)$$

where ℓ_z is the effective scale size along the LOS (Equation 2-17), and γ is a (unitless) constant

$$\gamma = \frac{2\sqrt{\pi}\ \Gamma(n-1)}{\Gamma(n-3/2)} \qquad \text{for} \qquad n > 1.5 \qquad (2\text{-}39)$$

(See Equations 8 and 9 of DNA-IR-82-02[2].) The total phase variance along the path is obtained by multiplying the differential phase variance by the path segment length at the point and summing over the N points along the path

$$\sigma_\phi^2 = \sum_i^N \frac{d\sigma^2}{dz} \Delta z \qquad [\text{rad}^2] \qquad (2\text{-}40)$$

Also, calculate the phase weighted sum of the B_n coefficient (Equation 2-31) which is used to generalize the frequency selective bandwidth calculation from a delta layer approximation to a layer of finite thickness

$$\text{sum}(h) = \sum_i^N B_n \frac{d\sigma^2}{dz} \Delta z \qquad [\text{rad}^2] \qquad (2\text{-}41)$$

(See equation preceding Equation 32 in DNA-IR-82-02[2].)

Next, we calculate the [unitless] function

$$M(z) = \frac{(L_x^2+L_y^2)(z_{end}-z)(z/z_{end})}{K \det(L)} \qquad (2\text{-}42)$$

and the three associated primitive integrals required to compute the mean square log amplititude fluctuation of the signal

$$\text{sum}(x_0) = \frac{1}{2} \sum_{i}^{N} \Delta z \, \frac{d\sigma^2}{dz} \, (n-1) \, f(n,z) \, I_0(z) \tag{2-43}$$

$$\text{sum}(x_1) = \frac{1}{2} \sum_{i}^{N} \Delta z \, \frac{d\sigma^2}{dz} \, (n-1) \, f(n,z) \, I_1(z) \tag{2-44}$$

$$\text{sum}(x_2) = \frac{1}{2} \sum_{i}^{N} \Delta z \, \frac{d\sigma^2}{dz} \, (n-1) \, f(n,z) \, I_2(z) \tag{2-45}$$

where

$$f(n,z) = \left(\frac{f'(n) + \frac{1}{n} M(z)}{1 + M(z)}\right) \left\{1 - \frac{n}{12} \exp\left[-\left(\frac{M(z)}{3} - \frac{1}{10M(z)} - 1\right)^2\right]\right\} \tag{2-46}$$

$$f'(n) = 1.1 - \text{maximum } (0, (n-2.4)/2) \tag{2-47}$$

and

$$I_0(z) = \begin{cases} 16c_1^{2n}\left(c_2^{6-2n} - a_1^{6-2n}\right) \dfrac{M(z)^{n-1}}{6-2n} & n \neq 3 \\ 16c_1^{2n} \ln (c_2/a_1) \, M(z)^{n-1} & n=3 \end{cases} \tag{2-48}$$

$$I_1(z) = 8\left[\frac{1}{3} a_1^6 + c_2^4 \left(a_2^2 - c_2^2\right)\right] M(z)^{-1} \tag{2-49}$$

$$I_2(z) = 8c_1^{2n} c_2^4 a_2^{2-2n} \frac{M(z)^{n-1}}{n-1} \tag{2-50}$$

where

$$a_1 = \text{minimum } \left[c_2, c_1\sqrt{M(z)}\right] \tag{2-51}$$

$$a_2 = \text{maximum } \left[c_2, c_1\sqrt{M(z)}\right] \tag{2-52}$$

with $c_1 = 0.5$ and $c_2 = 0.84$. (See equations following Equation A-3 of DNA-IR-82-02[2].) Note that M and all the primitive sums are unitless quantities. This derivation for the mean square log amplitude is valid for all values of M and for n within the range $1.2 \leq n \leq 4$. Also, RFPROP stores the [unitless] auxiliary sums

$$J_1 = \frac{1}{2} \sum_i^N \Delta z \frac{d\sigma^2}{dz} [M(z)]^2 \tag{2-53}$$

$$J_2 = \begin{cases} \frac{1}{2} \sum_i^N \Delta z \frac{d\sigma^2}{dz} M(z)^{n-1} & n \neq 3 \\ -\frac{1}{4} \sum_i^N \Delta z \frac{d\sigma^2}{dz} \ln[M(z)] M(z)^2 & n=3 \end{cases} \tag{2-54}$$

which will be used to evaluate the Rayleigh phase variance. (See Equations A-8a through A-8c of DNA-IR-82-02[2].)

Calculate the integral to be used to compute the signal decorrelation time in the direction perpendicular to the LOS

$$\text{sum}(\tau) = \sum_i^N \Delta z \frac{d\sigma^2}{dz} B_n (\rho_v z / z_{end})^m \qquad [\text{sec}^{-m}] \tag{2-55}$$

where B_n is the coefficient from Equation 2-32 and ρ_v is given by Equation 2-25. (See Equation 14 of DNA-IR-82-02[2].)

Sum the weighted plasma velocity relative to the receiver in the directions parallel and perpendicular to the LOS:

$$\text{sum}(v_\perp) = \sum_i^N \Delta z \frac{d\sigma^2}{dz} \left| (\vec{V}_{ion} - \vec{V}_{end}) \cdot \hat{z} \right| \qquad [\text{cm sec}^{-1}] \tag{2-56}$$

and

$$\text{sum}(v_{\perp}) = \sum_{i}^{N} \Delta z \frac{d\sigma^2}{dz} V_{trans} \qquad [\text{cm sec}^{-1}] \quad (2\text{-}57)$$

where

$$V_{trans} = \{[(\vec{V}_{ion} - \vec{V}_{end}) \cdot \hat{u}]^2 + [(\vec{V}_{ion} - \vec{V}_{end}) \cdot \hat{v}]^2\}^{1/2} \qquad [\text{cm sec}^{-1}] \quad (2\text{-}58)$$

Calculate and sum the increments of the primitive integrals needed to calculate the moments of the coherence function at the receiver:

$$\text{sum}(C_u) = \sum_{i}^{N} B_n \frac{d\sigma^2}{dz} \Delta z \left[(z/z_{end})^2 \frac{L_u^2}{\det(L)}\right]^{m/2} \qquad [\text{cm}^{-m}] \quad (2\text{-}59)$$

$$\text{sum}(C_v) = \sum_{i}^{N} B_n \frac{d\sigma^2}{dz} \Delta z \left[(z/z_{end})^2 \frac{L_v^2}{\det(L)}\right]^{m/2} \qquad [\text{cm}^{-m}] \quad (2\text{-}60)$$

$$\text{sum}(C_{uv}) = \sum_{i}^{N} B_n \frac{d\sigma^2}{dz} \Delta z \left[(z/z_{end})^2 \frac{2|L_{uv}|}{\det(L)}\right]^{m/2} \text{sign}(L_{uv}) \qquad [\text{cm}^{-m}] \quad (2\text{-}61)$$

(See Equations 20-a through 20-d of DNA-IR-82-02[2].) The analogous quantities are computed at the transmitter by replacing z in Equations 2-59 through 2-61 by $(z_{end} - z)$.

The signal time delay variance (σ_t^2) and frequency selective bandwidth (f_0) have been derived by Wittwer (see Equations 31-33 of DNA-IR-82-02[2])

$$\sigma_t^2 = (2\pi f_c)^{-2} \left\{\sigma_R^2 + \frac{H_m}{K^2} \int_0^{z_{end}} \frac{dz}{z^2} \int_0^{z} \frac{dz'}{z'^2} \left[I_u^2(z') + I_v^2(z') + 2I_{uv}^2(z)\right]\right\} \qquad [\text{sec}^2] \quad (2\text{-}62)$$

and

$$f_0 = (4\pi^2 \sigma_t^2)^{-1/2} \qquad [\text{Hz}] \quad (2\text{-}63)$$

where

σ_R^2 is the phase variance of the Rayleigh distributed component of the signal

H_m is the parameter derived in Equation 2-127

z_{end} is the length of the path [cm]

and

$$I_u(z') = 2\int_0^{z'} B_n dz \left(\frac{d\sigma_\phi^2}{dz}\right) z^2 L_u^2 [\det(L)]^{-1} \qquad (2\text{-}64)$$

$$I_v(z') = 2\int_0^{z'} B_n dz \left(\frac{d\sigma_\phi^2}{dz}\right) z^2 L_v^2 [\det(L)]^{-1} \qquad (2\text{-}65)$$

$$I_{uv}(z') = 2\int_0^{z'} B_n dz \left(\frac{d\sigma_\phi^2}{dz}\right) z^2 L_{uv} [\det(L)]^{-1} \qquad (2\text{-}66)$$

where $(d\sigma_\phi^2/dz)$ is the differential phase variance (Equation 2-38), B_n is defined in Equation 2-31, det(L) is the determinant of the scale size operator (Equation 2-18), and L_u^2 etc., are the transformed elements of the scale size operator (Equations 2-14 through 2-16).

Since the calculation depends on a linear combination of the squares of the innermost integrals (Equations 2-64 through 2-66), we shall limit the remainder of this discussion to the evaluation of the single 3-level nested integral

$$\Gamma = \int_0^{x_{end}} \frac{dx}{x^2} \left[\int_0^{x} \frac{dx'}{x'^2} \left[\int_0^{x'} d\xi \; \xi^2 \; f(\xi) \right]^2 \right] \quad [cm^{-2}] \qquad (2\text{-}67)$$

All the other integrals computed by RFPROP are evaluated using a mean-rectangular integration algorithm (see Equation 2-3). The accuracy of this technique is unsatisfactory for the triply nested integral of Equation 2-67, however. First, we simplify the integral using integration by parts of the outermost integral to yield the 2-level nested integral

$$\Gamma = \int_0^{x_{end}} \frac{dx}{x^2} \left(\frac{1}{x} - \frac{1}{x_{end}} \right) \left[\int_0^{x} dx' x'^2 f(x') \right]^2 \quad [cm^{-2}] \qquad (2\text{-}68)$$

Then, approximate the integrand $f(x)$ by a piecewise linear function between the $n+1$ discrete points on the path

$$f(x) = \begin{cases} \alpha_1 x + \beta_1 & \text{on } x_0 < x \leq x_1 \\ \alpha_2 x + \beta_2 & \text{on } x_1 < x \leq x_2 \\ \quad \cdots & \quad \cdots \\ \alpha_n x + \beta_n & \text{on } x_{n-1} < x \leq x_n \end{cases} \qquad (2\text{-}69)$$

where

$$\alpha_j = (y_j - y_{j-1})/(x_j - x_{j-1}) \qquad (2\text{-}70)$$

and

$$\beta_j = (x_j y_{j-1} - x_{j-1} y_j)/(x_j - x_{j-1}) \qquad (2\text{-}71)$$

for $j = 1, 2, \ldots, n$.

It can be shown that the innermost integral can be calculated by the recursion relation

$$\gamma'_j = \xi_j^3 \gamma'_{j-1} + \left[\frac{1}{4} r^{(3)}(\xi_j)\Delta y_j^{(1)} - \frac{1}{3} r^{(2)}(\xi_j)\ \Delta y_j^{(2)}\right] \qquad (2\text{-}72)$$

where

$$\xi_j = x_{j-1}/x_j \qquad (2\text{-}73)$$

$$r^{(n)}(\xi_j) = 1 + \xi_j + \xi_j^2 + \ldots + \xi_j^n \qquad (2\text{-}74)$$

$$\Delta y_j^{(1)} = y_j - y_{j-1} \qquad (2\text{-}75)$$

$$\Delta y_j^{(2)} = \xi_j y_j - y_{j-1} \qquad (2\text{-}76)$$

Also, define the quantity

$$C'_j = \xi_j^3 \left[\gamma'_{j-1} - (1-\varepsilon_j)^{-1} \left(\frac{1}{4} \xi_j \Delta y_j^{(1)} - \frac{1}{3} \Delta y_j^{(2)}\right)\right] \qquad (2\text{-}77)$$

Then, it can be shown that the integral of Equation 2-68 may be written

$$\Gamma = \Gamma_n^{(1)} - \frac{1}{x_{end}} \Gamma_n^{(2)} \qquad [cm^{-2}] \qquad (2\text{-}78)$$

where the Γ_j are calculated by the recursion relations

$$\Gamma_j^{(1)} = \Gamma_{j-1}^{(1)} + x_j^4 \left\{(1-\xi_j)^{-1} \left[\frac{1}{96} r^{(5)}(\xi_j)(\Delta y_j^{(1)})^2 + \frac{1}{36} r^{(3)}(\xi_j)(\Delta y_j^{(2)})^2 \right.\right.$$

$$\left. - \frac{1}{30} r^{(4)}(\xi_j)\ \Delta y_j^{(1)}\ \Delta y_j^{(2)}\right]$$

$$\left. + C'_j \left[\frac{1}{4} r^{(1)}(\xi_j)\ \Delta y_j^{(1)} - \frac{2}{3} \Delta y_j^{(2)} - \frac{1}{2} C'_j\ (1-\xi_j^{-2})\right]\right\} \qquad (2\text{-}79)$$

and

$$r_j^{(2)} = r_{j-1}^{(2)} + x_j^5 \left[(1-\xi_j)^{-1} \left[\frac{1}{112} r^{(6)}(\xi_j)(\Delta y_j^{(1)})^2 + \frac{1}{45} r^{(4)}(\xi_j)(\Delta y_j^{(2)})^2 \right.\right.$$

$$\left. - \frac{1}{36} r^{(5)}(\xi_j)\Delta y_j^{(1)}\Delta y_j^{(2)}\right]$$

$$\left. + C_j' \left[\frac{1}{6} r^{(2)}(\xi_j)\Delta y_j^{(1)} - \frac{1}{3} r^{(1)}(\xi_j)\Delta y_j^{(2)} - C_j'(1-\xi_j^{-1})\right]\right] \qquad (2\text{-}80)$$

The summation registers containing the sums of the terms of Equations 2-79 and 2-80 are incremented inside the grid only. When the LOS extends beyond the edge of the grid (i.e., whenever the receiver is not located inside the grid), it is necessary to correct the sum to account for the finite distance from the edge of the grid to the receiver. It can be shown that the necessary correction factor to be added to Equation 2-78 is

$$\varepsilon = \frac{1}{2} \gamma_n'^2 \left(\frac{x_n}{x_{end}} - 1\right)^2 \left(\frac{x_n}{x_{end}}\right)^4 \qquad (2\text{-}81)$$

where x_n is the distance from the origin (transmitter) to the far edge of the grid, x_{end} is the length of the LOS, and γ_n' is the innermost integral obtained from Equation 2-72. (For a more complete explanation of the derivation of these equations, refer to MRC-N-273[16].)

All the remaining basic parameters calculated by RFPROP are used to derive the mean ionization effects. We calculate the real part of the index of refraction, the absorption coefficient, and the effective electron density using the Appleton-Hartree equations. PRPSIM considers only the contribution of electron-ion collisions and electron-neutral collisions. The magnetic field and ion-neutral collisions can be neglected at the propagation frequencies of interest here. Now let

$$X = \frac{e^2}{\varepsilon_0 m} \frac{N_e}{\omega^2} = 3.1833 \times 10^9 \, N_e/\omega^2 \qquad (2\text{-}82)$$

where e and m are the electronic charge (4.803E-10 statcoulombs) and mass (9.107E-28 gm), respectively, ε_0 is the permittivity of free space ($(4\pi)^{-1}$ = 7.958E-2 in cgs units), N_e is the local electron density [cm^{-3}], and ω is the angular frequency of the signal [rad sec^{-1}]; and let

$$Z = \frac{\nu_{ei} + \nu_{en}}{\omega} \qquad (2\text{-}83)$$

where ν_{ei} and ν_{en} are the electron-ion and electron-neutral collision frequencies, respectively. These parameters are then modified to account for the velocity dependence of the electron collision frequency:

$$X_{eff} = \frac{1}{H} X \qquad (2\text{-}84)$$

$$Z_{eff} = \frac{G}{H} Z \qquad (2\text{-}85)$$

where

$$G = \begin{cases} \dfrac{1+Z/2.5}{1+Z/1.5} & \nu_{en} > \nu_{ei} \\ 1 & \nu_{en} \leq \nu_{ei} \end{cases} \qquad (2\text{-}86)$$

and

$$H = \begin{cases} \dfrac{1 + .15Z}{1 + .05Z} & \nu_{en} > \nu_{ei} \\ 1 & \nu_{en} \leq \nu_{ei} \end{cases} \qquad (2\text{-}87)$$

(See Shkarofsky, 1961[4].) The real part of the [unitless] index of refraction is given by

$$\mu = \frac{1}{\sqrt{2}}\sqrt{(1-Y) + \sqrt{(1-Y)^2 + Z_{eff}^2\, Y^2}} \qquad (2\text{-}88)$$

where

$$Y = \frac{X_{eff}}{1 + Z_{eff}^2} \qquad (2\text{-}89)$$

(See Equation 2.93 of Davies, 1965[5].)

The linear coefficient of absorption is given by

$$\alpha = \frac{20}{\ln(10)} \frac{1}{2c} \frac{\omega}{\mu} YZ_{eff} = 1.449 \times 10^{-10} \frac{\omega}{\mu} YZ_{eff} \quad [\text{dB cm}^{-1}] \qquad (2\text{-}90)$$

(See Equation 2.98 of Davies, 1965[5].) If one can assume that the carrier frequency is large compared to the collision frequencies, the coefficient of absorption may be approximated as

$$\alpha \simeq \frac{0.461}{\mu\omega^2} N_e(\nu_{ei} + \nu_{en}) \quad [\text{dB cm}^{-1}] \qquad (2\text{-}91)$$

RFPROP calculates the mean absorption coefficient for the cell

$$\overline{\alpha} = \int_0^\infty \alpha(N_e)\, p(N_e)\, dN_e \qquad (2\text{-}92)$$

where $p(N_e)$ is the unknown distribution function of the electron density within the cell. From Equations 3-28 and 3-30, it is seen that the neutral-electron collision frequency (per electron) is independent of the electron density, and that the ion-electron collision frequency is proportional to the electron density. Thus

$$\alpha = \int_0^\infty (a_1 N_e^2 + a_2 N_e)\, p(N_e)\, dN_e$$

$$= a_1 \overline{N_e^2} + a_2 \overline{N_e} \qquad (2\text{-}93)$$

Hence, the mean absorption coefficient can be computed as the sum of two coefficients with the first being a function of the ion-electron collision frequency and the root-mean-square electron density, and the second being a function of the neutral-electron collision frequency and the mean electron density.

The effective mean electron density at the signal propagation frequency is given by

$$Ne_{eff} = \frac{N_e}{1 + Z_{eff}^2} \qquad [cm^{-3}] \qquad (2\text{-}94)$$

where N_e is the mean electron density provided by DATAPT, and Z_{eff} is the Z coefficient calculated using only the electron-neutral collisions. Note that the effective density differs significantly from the actual density only when the signal propagation frequency is comparable to or smaller than the electron-neutral collision frequency. This value is added to the electron content register to calculate the mean total electron content (TEC) along the path.

$$\langle TEC \rangle = \sum_i^N \Delta z\, Ne_{eff} \qquad [cm^{-2}] \qquad (2\text{-}95)$$

The first three time derivatives of the local mean electron density (calculated by SCENARIO and in Equations 2-22 and 2-23 above, respectively) are also summed into individual registers to calculate the

three time derivatives of the <TEC>. Similarly, the total absorption is calculated as the sum of the absorption coefficients (Equation 2-93) multiplied by the path segment lengths.

The incremental Faraday rotation of the plane of polarization of the electric vector of the signal is calculated for the case of quasi-longitudinal propagation in the absence of absorption:

$$\frac{d\omega}{dz} = \frac{1}{2c^2}\left(\frac{e^2}{4\pi^2\varepsilon_0 m}\right)\left(\frac{e}{m}\right)\frac{N_e B_w}{f^2} = 2.365\times10^4\,\frac{N_e B_w}{f^2} \qquad [\text{rad cm}^{-1}] \quad (2\text{-}96)$$

where c is the speed of light, ε_0 is the permittivity of free space, e and m are the charge and mass of the electron, respectively, N_e is the effective mean electron density [cm^{-3}], and B_w is the component of the magnetic field [Gauss] parallel to the LOS. (See Equation 4.39 of Davies, 1965[5].) The total angle of rotation is calculated as the sum of the incremental rotations multiplied by the path segment lengths.

The last frequency dependent integrands to be computed are the weighted distance to the point and the weighted square of the distance with the phase variance as the weighting function. These are used to provide measures of the distance to the most intense region along the path and of the extent of the active region. Let

$$\text{sum}(Z) = \sum_i^N z\,\Delta z\left(\frac{d\sigma^2}{dz}\right) \qquad [\text{cm}] \quad (2\text{-}97)$$

$$\text{sum}(Z^2) = \sum_i^N z^2\,\Delta z\left(\frac{d\sigma^2}{dz}\right) \qquad [\text{cm}^2] \quad (2\text{-}98)$$

This point marks the end of the loop for which the integrands are calculated as functions of frequency and also the end of the loop over

the points along the path at which the integrands are summed into their appropriate integral registers.

2.2.3 Calculation of Signal Parameters from Primitive Integrals.

Next, RFPROP begins to loop over frequency to derive the signal parameters from the primitive integrals which were summed over the individual points along the path. First, the principal moments and the orientation of the decorrelation matrix at the receiver are computed:

$$C_u = [\,\mathrm{sum}(C_u)\,]^{2/m} \qquad [cm^{-2}] \qquad (2\text{-}99)$$

$$C_v = [\,\mathrm{sum}(C_v)\,]^{2/m} \qquad [cm^{-2}] \qquad (2\text{-}100)$$

$$C_{uv} = \mathrm{sign}[\,\mathrm{sum}(C_{uv})\,]\,|\mathrm{sum}(C_{uv})|^{2/m} \qquad [cm^{-2}] \qquad (2\text{-}101)$$

where $\mathrm{sum}(C_u)$, $\mathrm{sum}(C_v)$, and $\mathrm{sum}(C_{uv})$ are the primitive integrals by Equations 2-59 through 2-61. (See Equations 20a-d of DNA-IR-82-02[2].) Find the maximum and mininum eigenvalues of the matrix, C_p and C_q:

$$C_p = \frac{1}{2}\left[(C_u+C_v) + \sqrt{(C_u-C_v)^2 + 4C_{uv}^2}\right] \qquad [cm^{-2}] \qquad (2\text{-}102)$$

$$C_q = \frac{1}{2}\left[(C_u+C_v) - \sqrt{(C_u-C_v)^2 + 4C_{uv}^2}\right] \qquad [cm^{-2}] \qquad (2\text{-}103)$$

and the orientation of the maximum eigenvector:

$$\varepsilon = \frac{1}{2}\arctan\left[\frac{2C_{uv}}{C_u-C_v}\right] \qquad [rad] \qquad (2\text{-}104)$$

(See equations preceding Equation 21 of DNA-IR-82-02[2].) Note that C_p and C_q denote the maximum and minimum eigenvalues, respectively of the decorrelation matrix. The analogous decorrelation matrix at the transmitter is calculated also. The decorrelation distances along the p and q axes are derived from the eigenvalues of the decorrelation matrix:

$$\ell_p = \frac{B(n,\sigma_\phi^2)}{\sqrt{C_p}} \qquad [cm] \qquad (2\text{-}105)$$

$$\ell_q = \frac{B(n,\sigma_\phi^2)}{\sqrt{C_q}} \qquad [cm] \qquad (2\text{-}106)$$

where $B(n,\sigma_\phi^2)$ is the empirical function defined in Equation 2-112. (See Equation 41 of DNA-5304D[1].) Note that ℓ_p and ℓ_q denote the *minimum* and maximum decorrelation distances, respectively. The decorrelation distance is defined as the distance from the LOS on the perpendicular plane at which the mutual coherence function decreases by a factor of 2.718. (See Equation 21 of DNA-IR-82-02[2].) The mean square angles of the signal energy arrival at the receiver and transmitter are derived from the decorrelation matrix also:

$$\sigma_p^2 = \frac{2C_p}{K^2} \qquad [rad^2] \qquad (2\text{-}107)$$

$$\sigma_q^2 = \frac{2C_q}{K^2} \qquad [rad^2] \qquad (2\text{-}108)$$

(See Equations 26a and 26b of DNA-IR-82-02[2].) Note that σ_p^2 and σ_q^2 denote the maximum and minimum values, respectively. Also note that each of the Equations 2-99 through 2-108 denotes the calculation of two quantities -- one at the receiver and one at the transmitter.

The signal decorrelation time at the receiver in the direction parallel to the LOS is approximated by

$$\tau_{\parallel} = \frac{3.5\ K}{\left[C_p^{2/3} + C_q^{2/3}\right]^{3/2} \langle v_{\parallel} \rangle} \qquad [\text{sec}] \qquad (2\text{-}109)$$

where $\langle v_{\parallel} \rangle$ is the weighted average magnitude of the plasma velocity relative to the receiver and parallel to the LOS (from Equation 2-56)

$$\langle v_{\parallel} \rangle = \text{sum}(v_{\parallel})/\sigma_{\phi}^2 \qquad [\text{cm sec}^{-1}] \qquad (2\text{-}110)$$

(See Equation 2-56 above and Equation 22 of DNA-IR-82-02[2].)

The signal decorrelation time at the receiver in the plane perpendicular to the LOS is

$$\tau_{\perp} = \frac{B(n,\sigma_{\phi}^2)}{\left(\text{sum}(\tau)\right)^{1/m}} \qquad [\text{sec}] \qquad (2\text{-}111)$$

where sum(τ) is the primitive integral of Equation 2-55, m is defined in Equation 2-29, and B is a [unitless] function of the spectral index and the total phase variance:

$$B(n,\sigma_{\phi}^2) = \min\left[1,(-0.34n^2 + 2.51n - 2.0)\right]\left[\text{sum}(h)\right]^{1/m} \qquad (2\text{-}112)$$

where sum(h) is the phase weighted sum (Equation 2-41) of the B_n coefficient calculated in Equation 2-31. (See Equation 14 of DNA-IR-82-02[2].) The B function imposes an emperically determined lower limit for

the perpendicular decorrelation time when the total phase variance along the path becomes vanishingly small.

The smaller value of the $\tau_{\perp}$ - $\tau_{\parallel}$ pair is designated as the signal decorrelation time:

$$\tau_0 = \min(\tau_{\perp},\tau_{\parallel}) \qquad [\text{sec}] \tag{2-113}$$

(See Equation 23 of DNA-IR-82-02[2].)

Next, calculate the mean weighted distance to the region and its standard deviation:

$$\langle Z\rangle_{\sigma} = \text{sum}(Z)/\sigma_{\phi}^2 \qquad [\text{cm}] \tag{2-114}$$

$$\text{sd}(Z) = \left[\text{sum}(Z^2)/\sigma_{\phi}^2 - \langle Z\rangle^2\right]^{1/2} \qquad [\text{cm}] \tag{2-115}$$

using the sums calculated in Equations 2-97 and 2-98.

The mean square log amplitude fluctuation (MSLAF) is required in order to calculate the portion of the total phase variance whose amplitude is Rayleigh distributed. Calculate the MSLAF using the primitive integrals of Equations 2-43 through 2-45:

$$\chi^2 = \text{sum}(\chi_0) + \text{sum}(\chi_1) + \text{sum}(\chi_2) \tag{2-116}$$

(See Equation A-3 of DNA-IR-82-02[2].) Then to determine the portion of the phase variance which is Rayleigh distributed, let

$$J_3 = \begin{cases} \left[c_2^{(6-2n)} J_2 - c_1^{(6-2n)} J_1\right]/(6-2n) & n\neq 3 \\ J_2 + J_1 \ln(c_2/c_1) & n=3 \end{cases} \tag{2-117}$$

where J_1 and J_2 are the integrals computed in Equations 2-53 and 2-54, and c_1 and c_2 are constants: $c_1 = 0.5$, $c_2 = 0.84$. (See Equations A-9a and A-9b of DNA-IR-82-02[2].) And let

$$\chi_s^2 = 16(n-1)f(n)\ c_1^{2n}\ J_3 + \text{sum}(\chi_1) \tag{2-118}$$

where $\text{sum}(\chi_1)$ is the integral computed in Equation 2-44, and $f(n)$ is the phase weighted mean of the function $f(n,z)$ defined in Equation 2-46:

$$f(n) = \left[\sum_i^N f(n,z_i)\ \frac{d\sigma^2}{dz}\ \Delta z\right] / \sigma_\phi^2 \tag{2-119}$$

The phase spectrum is arbitrarily divided into two regions so that fluctuations whose wave number is smaller than some critical value can be considered to contribute negligibly to the total phase variance. Denote the value of the MSLAF integrated up to that wave number as χ_c^2. The Rayleigh threshold is usually defined to be $\chi^2 = 0.10$. PRPSIM uses the following procedure to compute the Rayleigh distributed contribution to the phase variance:

If $\chi^2 \leq \chi_c^2$ or $(J_3 \leq 0$ and $\sigma_\phi^2/2 < \chi_c^2)$ then

$$\sigma_R^2 = 0 \tag{2-120}$$

else if $\text{sum}(\chi_1) \leq \chi_c^2$ or $(J_3 \leq 0$ and $\sigma_\phi^2/2 \geq \chi_c^2)$ then

$$\sigma_R^2 = \sigma_\phi^2 \qquad [\text{rad}^2] \tag{2-121}$$

(where $\text{sum}(\chi_1)$ is the integral computed in Equation 2-44 and σ_ϕ^2 is the total phase variance computed in Equation 2-40); else calculate

$$\sigma_R^2 = \begin{cases} \min\left[\dfrac{2J_2}{4^{n-1}\, a_c^{(2n-2)}},\ \sigma_\phi^2\right] & n \neq 3 \\ \min\left[\dfrac{2J_1}{4^{n-1}\, a_c^{(2n-2)}},\ \sigma_\phi^2\right] & n = 3 \end{cases} \tag{2-122}$$

where, if $\chi_c < \chi_s^2$

$$a_c = \begin{cases} \left\{(6-2n)\left[\dfrac{\chi_c^2 - \chi_s^2}{16c_1^{2n}(n-1)f(n)J_2}\right] + c_2^{6-2n}\right\}^{\frac{1}{(6-2n)}} & n \neq 3 \\ c_2 \exp\left[\dfrac{\chi_c^2 - \chi_s^2}{16c_1^{2n}(n-1)f(n)J_1}\right] & n = 3 \end{cases} \tag{2-123}$$

or, if $\chi_c^2 \geq \chi_s^2$

$$a_c = \begin{cases} \left\{(2-2n)\left[\dfrac{\chi_c^2 - \chi_s^2}{16c_1^{2n}c_2^4(n-1)f(n)J_2}\right] + c_2^{2-2n}\right\}^{\frac{1}{(2-2n)}} & n \neq 3 \\ \left\{(2-2n)\left[\dfrac{\chi_c^2 - \chi_s^2}{16c_1^{2n}c_2^4(n-1)f(n)J_1}\right] + c_2^{2-2n}\right\}^{\frac{1}{(2-2n)}} & n = 3 \end{cases} \tag{2-124}$$

(See Equations A-11a through A-13b of DNA-IR-82-02[2].)

The S_4 scintillation index is also a unitless measure of the severity of the amplitude scintillation. We approximate it from the MSLAF by using the empirically derived relation

$$S_4 = \text{minimum } (1.42(\chi^2)^{0.44}, 1) \qquad (2\text{-}125)$$

where χ^2 is the MSLAF from Equation 2-116. (See Equation 10 of Reference 6.) Note that this approximation is most accurate at n = 2.

The frequency selective bandwidth is computed as

$$f_c = f_C \sqrt{\sigma_R^2 + \frac{H_m}{K^2}(\tau+\varepsilon)^{1-1/2}} \qquad [\text{Hz}] \qquad (2\text{-}126)$$

where

f_C	is the signal carrier frequency	[Hz]
K	is the signal wave-number	$[\text{cm}^{-1}]$
σ_R^2	is the Rayleigh phase variance from Equations 2-120 - 2-122	$[\text{rad}^2]$
ε	is the correction factor from Equation 2-81	$[\text{cm}^{-2}]$
τ	is the primitive sum from Equation 2-78	$[\text{cm}^{-2}]$

and

$$H_m = \sqrt{\text{sum}(h)^{4/m-2}} \qquad (2\text{-}127)$$

is the finite layer correction factor derived from the primitive sum from Equation 2-41. (See Equations 31-33 of DNA-IR-82-02[2].)

The Rayleigh frequency (f_R) is defined as the smallest frequency of the plasma oscillations which contributes to the Rayleigh phase variance:

$$\int_{-f_R}^{f_R} P_\phi(f)df = 2\int_0^{f_R} P_\phi(f)df = 1 - \sigma_R^2/\sigma_\phi^2 \qquad (2\text{-}128)$$

where σ_R^2 is the Rayleigh phase variance, σ_ϕ^2 is the total phase variance, and $P_\phi(f)$ is the probability distribution in frequency for the electron density fluctuations:

$$P_\phi(f) = 2\sqrt{\pi}\,\tau_0\, a^{2n-2}\,\frac{\Gamma(n-1/2)}{\Gamma(n-1)}\left[a^2 + (2\pi\tau_0 f)^2\right]^{-(n-1/2)} \qquad (2\text{-}129)$$

where τ_0 is the signal decorrelation time (Equation 2-113) and a is a unitless coefficient derived from the phase weighted sum of the B_n coefficient

$$a = \left[\text{sum}(h)\right]^{-1/m} \qquad (2\text{-}130)$$

(See Equations 2-29, 2-41, and Equation 39 of DNA-IR-82-02[2].) For convenience, we define the [unitless] scaled Rayleigh frequency

$$z_R = 2\pi\,(\tau_0/a)f_R \qquad (2\text{-}131)$$

Analytic solutions for z_R exist only for n = 3/2 and n = 2. For n = 2

$$z_R = \left\{\left[1 - \sigma_R^2/\sigma_\phi^2\right]^{-2} - 1\right\}^{-1/2} \qquad (2\text{-}132)$$

For other values of n, it is easy to show that the limiting solutions for z_R are

$$z_R \overset{\lim}{\to} 0,\ z_R \simeq \frac{\sqrt{\pi}}{2} \frac{\Gamma(n-1)}{\Gamma(n-1/2)} \left[1 - \sigma_R^2/\sigma_\phi^2\right] \qquad (2\text{-}133)$$

and

$$z_R \overset{\lim}{\to} \infty,\ z_R \simeq \{(2n-2) \frac{\sqrt{\pi}}{2} \frac{\Gamma(n-1)}{\Gamma(n-1/2)} (\sigma_R^2/\sigma_\phi^2)\}^{-1/(2n-2)} \qquad (2\text{-}134)$$

Note that Equation 2-133 always underestimates the true value of z_R whereas Equation 2-134 always overestimates it. To compute the true value, we numerically calculate the value of the integral (using Equation 2-128) to the low estimate and to the high estimate of z_R, and compare these quantities to the known value of the integral. We interpolate logarithmically between the low and high estimates to obtain a new estimate of z_R, and numerically calculate the integral to this value. If that integral exceeds the known integral to the true value, we replace the high estimate of z_R by the new estimate and repeat the process. Otherwise if the integral is smaller than the known integral, we replace the low estimate of z_R by the new estimate and repeat the process. In practice, 2 to 4 iterations are usually sufficient to calculate z_R to within 1 percent accuracy.

The final quantities to be calculated by the module RFPROP are the means and standard deviations of a set of eight parameters which are proportional to the mean and standard deviation of the TEC and its time derivatives. The variance of the j^{th} order time derivative of the TEC is obtained from the expression

$$\sigma_{N_j}^2 = \frac{2}{\pi} \left(\frac{f_c}{cr_e}\right)^2 a^{-m} \int_0^{f_R} P_\phi(f)\ (2\pi f)^{2j}\ df \qquad (2\text{-}135)$$

where $P_\phi(f)$ and a are defined in Equations 2-129 and 2-130, and f_c is the carrier frequency [Hz] (see Equation A-21b of DNA-5662D[8]). Equation 2-135 can be expressed more conveniently as

$$\sigma^2_{N_j} = \frac{1}{\pi} \left(\frac{f_c}{cr_e}\right)^2 a^{-m} \left(\frac{a}{\tau_0}\right)^{2j} f_{n,j}(z_R) \tag{2-136}$$

where

$$f_{n,j}(z_R) = \int_0^{z_R} dz\ z^{2j}\ (1+z^2)^{-(n-1/2)} \tag{2-137}$$

The zeroth order derivative may be evaluated analytically for all values of n, i.e.,

$$\sigma^2_{N_0} = \frac{1}{\pi} \left(\frac{f_c}{cr_e}\right)^2 a^{-m} \left[1-\sigma_R^2/\sigma_\phi^2\right] \tag{2-138}$$

Analytic solutions for the higher order derivatives exist only for n = 2

$$f_{2,1}(z_R) = \log\left(z_R + \sqrt{1+z_R^2}\right) - (1+z_R^{-2})^{-1/2} \tag{2-139}$$

$$f_{2,2}(z_R) = \frac{1}{2}\left[z_R^2(1+z_R^{-2})^{-1/2} - 3f_{2,1}(z_R)\right] \tag{2-140}$$

$$f_{2,3}(z_R) = \frac{1}{8}\left[z_R^4(2-5z_R^{-2})(1+z_R^{-2})^{-1/2} + 15f_{2,1}(z_R)\right] \tag{2-141}$$

For the limiting solutions when n = 2

$$\lim_{z_R \to 0},\ f_{2,j}(z_R) = \frac{1}{(2j+1)}\, z_R^{2j+1} \quad j = 1, 2, \ldots \tag{2-142}$$

and

$$\lim_{z_R \to \infty} f_{2,j(z_R)} = \begin{cases} \log(2z_R)-1 & j = 1 \\ \frac{1}{(2j-1)} z_R^{2j-1} & j \neq 1 \end{cases} \quad (2\text{-}143)$$

For $n \neq 2$, no analytic solutions exist for the integral Equation 2-137. PRPSIM resorts to Simpson's rule to solve the integral numerically.

The mean and standard deviataion of the eight additional signal parameters are derived from the mean and standard deviation of the TEC and its time derivatives as listed below:

Mean signal phase shift and its standard deviation:

$$\langle \text{phase shift} \rangle = A\langle \text{TEC} \rangle \quad [\text{rad}] \quad (2\text{-}144)$$

$$\sigma(\text{phase shift}) = A\,\sigma_{N_0} \quad [\text{rad}] \quad (2\text{-}145)$$

Mean Doppler shift and its standard deviation:

$$\langle \text{Doppler shift} \rangle = \left(\frac{A}{2\pi}\right) \frac{d}{dt} \langle \text{TEC} \rangle \quad [\text{Hz}] \quad (2\text{-}146)$$

$$\sigma(\text{Dopler shift}) = \left(\frac{A}{2\pi}\right) \sigma_{N1} \quad [\text{Hz}] \quad (2\text{-}147)$$

Mean Doppler rate and its standard deviation:

$$\langle \text{Doppler rate} \rangle = \left(\frac{A}{2\pi}\right) \frac{d^2}{dt^2} \langle \text{TEC} \rangle \quad [\text{Hz sec}^{-1}] \quad (2\text{-}148)$$

$$\sigma(\text{Doppler rate}) = \left(\frac{A}{2\pi}\right) \sigma_{N2} \quad [\text{Hz sec}^{-1}] \quad (2\text{-}149)$$

Mean phase "jerk" and its standard deviation:

$$\langle \text{phase jerk} \rangle = \left(\frac{A}{2\pi}\right) \frac{d^3}{dt^3} \langle \text{TEC} \rangle \qquad [\text{Hz sec}^{-2}] \qquad (2\text{-}150)$$

$$\sigma(\text{phase jerk}) = \left(\frac{A}{2\pi}\right) \sigma_{N3} \qquad [\text{Hz sec}^{-2}] \qquad (2\text{-}151)$$

Mean signal time delay and its standard deviation:

$$\langle \text{time delay} \rangle = B \langle \text{TEC} \rangle \qquad [\mu\text{sec}] \qquad (2\text{-}152)$$

$$\sigma(\text{time delay}) = B \sigma_{N0} \qquad [\mu\text{sec}] \qquad (2\text{-}153)$$

Mean time delay rate and its standard deviation:

$$\langle \text{time delay rate} \rangle = B \frac{d}{dt} \langle \text{TEC} \rangle \qquad [\mu\text{sec sec}^{-1}] \qquad (2\text{-}154)$$

$$\sigma(\text{time delay rate}) = B \sigma_{N1} \qquad [\mu\text{sec sec}^{-1}] \qquad (2\text{-}155)$$

Mean time delay acceleration and its standard deviation:

$$\langle \text{time delay acceleration} \rangle = B \frac{d^2}{dt^2} \langle \text{TEC} \rangle \qquad [\mu\text{sec sec}^{-2}] \qquad (2\text{-}156)$$

$$\sigma(\text{time delay acceleration}) = B \sigma_{N2} \qquad [\mu\text{sec sec}^{-2}] \qquad (2\text{-}157)$$

Mean time delay "jerk" and its standard deviation:

$$\langle \text{time delay jerk} \rangle = B \frac{d^3}{dt^3} \langle \text{TEC} \rangle \qquad [\mu\text{sec sec}^{-3}] \qquad (2\text{-}158)$$

$$\sigma(\text{time delay jerk}) = B \sigma_{N3} \qquad [\mu\text{sec sec}^{-3}] \qquad (2\text{-}159)$$

with

$$A = r_e \lambda \qquad [cm^2] \qquad (2\text{-}160)$$

$$B = 1 \times 10^6 \frac{c r_e}{2\pi f_c^2} \qquad [cm^2\ \mu sec] \qquad (2\text{-}161)$$

where c is the speed of light, r_e is the classical radius of the electron, f_c is the carrier frequency [Hz], and λ is the wavelength [cm]. This point marks the end of the loop in frequency in which the signal parameters are calculated.

Two additional subroutines (RFTEMP and REFRAC) are called by RFPROP to calculate the effective temperature of the receiving antenna due to nuclear enhanced sky temperature and to calculate the bending of the ray path by smooth gradient or "gross" refraction. These subroutines will be described in Sections 2.4 and 2.5 respectively.

Table 3 summarizes the major parameters calculated by RFPROP and indexes the numbers of the equations (in Section 2-2) pertinent to their calculation.

Table 3. **Summary of equation numbers for major parameters calculated by RFPROP.**

PARAMETERS	UNITS	EQUATION(s)
decorrelation distance	[cm]	106 105
decorrelation time	[sec]	113 111 109 55
Faraday rotation angle	[rad]	96
frequency selective bandwidth	[Hz]	126 78
mean square log amplitude fluctuation (MSLAF)		116 45 44 43
mean signal phase shift	[rad]	144
mean signal time delay	[μsec]	152
mean square angle of energy arrival	[rad^2]	108 107
mean weighted distance	[cm]	114 97
Rayleigh phase variance	[rad^2]	122 121 120
Rayleigh frequency	[Hz]	128
S_4 scintillation index		125
total absorption	[dB]	93 90
total electron content (TEC) and time derivatives	[cm^{-2} sec^{-j}]	94 23 22 19
total electron standard deviations and time derivatives	[cm^{-2} sec^{-j}]	136
total phase variance	[rad^2]	40 38

2.3 ANTENNA FILTERING.

The subroutine ANTMOD is called by PRPSIM to calculate the modification of the signal parameters resulting from the loss of signal power caused by angular scattering at the receiving and transmitting antennas. The equations used in ANTMOD are taken from those derived by Dana (1985).[9] The derivations assume that both antennas are characterized by Gaussian beam profiles and that both antennas are pointed along the line of sight. Four arrays of beamwidths are passed to ANTMOD by RFPROP. At each propagation frequency, each antenna is characterized by two beamwidths along two orthogonal axes perpendicular to the axis of the antenna. The beamwidth is defined as the angle [rad] subtended by the half power (3 dB) points on the directive gain function on opposite sides of the antenna axis. Currently, only circularly symmetric antennas are allowed by RFPROP, and the beamwidths in the two orthogonal directions are equal. Here we denote the beamwidths of the transmitting and receiving antennas along the X and Y-axes, respectively, as θ_{Tx}, θ_{Ty}, θ_{Rx}, and θ_{Ry}. The signal loss caused by scattering is given by

$$\alpha_s = 10 \log_{10}(\Delta x) + 10 \log_{10}(\Delta y) \qquad [dB] \qquad (2\text{-}162)$$

where

$$(\Delta x)^2 = 1 + k' \left(\frac{\sigma_{Tx}^2}{\theta_{Tx}^2} + \frac{\sigma_{Rx}^2}{\theta_{Rx}^2} \right) \qquad (2\text{-}163)$$

$$(\Delta y)^2 = 1 + k' \left(\frac{\sigma_{Ty}^2}{\theta_{Ty}^2} + \frac{\sigma_{Ry}^2}{\theta_{Ry}^2} \right) \qquad (2\text{-}164)$$

where σ_{Tx}^2 and σ_{Ty}^2 are the mean square angles of energy arrival in the x and y directions at the transmitter, σ_{Rx}^2 and σ_{Ry}^2 are the analogous quantities at the receiver, and k' is the constant $8\ln(2) = 5.545$. For a circular antenna we can replace the mean square angles in the x and y

directions by the minimum and maximum values in the p and q directions calculated in Equations 2-107 and 2-108. A beamwidth of π (180°) or greater is interpreted by ANTMOD as an omni-directional antenna with zero scattering loss ($(\Delta x)^2 = (\Delta y)^2 = 1$). ANTMOD also computes the total signal loss which is simply the sum of the absorption and the scattering loss. The apparant frequency selective bandwidth and decorrelation time are increased by scattering:

$$f_{ant} = \Lambda x \Lambda y \, f_0 \qquad [Hz] \qquad (2\text{-}165)$$

$$\tau_{ant} = \sqrt{\Lambda x \Lambda y} \, \tau_0 \qquad [sec] \qquad (2\text{-}166)$$

where f_0 and τ_0 are the antenna independent values calculated by Equations 2-126 and 2-113, respectively. Note that the degree of antenna filtering is frequency dependent.

2.4 ANTENNA NOISE TEMPERATURE.

PRPSIM calculates the effective antenna noise temperature of the receiving antenna due to a hot, ionized medium. The calculation includes only the contribution of the medium. All other sources (solar, cosmic, the earth, etc.) are not considered here. In theory the temperature must be integrated over every point in the grid weighted by the antenna gain function in the direction of the point. Such an analysis is beyond the scope of a propagation code whose primary purpose is the calculation of scintillation effects. We compromise by calculating the temperature with the "beam-filling" approximation formula at five points on the gain function, and computing the mean and standard deviation of these five values. One direction is along the line of sight (LOS) directed from the receiver to the transmitter. The other four directions are displaced one-half beamwidth from the LOS along two orthogonal directions perpendicular to the LOS. As before, the beamwidth of the antenna is defined to be the angle subtended by the half power (3 dB) points on the directive gain

function on opposite sides of the antenna axis. Currently, we assume that the antenna gain function is circularly symmetric and that the antenna axis is oriented along the LOS. RFPROP may easily be generalized to accomodate non-circular antennas, however. A warning flag is printed if the mean does not exceed the standard deviation by a factor of two or greater. The flag is intended to indicate that the variation of the temperature across the antenna gain function may be so large that the small number of points used may yield an inaccurate result. Although the absence of a flag indicates a reliable temperature calculation, a flag does not necessarily indicate that the resu't is inaccurate. Even when the result is flagged, the mean is a much better estimate of the true antenna temperature than the single beam-filled approximation calculated along the LOS only.

The antenna temperature calculation is performed by a submodule of RFPROP called RFTEMP. RFTEMP is called once by RFPROP for each link simulation. The arguments passed are the vectors containing the coordinates of the transmitter (path origin) and the receiver (path end), the number of RF carrier frequencies, the array containing those frequencies, the array containing the effective beamwidths along the X-axis at those frequencies, the array of beamwidths along the Y-axis (currently these equal those along the X-axis), and two integers which specify the sequential indices of the first and last point (relative to the transmitter) whose mean local electron density or standard deviation exceeds an arbitrary threshold. (Currently the threshold is 1 cm^{-3} for both parameters.)

The antenna temperature calculation can be the most time consuming of all PRPSIM calculations, and for that reason it is optional. Data retrieval, rather than the complexity of the calculations, constitutes the major demand for CPU time . Each of the five paths requires approximately the same number of data retrievals required for all

the computuations performed by RFPROP. Furthermore, because the antenna gain function and beamwidth are functions of frequency, a set of four different auxiliary paths must be defined for each operating frequency. If n operating frequencies are specified for a link, it is easy to show that the number of data retrievals will increase by a factor of 4n+2 if antenna temperature is calculated. (In theory, this ratio could be reduced to 4n+1 if the temperature along the central path were to be calculated by RFPROP. Owing to the directional asymmetry of the calculation of temperature and several of the other parameters, it is simpler for numerical reasons to calculate the temperature along the central path in RFTEMP.) We do reduce the CPU time somewhat by eliminating the construction of the auxiliary paths for situations in which it is easily demonstrated that the antenna beamwidth is filled by a homogeneous ionized region.

RFTEMP calls PATHPT to generate a set of points along the propagation path from "infinity" (at a point on the path located well outside the phenomenology grid) to the receiver. The indices (relative to the receiver) of the first and last point whose mean density exceeds the 1 cm^{-3} threshold are also computed. The code then begins to loop over those points along the path whose indices lie between the threshold indices to calculate the incremental contribution to the total antenna temperature from the plasma in that region. The submodule DATAPT (described in Section 3.4) is called to retrieve the set of interpolated environmental data for each point. The data set returned is truncated to only those data needed for the temperature calculation: (1) the mean electron density [cm^{-3}], (2) the electron density standard deviation [cm^{-3}], (3) the rms electron density [cm^{-3}], (4) the electron temperature [°K], (5) the electron-neutral collision frequency [sec^{-1}], and (6) the array of electron-ion collision frequencies [sec^{-1}]. (See Table 4 of Section 3.4.)

If we designate the local ion temperature of a plasma layer of thickness Δz_i as t_i, it can be shown that the temperature of the receiving antenna is

$$dT_i = t_i \{1 - \exp(-2K\nu_i \Delta z_i)\} Lp_i \qquad (2\text{-}167)$$

or

$$dT_i = t_i \{1 - 10^{-(\alpha_i \Delta z_i/10)}\} Lp_i \qquad (2\text{-}168)$$

if the layer is of uniform temperature and completely subtends the beamwidth of the antenna. (See Equation 27 of MRC-R-156, Volume II[7].) Lp_i is the loss caused by the absorption of the intervening material between the region and the receiver:

$$Lp_i = \exp\left\{-2 \sum_{j}^{i} K\nu_j \Delta z_j\right\} \qquad (2\text{-}169)$$

or

$$Lp_i = 10^{-\left(\sum_{j}^{i} \alpha_j \Delta z_j/10\right)} \qquad (2\text{-}170)$$

where $K\nu_j$ is the linear coefficient of absorption [cm^{-1}], and α is the coefficient of absorption which was derived in Equation 2-93 of Section 2.2. $K\nu$ and α are related by

$$\alpha = \frac{20}{\ln(10)} K\nu \qquad [dB\ cm^{-1}] \qquad (2\text{-}171)$$

The factor of two enters the exponential arguments because temperature is a measure of power whereas the coefficient of absorption is defined in terms of amplitude attenuation as a function of distance. Note that $K\nu$ is a function of both frequency and location. Thus, it is necessary to calculate the temperature increment for each carrier frequency and at each point along the path. The temperature of the receiver antenna (as

a function of frequency) is calculated by summing over all points along the path

$$T_{ant} = \sum_{i}^{N} dT_i = \sum_{i}^{N} t_i \left\{1-10^{-(\alpha_i \Delta z_i/10)}\right\} 10^{-\left(\sum_{j}^{i} \alpha_j \Delta z_j/10\right)} \quad [°K] \quad (2\text{-}172)$$

Note that Equation 2-172 depends on the order of summation. Because we want the temperature at the receiver, we must sum from the receiver (i=1) toward "infinity" (i=N). We also calculate the mean distance to the region weighted by the incremental temperature:

$$\langle z \rangle_T = \sum_{i}^{N} z_i \, dT_i / \sum_{i}^{N} dT_i \quad [cm] \quad (2\text{-}173)$$

Equation 2-172 is correct only if the medium is uniform over the beamwidth of the antenna. To test whether this is the case, we assume that the SCENARIO grid resolution is sufficiently good to assure that the properties of the medium are reasonably constant across a grid cell; and if we can show that the grid spacing at the most highly ionized region along the LOS is greater than the arc subtended by the beamwidth at that distance, then the beam-filling approximation may be used in lieu of integration over the gain function. First, using a simple search algorithm and the array of grid coordinates read and stored from the SCENARIO data file, we calculate the indices of the cell containing the point at the temperature weighted distance to the region computed in Equation 2-173. The dimensions of the cell along the three orthogonal coordinate axes are computed as

$$dx_i = h_i \, du_i \quad [cm] \quad (2\text{-}174)$$

where du_i are the differences between curvilinear coordinates read from the SCENARIO file, and h_i are the scale factors as calculated from Equations 3-40, 3-41, and 3-42 of Section 3.4. The angle subtended by the smallest of these dimensions at the temperature weighted distance to the cell is

$$\varepsilon = 2 \arctan \left[\frac{\min(dx_1, dx_2, dx_3)}{2\langle z \rangle_T} \right] \qquad (2\text{-}175)$$

If this angle is greater than the beamwidth of the antenna, the ionized medium is considered homogeneous throughout the beamwidth of the antenna so that the beam-filling approximation is valid. In that case we do not construct the four auxiliary paths as outlined below, and the antenna temperature is equated to the value obtained with Equation 2-172. The standard deviation of the temperature across the antenna face is set at zero.

RFTEMP then loops through the set of carrier frequencies. If ε does not exceed the antenna beamwidth for a given frequency, we proceed to construct a set of four auxiliary paths for that frequency. The paths are directed toward the half-power contour of the gain function and spaced at ninety degree increments in azimuth about the LOS (which is assumed to be coincident with the antenna normal). Define the path elevations and azimuths relative to the LOS:

$$\delta_i = \begin{cases} \pi/2 - \frac{1}{2}\,\text{beamwidth}_x & i = 1 \text{ or } 3 \\ \pi/2 - \frac{1}{2}\,\text{beamwidth}_y & i = 2 \text{ or } 4 \end{cases} \qquad (2\text{-}176)$$

and

$$\phi_i = 0,\ \pi/2,\ \pi,\ 3\pi/2 \qquad \text{for } i = 1,2,3,4 \tag{2-177}$$

(Note that the elevations of the auxiliary paths relative to the LOS are frequency dependent.) The end of each auxiliary path is located at "infinity" (i.e., outside the grid). All computations are done in the tangent plane (east, north, vertical) system of the antenna. To transform the coordinates of the four auxiliary paths from antenna coordinates to tangent plane coordinates: (1) rotate the system counterclockwise about the W-axis (normal to the antenna face) through the angle ψ to align the V-axis in the horizontal plane, (2) rotate counterclockwise about the V-axis through the angle $\pi/2-\varepsilon$ to align the W-axis with the Z-axis (vertical) and (3) rotate counterclockwise about the Z-axis through the angle $\pi/2+\lambda$ to align the U-axis with the X-axis (east) and the V-axis with the Y-axis (north). (See Figure 3.) Currently, only circular antennas are allowed by RFPROP, and ψ is undefined; for non-circular antennas, the U-axis would normally be defined to lie along the major axis of the gain function, and ψ would be defined as the angle (measured clockwise) from the horizontal to the V-axis.

RFTEMP tests to determine whether any of the auxiliary paths intersects the earth. If a path does intersect the earth, its length is redefined to be the distance from the receiver to the (nearest) intersection point. For each of the four auxiliary paths, let

$$b = \frac{1}{2}\left[z_0 + (r^2 - r_x^2)/z_0\right] \tag{2-178}$$

and

$$c = r^2 - r_e^2 \tag{2-179}$$

where z_0 is the original length of the auxiliary path, r is the radial distance to the receiver from the center of the earth, r_x is the radial

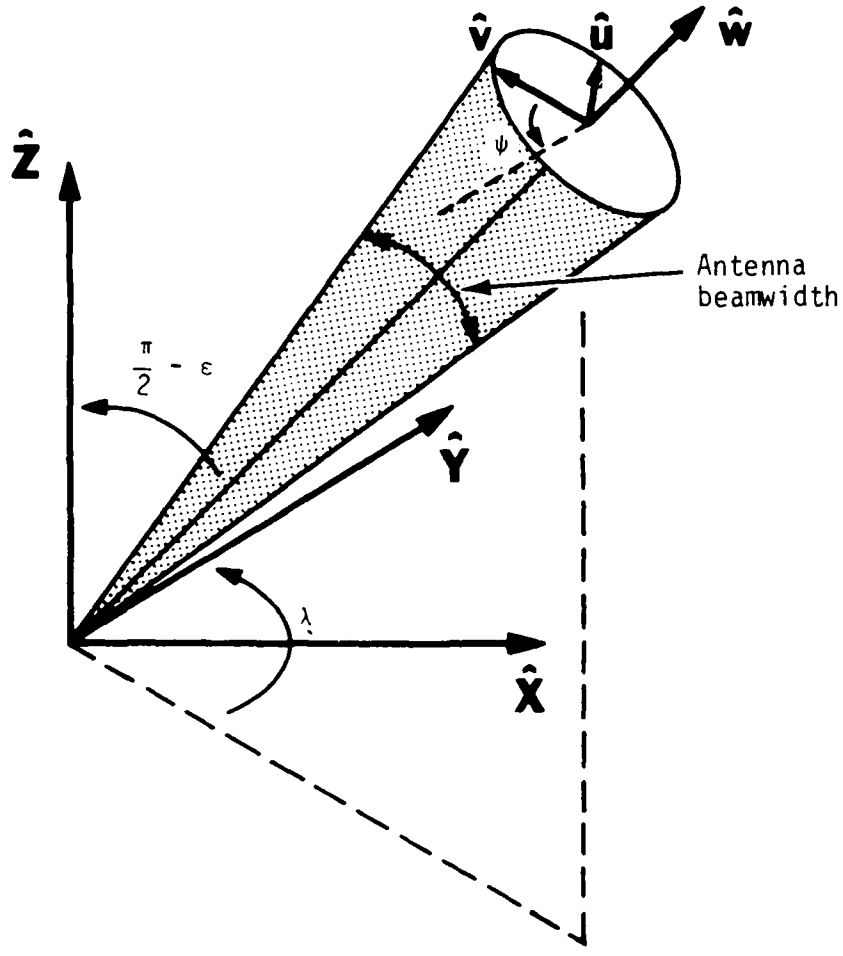

Figure 3. Geometric transformation from line of sight (LOS) coordinates to antenna tangent plane (east, north, vertical) coordinates.

distance to the transmitter, and r_e is the radius of the earth. If $b < 0$ or if $c > b^2$, the path does not intersect the earth, and we proceed to calculate the temperature by integrating along the entire length of the path. Otherwise, calculate the distance

$$x = b - \sqrt{b^2 - c} \qquad (2\text{-}180)$$

If $x < z_0$, the path intersects the earth, and we redefine the integration path length to be x.

PATHPT (see Section 3.3) is then called to generate a set of grid intersection points for the auxiliary path. The incremental temperature is calculated and summed along the auxiliary path in exactly the same manner as along the LOS except that there in no inner loop in frequency for the path point. Frequency is the outermost loop for the auxiliary paths rather than the innermost. The mean antenna temperature and the standard deviation are calculated by using the (frequency dependent) temperature integrated along the LOS and the four auxiliary paths:

$$\langle T \rangle = \sum_{i=0}^{4} W_i T_i / \sum_{i=0}^{4} W_i \qquad [^\circ K] \qquad (2\text{-}181)$$

$$\sigma_T = \left[\sum_{i=0}^{4} W_i T_i^2 / \sum_{i=0}^{4} W_i - \langle T \rangle^2 \right]^{1/2} \qquad [^\circ K] \qquad (2\text{-}182)$$

where T_0 is the temperature calculated along the LOS for that frequency, T_1 through T_4 are the temperatures calculated along the auxiliary paths and W_i are the weighting parameters. The gain function along the auxiliary paths is half that along the LOS, implying that we might choose $W_0 = 1$ and $W_i = 0.5$ for i=1 to 4. The contribution of each of the auxiliary paths to the total solid angle is somewhat greater than that of

the LOS, however, so that the W_i should be somewhat larger than 0.5 (but smaller than 1). Here, we have conservatively set all the weighting parameters to 1, even though this choice probably biases the estimate of the standard deviation toward values somwhat greater than its real value.

2.5 REFRACTION.

PRPSIM calculates the refractive effects on an RF signal propagating in an inhomogeneous ionized medium whose properties are known only at specified points. The primary objective is to provide reasonably accurate calculations of refraction, multipath, focusing and defocusing, phase shifts, and group delay in the disturbed environment modelled by SCENARIO. The refractive effects considered here are those effects caused by large-scale ionization structure in the propagation medium - often referred to as "gross" or "smooth gradient" refractive effects. That is, the index of refraction is a sufficiently slowly-varying function in space so that geometrical optics or "ray theory" is applicable; and furthermore, the index of refraction is a reasonably smooth and well-behaved function in the regions through which most of the received signal energy propagates. The approximation of geometrical optics imposes no significant constraint because, when the refractive index is well-behaved, this approximation requires that the properties of the medium change very little over dimensions comparable to a wavelength. At frequencies in the UHF band and higher, this requirement is easily satisfied whenever signals can propagate at all. Section 2.2 treats the effects of random inhomogeneities in the index of refraction due to relatively small-scale ionization structure encountered in the striated plasma.

2.5.1 Primary Angle Bending and Multipath.

The technique used here (implemented in routine REFRAC and its associated subroutines) to compute refractive effects on RF signal propagation is one derived in Reference 10. The technique, referred to as the

multiscreen method, is more soundly based in propagation theory than the simpler refraction computational methods used in system analysis codes, and it is much more efficient than ray-tracing techniques.

The multiscreen method is a stationary phase approach in which the phase shifts caused by the propagation medium are represented by a series of phase screens along the propagation path. Each phase screen is constructed by means of a Taylor series expansion about the line of sight (LOS) at each point at which environmental data are available. The geometry of the primary propagation path is estimated by applying Fermat's principle to a simplified equation for the phase path length through the multiple phase screens. The simplification is such that the condition for stationary phase requires the solution of 2n simultaneous linear equations, where n is the number of phase screens. The set of 2n equations is a five-diagonal system that is easily solved by a modification of the Crout reduction technique. The resulting path geometry is considered a 1st order approximation to the actual path geometry. A parameter that describes the perturbation of the actual path geometry from the representative geometry is then introduced. A more complete equation for the phase path length of the perturbed path through the multiple phase screen is formulated using higher-order terms in the series expansions. The final solution for the stationary paths involves a cubic equation in terms of the perturbation parameter, which yields up to three possible propagation paths.

The phase path length of a ray path is given by the following integral

$$\vartheta = -\frac{\omega}{c}\int_0^R \mu dr \qquad \text{[rad]} \qquad (2\text{-}183)$$

where ω is the angular signal frequency in rad sec^{-1}, c is the speed of light (2.998E+10 cm sec^{-1}), and μ has the following form:

$$\mu \approx \left(1 - \frac{\omega_p^2}{\omega^2}\right)^{1/2} \qquad (2\text{-}184)$$

where ω_p is the angular plasma frequency in rad sec^{-1}. Fermat's principle states that the paths along which the signal propagates are paths of stationary phase - that is, paths for which the phase is constant for small perturbations of the path geometry. The path geometry is the unknown to be determined. Hence, one first assumes some kind of reasonable geometry as a function of one or more independent parameters, and then solves for the parameter values that satisfy the condition of stationary phase.

In setting up the path geometry, we note that the information about the propagation medium consists of the mean electron density and its spatial derivatives (described in detail in section 3.4) at a sequence of points along the LOS path (described in detail in section 3.3) to the receiver. In effect, we have information on n phase screens along the path, as illustrated in figure 4. The points r_1, r_2, ..., r_n are calculation points along the LOS to the receiver located at r_{RCVR}. The electron density and its transverse spatial derivatives up to some reasonable order are known at each point. A possible refracted path is then postulated. The refracted path intersects the planes normal to the LOS at x_i, y_i, i = 1, 2, ..., n. The x-axis lies in the "vertical" plane and the y-axis lies in the plane normal to the "vertical" plane (traverse plane). (Note that the x and y axes here are the same as the U and V axes defined in section 2.2.1.)

With this geometry the phase can be evaluated from equations (2-183) and (2-184). Under the condition that $\omega^2 >> \omega_p^2$, which is well satisfied whenever absorption is not catastrophically large at the frequencies of interest, and assuming small refractive bending angles, the total phase shift along the refracted path is given by:

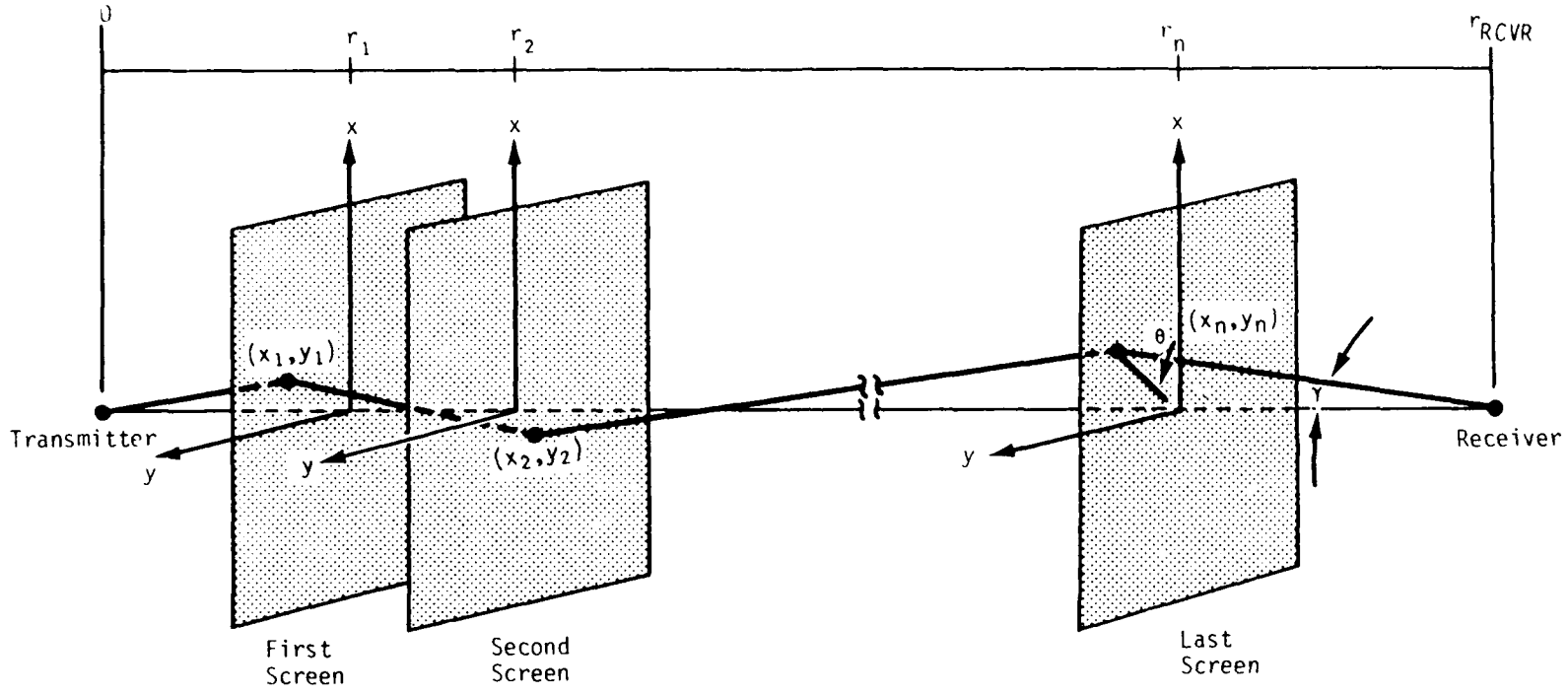

Figure 4. Multiple phase screen refraction geometry.

$$\Phi = -\frac{\omega}{c}\sum_{i=0}^{n}\left\{\Delta r_i + \frac{(x_{i+1}-x_i)^2}{2\Delta r_i} + \frac{(y_{i+1}-y_i)^2}{2\Delta r_i}\right.$$

$$\left. - \frac{\Delta r_i}{4N_c}\left[n_e(x_i, y_i, r_i) + n_e(x_{i+1}, y_{i+1}, r_{i+1})\right]\right\} \qquad (2\text{-}185)$$

where $\Delta r_i = r_{i+1} - r_i$, and N_c is the critical value of the electron density (for which ω_p^2 would be equal to ω^2):

$$N_c = \left(\frac{\omega^2}{\omega_p^2}\right) n_e = \frac{\pi}{r_e \lambda^2}$$

$$= 1.24 \times 10^4 \, f^2 \qquad [cm^{-3}] \qquad (2\text{-}186)$$

with the wave frequency f given in Hertz.

The displacements x_i, y_i are independent parameters that determine the geometry of the refracted path. Consequently the stationary phase paths that actually propagate are found by solving the following set of 2n simultaneous equations:

$$\frac{\partial \Phi}{\partial x_i} = 0 \quad , \quad i = 1, 2, \ldots, n$$

$$\frac{\partial \Phi}{\partial y_i} = 0 \quad , \quad i = 1, 2, \ldots, n \qquad (2\text{-}187)$$

Because the propagation paths must connect the transmitter and receiver, we have the following boundary conditions:

$$r_0 = 0$$

$$x_0 = y_0 = 0$$

$$r_{n+1} = r_{RCVR}$$

$$x_{n+1} = y_{n+1} = 0 \qquad (2\text{-}188)$$

The electron density at the intersection of the refracted path with each screen can be evaluated by means of a Taylor series expansion. To linearize the set of 2n simultaneous equations, only terms through second order are retained in the expansion at this stage. (A method of incorporating the effects of higher-order terms is introduced shortly.) Thus the system of 2n equations to be solved is:

$$\frac{x_i - x_{i-1}}{r_i - r_{i-1}} - \frac{x_{i+1} - x_i}{r_{i+1} - r_i} - \frac{r_{i+1} - r_{i-1}}{4N_c}\left(\frac{\partial n_{ei}}{\partial x} + \frac{\partial^2 n_{ei}}{\partial x^2} x_i + \frac{\partial^2 n_{ei}}{\partial x \partial y} y_i\right) = 0$$

$$\frac{y_i - y_{i-1}}{r_i - r_{i-1}} - \frac{y_{i+1} - y_i}{r_{i+1} - r_i} - \frac{r_{i+1} - r_{i-1}}{4N_c}\left(\frac{\partial n_{ei}}{\partial y} + \frac{\partial^2 n_{ei}}{\partial y^2} y_i + \frac{\partial^2 n_{ei}}{\partial x \partial y} x_i\right) = 0 \qquad (2\text{-}189)$$

where the subscript i denotes values calculated at the point r_i on the LOS.

If these 2n equations and the unknowns are arranged in the orders $x_1, y_1, x_2, y_2, \ldots, x_n, y_n$, the coefficient matrix has a five-diagonal form. This five-diagonal system can be readily solved using the Crout reduction method (see, for example, reference 11). The system of equations can be written as:

$$
\begin{aligned}
d_1x_1+h_1y_1+f_1x_2 &= c_1\\
g_2x_1+d_2y_1+h_2x_2+f_2y_2 &= c_2\\
e_3x_1+g_3y_1+d_3x_2+h_3y_2+f_3x_3 &= c_3\\
e_4y_1+g_4x_2+d_4y_2+h_4x_3+f_4y_3 &= c_4\\
e_5x_2+g_5y_2+d_5x_3+h_5y_3+f_5x_4 &= c_5\\
\cdots & \cdots\\
e_{2n-1}x_{n-1} + g_{2n-1}y_{n-1} + d_{2n-1}x_n + h_{2n-1}y_n &= c_{2n-1}\\
e_{2n}y_{n-1}+g_{2n}x_n+d_{2n}y_n &= c_{2n} \qquad (2\text{-}190)
\end{aligned}
$$

From Equations 2-189, the elements of the augmented matrix of the system are given by:

$$d_{2i-1} = (r_{i+1}-r_{i-1}) \left[\frac{1}{(r_i-r_{i-1})(r_{i+1}-r_i)} - \frac{1}{4N_c}\frac{\partial^2 n_{ei}}{\partial x^2}\right], \quad i = 1,2,\ldots,n$$

$$d_{2i} = (r_{i+1}-r_{i-1}) \left[\frac{1}{(r_i-r_{i-1})(r_{i+1}-r_i)} - \frac{1}{4N_c}\frac{\partial^2 n_{ei}}{\partial y^2}\right], \quad i = 1,2,\ldots,n$$

$$h_{2i-1} = -\frac{r_{i+1} - r_{i-1}}{4N_c}\frac{\partial^2 n_{ei}}{\partial x \partial y}, \quad i = 1,2,\ldots,n$$

$$h_{2i} = 0, \quad i = 1,2,\ldots,n$$

$$f_{2i-1} = f_{2i} = -\frac{1}{r_{i+1} - r_i}, \quad i = 1,2,\ldots,n-1$$

$$f_{2n-1} = f_{2n} = 0$$

$$e_1 = e_2 = 0$$

$$e_{2i-1} = e_{2i} = f_{2i-3} \quad , \; i = 2,3,\ldots,n$$

$$q_{2i-1} = 0 \quad , \; i = 1,2,\ldots,n$$

$$q_{2i} = q_{2i-1} \quad , \; i = 1,2,\ldots,n$$

$$c_{2i-1} = \frac{r_{i+1} - r_{i-1}}{4N_c} \frac{\partial n_{ei}}{\partial x} \quad , \; i = 1,2,\ldots,n$$

$$c_{2i} = \frac{r_{i+1} - r_{i-1}}{4N_c} \frac{\partial n_{ei}}{\partial y} \quad , \; i = 1,2,\ldots,n$$

It can be readily verified that the Crout reduction preserves the five-diagonal property, and that the elements of the auxiliary matrix are given by the simplified forms:

$$d_1' = d_1 \; , \; h_1' = \frac{h_1}{d_1'} \; , \; c_1' = \frac{c_1}{d_1'}$$

$$q_2' = q_2 \; , \; d_2' = d_2 - q_2' h_1' \; , \; c_2' = \frac{c_2 - q_2' c_1'}{d_2'}$$

$$e_k' = e_k \quad , \; k = 3,4,\ldots,2n$$

$$q_k' = q_k - e_k' h_{k-2}' \quad , \; k = 3,4,\ldots,2n$$

$$d_k' = d_k - e_k' f_{k-2}' - q_k' h_{k-1}' \quad , \; k = 3,4,\ldots,2n$$

$$f_k' = \frac{f_k}{d_k'} \quad , \; k = 1,2,\ldots,2n-2$$

$$h_k' = \frac{h_k - q_k' f_{k-1}'}{d_k'} \quad , \; k = 2,3,\ldots,2n-1$$

$$c'_k = \frac{c_k - e'_k c'_{k-2} - q'_k c'_{k-1}}{d'_k} \qquad , \; k = 3,4,\ldots,2n$$

The solutions for x_i, y_i are then determined in reverse order using the following equations:

$$y_n = c'_{2n}$$

$$x_n = c'_{2n-1} - h'_{2n-1} y_n$$

$$y_i = c'_{2i} - h'_{2i} x_{i+1} - f'_{2i} y_{i+1} \qquad , \; i = n-1,n-2,\ldots,1$$

$$x_i = c'_{2i-1} - h'_{2i-1} y_i - f'_{2i-1} x_{i+1} \qquad , \; i = n-1,n-2,\ldots,1$$

(2-191)

Within the limits of the small-angle approximations and the neglect of higher-order derivatives in the Taylor series expansions, these solutions for x_i and y_i provide an essentially exact solution for the propagation path when an adequate number of calculation points are used.

The simplest method of incorporating the effects of higher-order spatial derivatives in the Taylor series expansions is to assume that the solution just obtained is typical of the propagation path geometry, and that the actual path (or paths) can be represented by a perturbation of this geometry. In this case we consider the actual propagation path to intersect each phase screen at the point $(\delta x_i, \delta y_i)$, where x_i and y_i are the values just obtained from Equations 2-191, and δ is a parameter whose value is to be determined. Since only a single unknown parameter is now involved, terms in the Taylor series expansions through fourth order can be retained, which yields a single cubic equation in δ to solve for the stationary phase paths:

$$s_0 + s_1\delta + s_2\delta^2 + s_3\delta^3 = 0 \tag{2-192}$$

where

$$s_0 = -\frac{1}{4N_c}\sum_{i=1}^{n}(r_{i+1}-r_{i-1})\left(\frac{\partial n_{ei}}{\partial x}x_i + \frac{\partial n_{ei}}{\partial y}y_i\right) \tag{2-193}$$

$$s_1 = \sum_{i=0}^{n}\left[\frac{(x_{i+1}-x_i)^2 + (y_{i+1}-y_i)^2}{r_{i+1} - r_i}\right] - \frac{1}{4N_c}\sum_{i=1}^{n}(r_{i+1}-r_{i-1})\left(\frac{\partial^2 n_{ei}}{\partial x^2}x_i^2 + 2\frac{\partial^2 n_{ei}}{\partial x\partial y}x_iy_i + \frac{\partial^2 n_{ei}}{\partial y^2}y_i^2\right) \tag{2-194}$$

$$s_2 = -\frac{1}{4N_c}\sum_{i=1}^{n}\left(\frac{r_{i+1}-r_{i-1}}{2}\right)\left(\frac{\partial^3 n_{ei}}{\partial x^3}x_i^3 + 3\frac{\partial^3 n_{ei}}{\partial x^2\partial y}x_i^2y_i + 3\frac{\partial^3 n_{ei}}{\partial x\partial^2 y}x_iy_i^2 + \frac{\partial^3 n_{ei}}{\partial y^3}y_i^3\right) \tag{2-195}$$

$$s_3 = -\frac{1}{4N_c}\sum_{i=1}^{n}\frac{(r_{i+1}-r_{i-1})}{6}\left(\frac{\partial^4 n_{ei}}{\partial x^4}x_i^4 + 4\frac{\partial^4 n_{ei}}{\partial x^3\partial y}x_i^3y_i + 6\frac{\partial^4 n_{ei}}{\partial x^2\partial y^2}x_i^2y_i^2 + 4\frac{\partial^4 n_{ei}}{\partial x\partial y^3}x_iy_i^3 + \frac{\partial^4 n_{ei}}{\partial y^4}y_i^4\right) \tag{2-196}$$

At this point we note that if all the third and fourth spatial derivatives of the electron concentration were zero, then s_2 and s_3 would vanish and δ would be equal to $-s_0/s_1$. However, under this condition we know that δ must equal unity, since the unknown x_i and y_i give the stationary phase path when the third and fourth derivatives are neglected. Therefore, we have the additional information that $s_0 = -s_1$, which can be used to simplify the computation or to check the multiscreen solution.

The cubic equation (Equation 2-192) can be solved by standard techniques. The values of the perturbation parameter δ thus obtained are used to modify the original multiscreen solutions to obtain improved solutions for the propagation paths. The procedure can yield any number of propagation paths from zero to three, depending upon the electron density gradients. Thus, refractive multipath conditions are directly treated by this procedure.

If one is to consider the transmitter as a radar and the receiver as a target, when more than one propagation path exists between the radar and target, say m paths, then m^2 returns are present at the radar receiver resulting from each combination of outgoing and incoming paths, interference between the multiple returns gives rise to amplitude fading and jitter in the radar measurements.

Using the values of δ in conjunction with the unperturbed screen solutions, the refractive bending angles at each end of the propagation path are given by (see figure 4):

$$\tan\theta_{r_0} = \delta \frac{\sqrt{x_1^2 + y_1^2}}{r_1} \tag{2-197}$$

$$\tan\theta_{r_{RCVR}} = \delta \frac{\sqrt{x_n^2 + y_n^2}}{r_{RCVR} - r_n} \tag{2-198}$$

The orientation of these refractive angles, relative to the vertical direction (x-axis), measured clockwise as seen from the transmitter end of the path, are given by:

$$\gamma_{r_0} = \tan^{-1}\left(\frac{y_1}{x_1}\right) \tag{2-199}$$

$$\gamma_{r_{RCVR}} = \tan^{-1}\left(\frac{y_n}{x_n}\right) \tag{2-200}$$

2.5.2 Focusing and Defocusing.

Focusing and defocusing can also occur in a refractive environment. In such cases the ionosphere acts somewhat as a lens, causing either enhanced or reduced signal strength at the receiver depending on the characteristics of the spatial variation of the refractive index. Focusing and defocusing are usually significant only when a propagation mode is just on the verge of disappearing or reappearing.

Assume that the first path solution to the receiver (located at $r_{n+1} = r_{RCVR}$, $x_{n+1} = 0$, $y_{n+1} = 0$) has been obtained, and the coefficients of the cubic perturbation equation have been computed. To estimate the focusing/defocusing properties of the medium in the refractive gradient direction, another propagation path solution is obtained for a point displaced slightly in the receiver plane in the direction in which the path intersection with the last screen is displaced.

Thus, for the gradient, direction, we take the displaced point to be located in the receiver plane at

$$x_{n+1} = \frac{\varepsilon x_n}{\sqrt{x_n^2 + y_n^2}} \tag{2-201}$$

$$y_{n+1} = \frac{\varepsilon y_n}{\sqrt{x_n^2 + y_n^2}} \tag{2-202}$$

where ε is a constant displacement from the receiver, and x_n, y_n are the coordinates of the point at which the previously computed path to the receiver intersected the last screen. Note that these values of x_{n+1}, y_{n+1} are constants, not variables, in the equations to be solved for the propagation paths to this displaced point.

Similarly, in the direction normal to the gradient direction, we take the displaced point in the receiver plane at

$$x_{n+1} = \frac{\varepsilon y_n}{\sqrt{x_n^2 + y_n^2}} \tag{2-203}$$

$$y_{n+1} = \frac{\varepsilon x_n}{\sqrt{x_n^2 + y_n^2}} \tag{2-204}$$

In either case, the resulting system of simultaneous linear equations that must be solved to obtain the propagation path to the displaced point is identical to Equation 2-189, with the exception that x_{n+1}, y_{n+1} are no longer zero. In fact, the only changes in the elements of the augmented matrix of the system are that the final two members of the column vector c each contain one additional term:

$$c_{2n-1} = \frac{r_{n+1} - r_{n-1}}{4N_c} \frac{\partial n_{en}}{\partial x} + \frac{x_{n+1}}{r_{n+1} - r_n} \tag{2-205}$$

$$c_{2n} = \frac{r_{n+1} - r_{n-1}}{4N_c} \frac{\partial n_{en}}{\partial y} + \frac{y_{n+1}}{r_{n+1} - r_n} \tag{2-206}$$

With the Crout reduction method of solution, it is seen that the above affects only the last two values of c' in the auxiliary matrix:

$$c'_{2n-1}(new) = c'_{2n-1}(old) + \frac{1}{d'_{2n-1}} \left(\frac{x_{n+1}}{r_{n+1}-r_n}\right) \qquad (2\text{-}207)$$

$$c'_{2n}(new) = c'_{2n}(old) + \frac{1}{d'_{2n}} \left(\frac{y_{n+1}}{r_{n+1} - r_n}\right) - \frac{g'_{2n}}{d'_{2n}d'_{2n-1}} \left(\frac{x_{n+1}}{r_{n+1} - r_n}\right) \qquad (2\text{-}208)$$

These two changes propagate back and modify all of the x_i, y_i, i=1,2, ...,n. The focusing/defocusing properties in each of the two directions are then computed by determining the angular separations between the receiver path and the displaced paths compared to those which would result in free-space.

Once the screen equations are solved for the displaced path, the one-dimensional one-way defocusing ratio in the refractive gradient direction is computed as:

$$f_1 = \frac{r_1}{r_{RCVR}} \frac{\delta}{\sqrt{(x_1-x'_1)^2 + (y_1-y'_1)^2}} \qquad (2\text{-}209)$$

where primes denote values obtained for the displaced focusing path. For the direction orthogonal to the gradient direction a similar solution is obtained. (Note that a defocusing ratio greater than one implies a loss of signal energy and the complement of this condition implies a focusing or increase in signal power measured at the receiver.)

2.5.3 Refractive Effects on Phase and Time Delay.

Refractive bending of the propagation path causes the phase and group path lengths to be changed from the values they would have if the wave propagated along the LOS to the receiver. These changes can be readily calculated using the multiscreen method.

When the multiscreen solution for the primary propagation path has been obtained and the coefficients of the cubic perturbation equation have been calculated, the phase shift along each of the possible propagation paths is determined as follows. Integration of Equation 2-192 with respect to δ yields the phase path length for each of the paths. This in conjunction with Equation 2-183 gives the phase shift along the refracted paths:

$$\theta = \frac{\omega}{c}\left(s_0\delta + \frac{1}{2}s_1\delta^2 + \frac{1}{3}s_2\delta^3 + \frac{1}{4}s_3\delta^4\right) + \theta_0 \qquad \text{[rad]} \quad (2\text{-}210)$$

where θ_0 is the phase shift evaluated along the LOS to the receiver, including the effects of electron content along the LOS. When absorption is not catastrophically large, the real part of the index of refraction (Equation 2-184) can be used to write a simple expression for θ_0:

$$\theta_0 = -\frac{\omega}{c}\int_0^R \left(1 - \frac{\omega_p^2}{\omega^2}\right)^{1/2} dr$$

$$\simeq -\frac{2\pi}{\lambda}R + r_e\lambda \qquad \text{[rad]} \quad (2\text{-}211)$$

where λ is the RF wavelength, R is the distance along the LOS from transmitter to receiver, and r_e is the classical electron radius (2.8184E-13 cm).

A similar situation exists for the time delay. The equation for the group path length is the same as that for the phase path length except that the term involving the electron content is reversed in sign. This leads to the following equation for time delay along the refracted paths:

$$t_d = \frac{1}{c}\left(-s_0\delta + \frac{1}{2}g_1\delta^2 - \frac{1}{3}s_2\delta^3 - \frac{1}{4}s_3\delta^4\right) + t_{do} \qquad \text{[sec]} \quad (2\text{-}212)$$

where t_{do} is the time delay along the LOS (including electron content thereon), and g_1 is given by a summation identical to that of s_1 (Equation 2-194) except that the second term (involving the electron content) is reversed in sign. Similarly to θ_0, t_{do} may be written in the following simplified form:

$$t_{do} = \frac{1}{c} \int_0^R \left(1 - \frac{\omega_p^2}{\omega^2}\right)^{-1/2} dr$$

$$\approx \frac{R}{c} + \frac{r_e \lambda^2}{2\pi c} \qquad [\text{sec}] \qquad (2\text{-}213)$$

2.5.4 Model Implementation Comments.

Implementation of the refraction models in PRPSIM follows the descriptions found in sections 2.5.1, 2.5.2, and 2.5.3. There are, however, a few details and assumptions worth mentioning.

Typical applications of the multiscreen modeling require environment data at a set of points along the LOS only within a spatial region where the refractive properties are not negligible. The physical path end points may be far removed from the intervening refractive region. The multiscreen method, by virtue of the boundary condition that the propagation paths must connect the physical path end points, in effect averages the properties of the first and last phase screens over the path segments connecting the associated end points. Depending on the distances involved and the refractive properties of the first and last screens, it is sometimes appropriate to insert an additional "null screen" (i.e., one which has zero spatial derivatives) between one or both of the physical end points and the associated closest calculation point. This procedure (implemented in subroutine SCREEN) assures that regions of negligible refraction are treated as such. Subroutine REFRAC calls subroutine SCREEN once for each propagation path to initialize the phase screens.

The multiscreen method implemented in PRPSIM requires the values of the spatial derivatives of N_e (mean electron density) in the two orthogonal directions (vertical and traverse planes), up to fourth order, at each screen. DATAPT (see section 3.4), calculates the 3 components of the electron density gradient and the 6 components of the second spatial derivative of the electron density at each screen using first and second order differencing respectively. However, this technique is inappropriate for the higher order (third and fourth) spatial derivatives needed by the multiscreen method. The following two techniques, dependent upon the magnitudes and signs of the mean N_e and the first and second spatial derivatives, are used to estimate the third and fourth spatial derivatives. For notational convenience we define the following values:

$$f_0 = N_e \tag{2-214}$$

$$f_1 = \frac{\partial N_e}{\partial x} \tag{2-215}$$

$$f_2 = \frac{\partial^2 N_e}{\partial x^2} \tag{2-216}$$

If $f_2 \leq f_1^2/f_0$ then a Gaussian profile aproximation is used for the higher order derivatives:

$$\frac{\partial^3 N_e}{\partial x^3} = 3\,\frac{f_1 f_2}{f_0} - 2\,\frac{f_1^3}{f_0^2} \tag{2-217}$$

$$\frac{\partial^4 N_e}{\partial x^4} = 3\,\frac{f_2^2}{f_0} - 2\,\frac{f_1^4}{f_0^3} \tag{2-218}$$

The above inequality provides that the variance of the Gaussian profile will be sensible. If this inequality fails, the power-law profile approximation is used:

$$\frac{\partial^3 N_e}{\partial x^3} = 2\,\frac{f_2^2}{f_1} - \frac{f_1 f_2}{f_0} \tag{2-219}$$

$$\frac{\partial^4 N_e}{\partial x^4} = 2\,\frac{f_1^2 f_2^2}{f_0^2} + 6\,\frac{f_2^3}{f_1^2} - 7\,\frac{f_2^2}{f_0} \tag{2-220}$$

The use of this profile is necessary when the known second derivative, f_2, is so large in the positive direction that neither the Gaussian nor the exponential profiles is a reasonable form to assume.

The higher order mixed partials are calculated using the usual product function approximations:

$$\frac{\partial^3 N_e}{\partial^2 x\,\partial y} = \left(\frac{\partial^2 N_e}{\partial^2 x}\right)\left(\frac{\partial N_e}{\partial y}\right)\left(\frac{1}{N_e}\right) \tag{2-221}$$

$$\frac{\partial^3 N_e}{\partial x\,\partial^2 y} = \left(\frac{\partial N_e}{\partial x}\right)\left(\frac{\partial^2 N_e}{\partial^2 y}\right)\left(\frac{1}{N_e}\right) \tag{2-222}$$

$$\frac{\partial^4 N_e}{\partial^3 x\,\partial y} \quad \left(\frac{\partial^3 N_e}{\partial^3 x}\right)\left(\frac{\partial N_e}{\partial y}\right)\left(\frac{1}{N_e}\right) \tag{2-223}$$

$$\frac{\partial^4 N_e}{\partial^2 x\,\partial^2 y} = \left(\frac{\partial^2 N_e}{\partial^2 x}\right)\left(\frac{\partial^2 N_e}{\partial^2 y}\right)\left(\frac{1}{N_e}\right) \tag{2-224}$$

$$\frac{\partial^4 N_e}{\partial x\,\partial^3 y} = \left(\frac{\partial N_e}{\partial x}\right)\left(\frac{\partial^3 N_e}{\partial^3 y}\right)\left(\frac{1}{N_e}\right) \tag{2-225}$$

The focusing/defocusing parameter ε (see Equations 2-201 through 2-204) is chosen to be consistent with a 1 mrad displacement of the LOS.

$$\varepsilon = .001\ r_{RCVR} \qquad (2\text{-}226)$$

In some cases near the "caustic" region (where there is no RF propagation due to the extreme ionization), the path to the receiver may propagate but the one displaced in the refractive gradient direction will not (because it is beyond the caustic). In such cases we rather arbitrarily set the one-dimensional one-way defocusing ratio in this direction equal to a small value (0.1) corresponding to appreciable focusing which is typical of this type of situation. Conversely, it is possible in some cases to obtain only one real root for the cubic perturbation equation (Equation 2-192) on the path to the receiver, but three real roots on one of the displaced paths. In these cases two of the three roots do not correspond to physically reasonable paths, and hence there is no problem as long as one is careful to associate real main paths with real displaced paths when computing the focusing effects.

SECTION 3
INTERFACE WITH THE PROPAGATION ENVIRONMENT

3.1 INTRODUCTION.

The SCENARIO code was developed to provide reliable estimates of the phenomenology of high altitude nuclear bursts. Preexisting research phenomenology codes were capable of providing the necessary data for individual situations, but they are much too expensive and difficult to run to be of practical use in analyzing a wide variety of nuclear scenarios. SCENARIO is thus a compromise in that it calculates only those environmental parameters which have the most significant impact on the propagation of satellite signals. Although the SCENARIO geometry cannot provide as high a degree of resolution at early times as the research codes provide, it is adequate to model a very broad range of realistic nuclear scenarios. The fundamental objective of the SCENARIO code is to predict the evolution of the power spectral density function of the electron density fluctuations over a CONUS sized region on a time scale of hours during and following a series of high altitude nuclear events. The purpose of this section is to provide the user with a very basic description of the data contained in the files generated by the SCENARIO code and how the PRPSIM code interfaces with them. For a more complete description of the SCENARIO code, the user should refer to the reports MRC-R-404[12], MRC-R-539[13], or MRC-R-994[14]. For a description of the format of SCENARIO data files, refer to MRC-N-718R[15].

3.2 RETRIEVAL AND STORAGE OF SCENARIO DATA.

The storage and retrieval of MHD environmental data read from SCENARIO data files requires more CPU time than all other PRPSIM operations. For that reason, simulation time is designated to be the outermost loop in the hierarchy of PRPSIM's structure. With such a structure, data for a single grid dump time need be stored only once per simulation, regardless of the number of links, frequencies, etc. requested for that simulation time. Environmental data are read from SCENARIO files and stored in memory by the PROPEN routine. They may then be retrieved from memory by the DATAPT routine. PROPEN is called once by PRPSIM for each simulation time specified - provided that the simulation time does not correspond to the grid dump time of a file already in memory, or that it is not bracketed by the grid dump times of two files already in memory.

In order for PROPEN to operate, it must share the following data with PRPSIM in common storage: (1) the number of SCENARIO data files available to the simulation, (2) the array containing the names of those files (here referred to as the "file name array"), (3) the array of the initial grid times in those files (here referred to as the "initial time array"), (4) the total number grid times in the designated files (a physical file may contain more than one grid dump), (5) the array of all grid times in the designated files (here referred to as the "grid time array"), (6) the current simulation time, and (7) the grid dump time(s) of the data currently in extended memory. (Note that the number of times in the initial time array equals the number of names in the file name array.)

It is assumed that the data file names are ordered in increasing initial grid time and that the data within individual files (should the file contain more than one grid time) are ordered in increasing grid time. Also, the initial grid time of a file must be larger that the last

grid time of the previous file. It is the responsibility of the INDATA module to insure that these requirements are satisfied. Upon being called, PROPEN first checks to determine whether the current simulation time is within the range of grid dump times in the designated files. If it is not, an error message is printed and the job is aborted immediately.

All file manipulation and bookkeeping are accomplished by two pointers. Upon being called, PROPEN sets the "file pointer" to the largest time in the initial time array which does not exceed the current simulation time. If the file pointer changes from its previous value, the currently open data file is closed. Similarly, the "grid pointer" is set to the largest time in the grid time array which does not exceed the current simulation time. A file inquiry is conducted to determine if the file in the file name array indicated by the file pointer can be located on disk. If not, an error message is printed and the job is aborted. Note that PROPEN always returns to this point in the code whenever the file pointer is incremented. If the file indicated by the file pointer is not open, it is opened and rewound. Before proceeding further with this description of the PROPEN routine, the user should refer to MRC-N-718R [15] to familiarize himself with the format of the SCENARIO data files.

A SCENARIO logical file consists of the following records: (1) the header record, (2) the burst history record, (3) the grid geometry record, (4) the ambient atmosphere ionosphere record, (5) the active/inactive tube map record, (6) the first plasma tube record, (7) the second plasma tube record, and so on. Two optional records may follow the data records. Neither of these optional records is used by PRPSIM, and they will not be discussed further here.

PROPEN first attempts to read a header record from the designated SCENARIO file. Should this be an end-of-file (EOF) marker, PROPEN then attempts to read the next record. If more than two EOFs are read in

succession, PROPEN assumes that it has reached the end of the physical file. It then closes that file, increments the file pointer by one, and returns to the point indicated above to inquire about the existence of the next file in the file name array. If the record is not an EOF, PROPEN assumes that the record is the header record of the next logical file and proceeds to read that record and to store the information contained on it. The header record contains all the information that PROPEN needs in order to be able to interpret the information contained in all the remaining records in the logical file. The first information from the header record to be used by PROPEN is the grid dump time which determines whether the data from this grid dump (logical file) will be stored. To determine whether the data in the current logical file should be stored, PROPEN compares the current simulation time to the current grid dump time and the time in the grid time array to which the grid pointer points. If the simulation time equals the grid dump time, or if it is less than either the indexed array time or the following array time, the data will be read and stored by PROPEN; otherwise, PROPEN merely reads over all the records in the current grid dump with dummy read statements and then returns to the point in the code at which to read the header record of the next file (or the EOF[s] at the end of the file.) Conversely, if the data were stored, and if the grid dump time equals or exceeds the simulation time (so that no additional data are required for time interpolation), PROPEN returns control to PRPSIM after reading the last record in the file. Note that the current input data file is always left open when PROPEN returns control to PRPSIM.

The contents of the second record, the event history record, are read and printed by PROPEN if the diagnostic level is set to 1 or higher. Otherwise, they are not used by PRPSIM.

The third record is the grid geometry record that contains all the information needed by the path intersection routine (PATHPT) to determine the intersection of the propagation path with the grid. Because the size and location may or may not change from one grid dump to another, PROPEN maintains a logical array (GRDFLG) that is shared with PATHPT to inform it of any changes in the grid geometry. GRDFLG(1) is set true if the grid geometry data in register one are replaced by new data, and GRDFLG(2) is set true if those in register two are replaced. They are reset to false by PATHPT when it processes the new geometry data. GRDFLG(3) is set false by PROPEN if the geometries of the grids for the data in both registers are identical; otherwise it is set true.

The fourth record is the ambient atmosphere ionosphere record which contains a simple (radial) ambient atmosphere/ionosphere model which the data retrieval module (DATAPT) can use to generate data for points found in inactive tubes. Because the ambient model may also change with time, PROPEN maintains two registers in which these data are stored.

The fifth record is the active/inactive plasma tube map record. This record consists of a sequential list of indices for every data tube in the grid. If the tube is active, its index is its position in the sequence of data tube records; if it is inactive, its index is zero.

The remaining records are the (active) plasma data tube records. Currently, files are written with one tube per data record. PROPEN can read multiple tube records, however, provided that the necessary information is included on the header record.

Normally, PROPEN maintains two registers in which to store the SCENARIO data so that data can be interpolated between simulation times which do not coincide with a grid dump time. Should the storage requirements of two registers exceed the storage capacity available to you

on your machine, the second register may be dispensed with -- provided that no time interpolation is required. This is accomplished readily by setting the value of the parameter ISTACK to 1, rather than the usual value of 2. When both registers are used, storage of the SCENARIO data alternates between them. The value of of the register pointer IREG (1 or 2) indicates which register was last filled. Each register has its own time register which is equated to the current grid dump time when data are stored in the register.

On virtual storage machines such as the VAX/VMS system, data from the active plasma tubes are stored in a large array which is accessed only by the storage routine PROPEN and the retrieval routine DATAPT. On other machines such as the CDC/Cyber series, the data are stored in extended core memory. All other data read by PROPEN are stored in arrays.

Table 4. SCENARIO cell quantities stored in mass storage by PROPEN module.

PARAMETERS	UNITS
(1) mean electron density in the cell	[cm^{-3}]
(2) standard deviation of electron density in the cell	[cm^{-3}]
(3) partial time derivative of mean electron density	[cm^{-3} sec^{-1}]
(4) mean electron temperature within the cell	[°K]
(5) α component of the mean ion velocity	[cm/sec]
(6) β component of the mean ion velocity	[cm/sec]
(7) ϕ component of the mean ion velocity	[cm/sec]
(8) mean neutral mass density	[gm/cm]
(9) transverse outer striation scale size	[cm]

3.3 PROPAGATION PATH INTERSECTION WITH THE SCENARIO GRID.

PATHPT is the PRPSIM routine which generates the set of analysis points along the line of sight (LOS) connecting each pair of linked objects. PATHPT is called once by RFPROP for each link at each simulation time. The geographic coordinates of the transmitter (origin) and receiver (end) are passed to PATHPT by RFPROP as arguments. PATHPT then proceeds to calculate the number of cells in the MHD environmental grid which are intersected by the LOS, the lengths of the path segments that are defined by the intersections of the LOS and the cell boundaries, and the distance from the LOS origin to the midpoint of each of the segments. The midpoints of the segments define the set of analysis points at which RFPROP calculates the integrands needed to compute the various signal parameters.

A logical array (GRDFLG) is shared between PATHPT and the environmental data storage routine PROPEN (described in section 3.2) in order to avoid unnecessary work by PATHPT when the grid geometry does not change between successive grid dumps. In general, PROPEN maintains two registers in which grid dumps at two different times are stored. The first element of the logical array is set true by PROPEN if (and only if) the grid geometry of the new dump to be stored in register one differs from that of the old dump (which is to be replaced) in register one. The second element is analogous and refers to the data stored in the second register. If either of these two logical flags is true, PATHPT calculates the coordinates of the grid boundaries from the cell widths and the cell center coordinates provided by PROPEN and sets the flag false. Otherwise, it calls the subroutine X1TOX2 which is responsible for the calculation of the set of the path segment lengths and the distance to the midpoint of the first segment. The third element of the logical array is set true by PROPEN if the grid geometries of the dumps in the two registers differ from one another. If this flag is set, and if time interpolation is required, X1TOX2 is called twice, otherwise it is called only once. (The

manner in which the two sets are merged to form a single set of intersections will be described after we describe the operation of the subroutine X1TOX2.)

The first task of X1TOX2 is to determine the maximum and minimum coordinates of the LOS along each of the three grid directions, α, β, and ϕ. If these lie outside the range of the grid boundaries along any of the three grid directions, a null LOS-grid intersection is obvious, and X1TOX2 returns control to PATHPT with the number of intersections set to zero. If the respective maxima and minima lie within the limits of the grid along each of the three grid directions, X1TOX2 proceeds to calculate the distance to the intersection of the LOS with each of the boundary surfaces of the grid. Note that when we calculate the distances, we may deal with the intersections with each of the three sets of surfaces (i.e., those surfaces with constant α, β, and ϕ, respectively) independently of the other two. After computing all the intersections, it is only necessary to combine the three sets of distances so that they are arranged in order of increasing distance from the transmitter.

The set of surfaces of constant ϕ are easiest to visualize: they are simply a set of planes with a common line of intersection which coincides with the dipole axis. The β surfaces are curves with an axis of rotational symmetry which coincides with the dipole axis, and the α surfaces are curves th a plane of symmetry which coincides with the dipole equator (see figures 5 and 6). Let us define a Cartesian set of coordinates with the z-axis aligned along the dipole axis (pointing toward the north), and the y-axis defined by the cross product of the rotation axis and the dipole axis. The components of any point along the LOS may be computed as

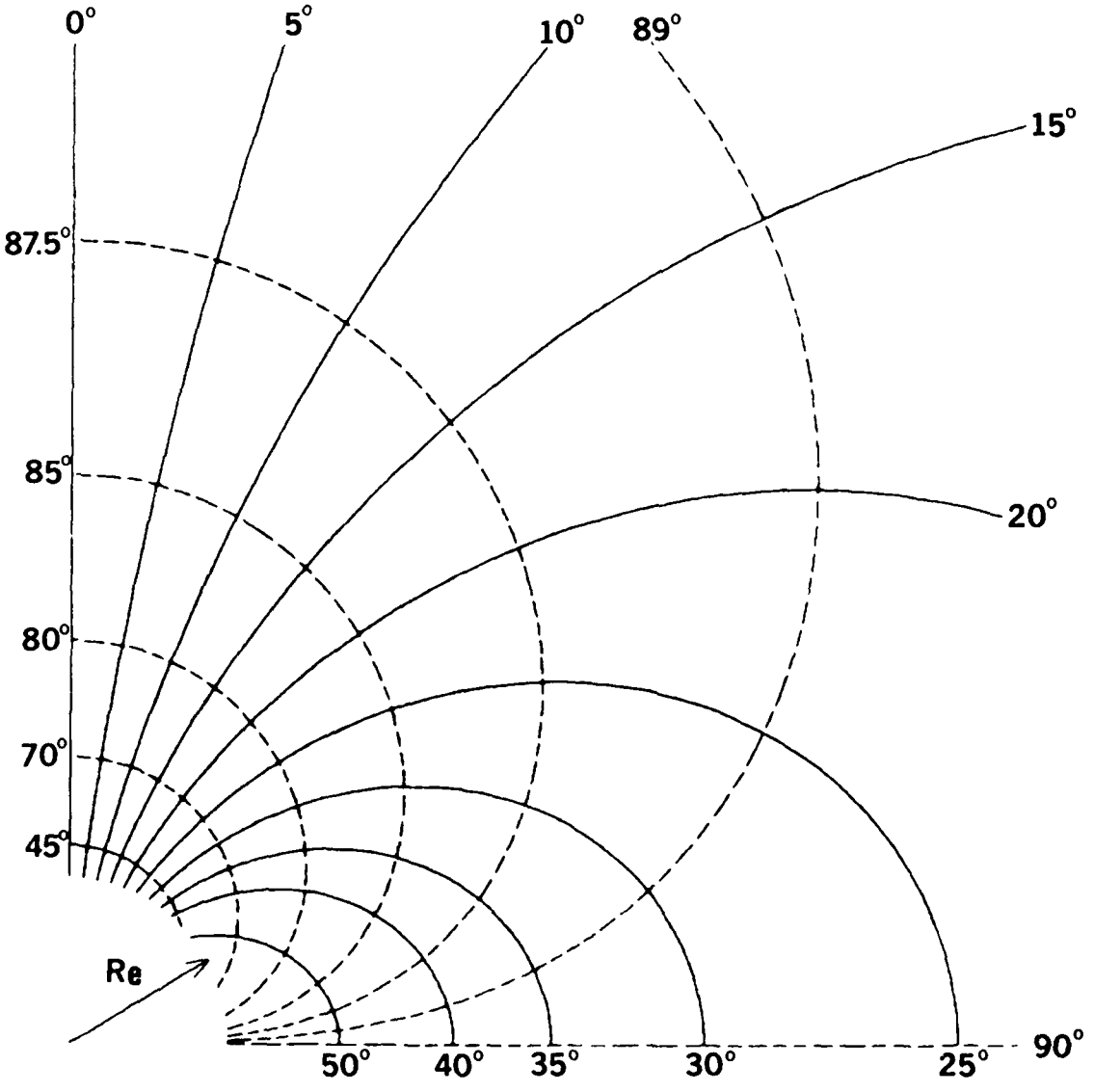

Figure 5. Cross-sectional view of a phi-plane in the dipole field aligned coordinate system of a uniform SCENARIO grid. Grid cell boundaries are formed by surfces of constant beta (solid lines) and constant alpha (dashed lines).

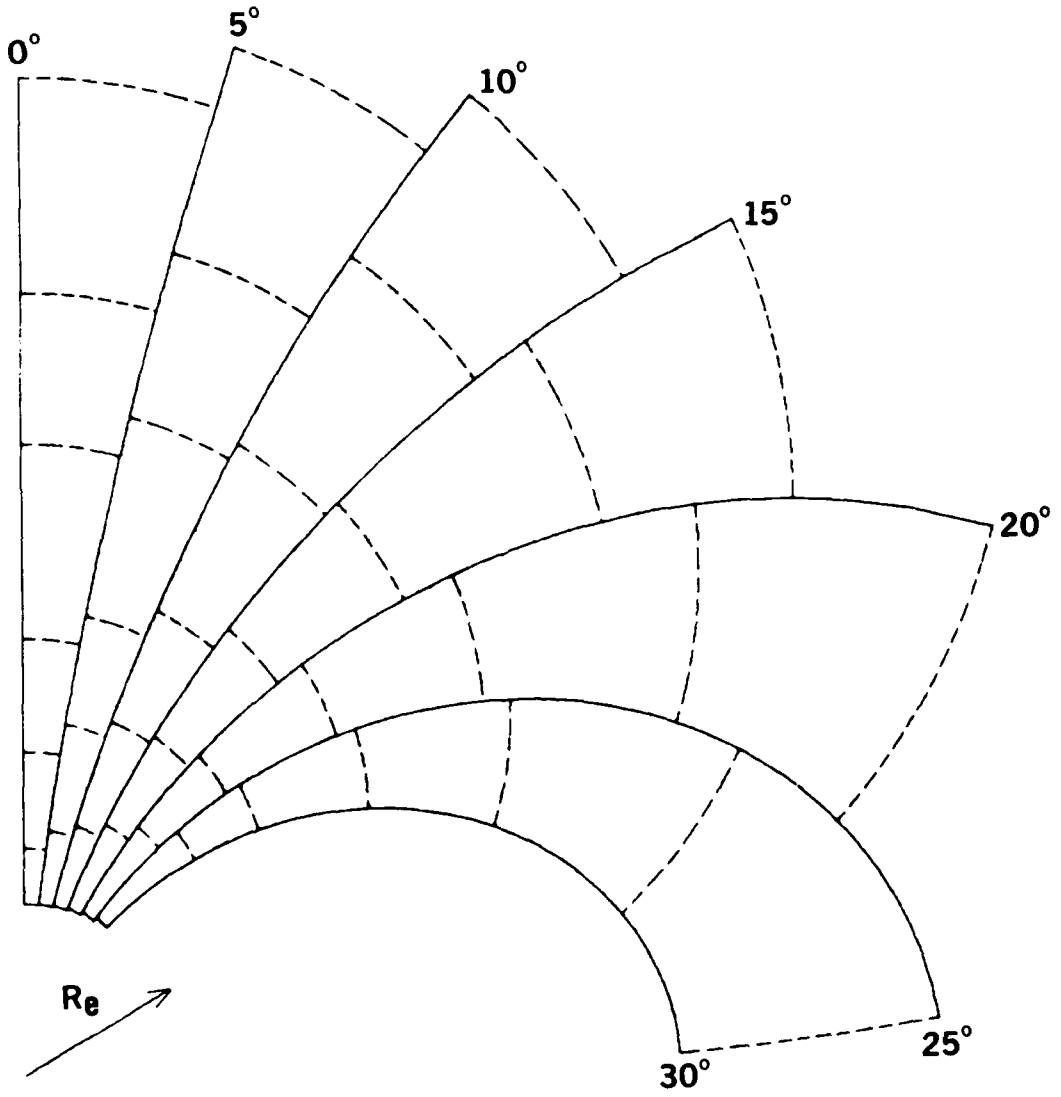

Figure 6. Cross-sectional view of a phi-plane in the dipole field aligned coordinate system of a "staggered" SCENARIO grid. Grid cell boundaries are formed by surfaces of constant beta (solid lines) and constant alpha (dashed line segments).

$$x = x_0 + at \tag{3-1}$$

$$y = y_0 + bt \tag{3-2}$$

$$z = z_0 + ct \tag{3-3}$$

where t is the distance from the origin to the point along the LOS; x_0, y_0, and z_0 are the coordinates of the origin; and a, b, and c are the direction cosines of the LOS along those axes, respectively,

$$a = (x_e - x_0)/t_{LOS} \tag{3-4}$$

$$b = (y_e - y_0)/t_{LOS} \tag{3-5}$$

$$c = (z_e - z_0)/t_{LOS} \tag{3-6}$$

where x_e, y_e, and z_e are the coordinates of the end point of the LOS, and

$$t_{LOS} = [(x_e - x_0)^2 + (y_e - y_0)^2 + (z_e - z_0)^2]^{1/2} \tag{3-7}$$

is the length of the LOS.

To compute the distances to the intersections with the set of ϕ planes with longitude ϕ_i, we use the relation

$$\phi_i = \tan^{-1}\left(\frac{y_i}{x_i}\right) \tag{3-8}$$

where i ranges between 1 and the number of ϕ planes defined in the grid. Then, from Equations 3-1, 3-2 and 3-8 we find the distances to the intersections

$$t_i = \frac{y_0 \cos\phi_i - x_0 \sin\phi_i}{a \sin\phi_i - b \cos\phi_i} \tag{3-9}$$

Note that if the LOS (when extended to infinity in both directions) intersects the dipole axis, there are no intersections of the LOS and the ϕ planes.

Equation 3-9 yields the intersection of the LOS with every ϕ plane in the grid. A real grid is bounded in α and β (as well as ϕ) so that we must test each of the points to determine whether it lies within these limits. Calculate the alpha coordinate of the ith point using

$$\cos\alpha_i = \frac{z_i R_e^2}{(x_i^2 + y_i^2 + z_i^2)^{3/2}} \tag{3-10}$$

and the beta coordinate using

$$\sin^2\beta_i = \frac{(x_i^2 + y_i^2)\ R_e}{(x_i^2 + y_i^2 + z_i^2)^{3/2}} \tag{3-11}$$

where R_e is the radius of the earth, and x_i, y_i, and z_i are obtained by inserting t_i from Equation 3-9 into Equations 3-1, 3-2, and 3-3. If either of these values falls outside the boundaries of the grid, the ith intersection is excluded from the set of grid intersections.

Equations 3-10 and 3-11 may be used to calculate the intersections of the LOS with the α and β surfaces, respectively. The distances, t_j, to the intersections with the β surfaces are given by all the real roots of the sixth order polynomial

$$[(x_0+at_j)^2 + (y_0+bt_j)^2 + (z_0+ct_j)^2]^3 = R_e^2[(x_0+at_j)^2 + (y_0+bt_j)^2]^2/\sin^4\beta_j \tag{3-12}$$

such that $0 < t_j < t_{LOS}$ where t_{LOS} is the length of the LOS, and j ranges over the number of β surfaces in the grid. Similarly, the distances to the intersections with the α surfaces are given by the real roots of the sixth order polynomial

$$\left[(x_0+at_k)^2 + (y_0+bt_k)^2 + (z_0+ct_k)^2\right]^3 = R_e^4(z_0+ct_k)^2/\cos^2\alpha_k \qquad (3\text{-}13)$$

such that $0 < t_k < t_{LOS}$ where t_{LOS} is the length of the LOS, and k ranges over the number of α surfaces in the grid. The SCENARIO grid is complicated by the fact that the α coordinates are "staggered" along different β coordinates. Specifically, for smaller values of β, the α coordinates decrease toward smaller values, but the number of α coordinates is the same for each of the β.

The number of real roots of Equation 3-12 on the interval $[0,t_{LOS}]$ is determined by applying Sturm's theorm. The first of these roots is then calculated precisely by applying Laguerre's method for root extraction with a "rough" initial estimate on the interval $[0,t_{LOS}]$. (For those rare instances in which Laguerre's method diverges, Sturm's method can be used to obtain a better initial estimate of the root, so that Laguerre's method can be applied again to converge to the root.) If more than one root (intersection) exists, the polynomial is "deflated" by dividing out the previously calculated root, and the root of the deflated polynomial is calculated as before. This process is continued until all the (up to four) real roots on the interval $[0,t_{LOS}]$ are calculated. Each of these distances must be checked by calculating (x_j, y_j, z_j) for each t_j (using Equations 3-1, 3-2, and 3-3) and inserting these values into Equations 3-8 and 3-10 to insure that the corresponding α and ϕ coordinates lie within the boundaries of the grid.

The roots of Equation 3-13 are calculated in analogous manner. Because the grid is staggered, however, it is convenient to analyze individually, each segment of the LOS between the intersections with adjacent β surfaces. If one (or both) end(s) of the LOS lie(s) within the grid boundaries, it is necessary to add one (or two) segments between the beginning and/or end of the LOS and the first and/or last intersected β surface.

The distances to the intersections between each of these segments and the α surfaces in the "tube" in which the segment lies are calculated by finding the real roots of Equation 3-13 on the interval $[0,t_j]$ where t_j is the length of the jth segment. (The x_0, y_0, and z_0 of Equation 3-13 must be replaced by the Cartesian coordinates of the beginning of the line segment.) The roots of this sixth order polynomial are computed in the same manner as those of Equation 3-12.

When the three sets of distances to the intersections of the LOS with each of the three sets of surfaces have been computed, X1TOX2 combines all three sets and reorders them according to increasing distance from the origin. The parameters that are passed back to PATHPT are the differences between distances to adjacent intersections (i.e., the set of path segment lengths, half the sum of the distances to the first two intersections (i.e., the distance to the center of the first segment), and the number of intersections minus one (i.e., the number of segments).

Because the grid is bounded by curved surfaces in α and β, it is possible that the LOS may exit the grid across a concave surface and then reenter. In such cases, X1TOX2 generates a path segment length for the extra-grid portion of the LOS as though it were enclosed by an ordinary grid cell. The data retrieval routine DATAPT recognizes this situation and returns null data (zeros) for such a segment. Path segments outside the grid but not bracketed by segments inside the grid are not generated by X1TOX2.

When time interpolation between two grids with different geometries is required, X1TOX2 must be called by PATHPT twice to generate two different sets of segments along the path. These must be merged into a single set of segments and distances to be used by RFPROP. The simplest means of doing this is just to combine both sets of intersections, and then determine the set of segment lengths between these intersections. If

the number of segments through the two grids is N1 and N2, then the number of combined segments is just N1+N2+1. Some of these may not be significant segments, however. Consider the case where the grids at the two times are identical but the second is shifted a minute linear distance relative to the first. (By minute, we mean that the distance of the shift is small when compared to any of the segment lengths along the LOS through either of the grids.) As one can easily visualize, the effect of combining the segments at the two times in the manner described above would be to insert minute segments of length equal to the shift between the original segments. In such a case, RFPROP would have to perform calculations at twice the number of points it actually needs. Our method of eliminating what we consider to be insignificant segments from the combined set is to merge a segment with its shortest neighbor if its length is less than one fourth the length of its shortest adjacent neighbor. Also all segments shorter than 5 m are merged with their shortest neighbor.

Finally, before returning control to RFPROP, PATHPT calculates the array of distances from the origin to the midpoint of each of the path segments. These constitute the set of points along which the propagation integrals will be calculated.

3.4 CALCULATION OF PRIMITIVE DATA FOR PROPAGATION INTEGRALS.

A set of nine SCENARIO data exists for every active cell within the plasma grid. Specifically, each of these data represents the mean value (and, in the case of the electron density, the standard deviation about the mean) of a particular variable within the cell. For a particular PROPSIM simulation of the progagation of a signal between a transmitter and receiver, a number of points along the propagation path is generated by the routine PATHPT. In theory, this set of points is the optimum set for the particular plasma grid because of the one-to-one correspondence

between the number of points and the number of grid cells which the propagation path intersects. (When time interpolation between two incongruent grids is required, the optimum set of points is harder to define, but that problem is beyond the scope of this section.) The basic task of the data retrieval routine (DATAPT) is to provide the integration module RFPROP with a set of data for each of these points along the path. The simplest means of doing this is to equate the data at each analysis point to the mean values for the cell in which it is located. DATAPT utilizes a method which somewhat more accurately represents the spatial variations of the variables in the grid by means of a three dimensional interpolation of the data from the coordinates of the nearest grid cell centers to the coordinates of the analysis point.

DATAPT operates in either of three computational modes. For the basic mode in which the spatial derivatives of the electron density are computed, data for four cells in each of twelve tubes surrounding the point are fetched. The data at the eight cell centers adjacent to the point are used for spatial interpolation, and the electron densities from the 24 "next nearest" neighbors are used to calculate the density gradient and second derivatives. For the second mode in which the derivatives are not computed, data from the eight nearest cell centers only are fetched and interpolated. The third mode is used for antenna temperature calculations and is similar to the second mode, but only a truncated data set is returned to RFPROP. In order to minimize the number of data fetches, DATAPT maintains an index of the subtubes for which data are currently available in the local buffer. (Here, a "subtube" refers to 4 [mode 1] or 2 [modes 2 and 3] adjacent cells in a tube.) For subsequent points along the path, the set of subtubes for which data are needed is compared to those already in the local buffer. The number of subtubes which must be fetched equals the number of subtubes in the buffer which are no longer needed, so that the former may be written over the latter, and the index updated. Figure 7 shows a schematic representation of the portion of the SCENARIO grid, relevant to a DATAPT operation at one point.

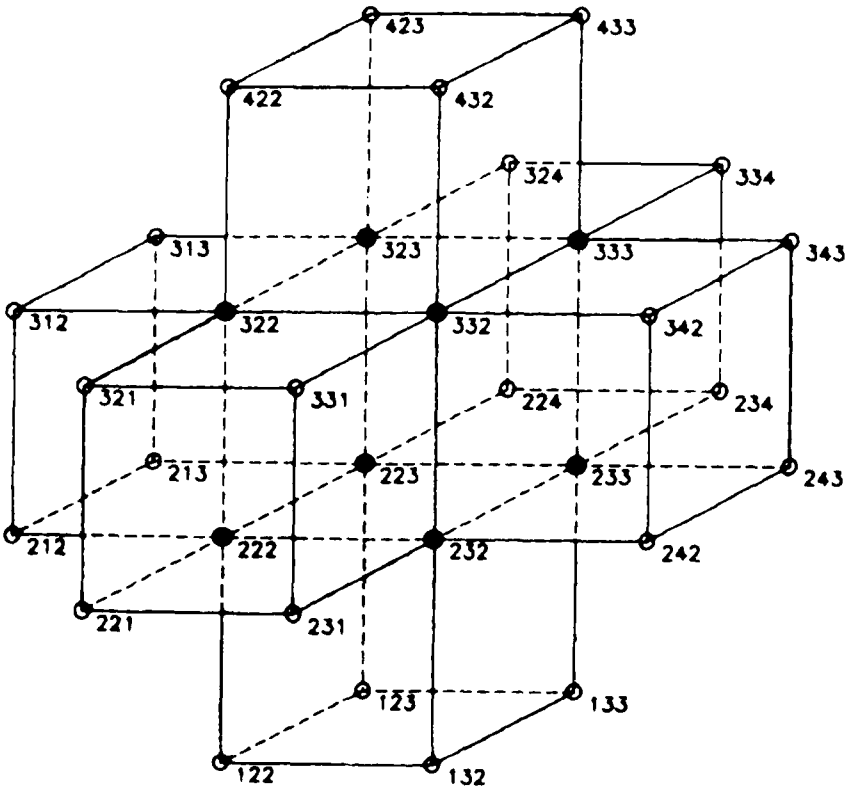

Figure 7. Cartesian representation of the portion of the SCENARIO grid used for a DATAPT calculation at a single point. The data from the 8 nearest cell centers (solid circles) are used to interpolate data to the coordinates of the point. The remaining 24 "next-nearest" neighbors (open circles) are used to approximate the mean electron density gradient and the spatial second derivatives. (Note that the grid shown is not "staggered.")

The data storage routine PROPEN insures that the current simulation time equals tne grid time of one of the grid data dumps currently in extended memory or that the grid times of the stored data bracket the simulation time. In the latter case, DATAPT must perform its calculations at each point twice using the data at both grid dump times. A single data set is then calculated from the two sets by interpolation in time. (Obviously, two local buffers are required to accomodate the data from all subtubes at both grid dump times.)

In addition to interpolation of SCENARIO data, DATAPT calculates several of its own parameters. These parameters calculated by DATAPT and interpolated from SCENARIO data are summarized in Table 5.

Table 5. Summary of parameters calculated or interpolated by DATAPT submodule.

I => interpolated from SCENARIO data
C => calculated by DATAPT
C/I => calculated using the interpolated SCENARIO data
Mode = 1/2 => ordinary calculation with/without local electron density derivatives
Mode = 3 => antenna temperature calculation

PARAMETER	UNITS	MODE
mean local electron density	[cm^{-3}]	I 1 2 3
electron temperature	[°K]	I 1 2 3
electron density standard deviation	[cm^{-3}]	I 1 2 3
rms electron density	[cm^{-3}]	C/I 1 2 3
electron-neutral collision frequencies	[sec^{-1}]	C/I 1 2 3
electron-ion collision frequency	[sec^{-1}]	C/I 1 2 3
3 components of the ion velocity	[cm sec^{-1}]	I 1 2
partial time derivative of electron density	[$cm^{-3}sec^{-1}$]	I 1 2
2 transverse outer striation scale sizes	[cm]	I 1 2
orientation of outer transverse scale sizes	[rad]	C 1 2
parallel outer striation scale size	[cm]	C 1 2
isotropic inner striation scale size	[cm]	C 1 2
3 components of the magnetic field	[Gauss]	C 1 2
3 components of electron density gradient	[cm^{-4}]	C/I 1
6 components of second derivative of density	[cm^{-5}]	C/I 1

The argument list for DATAPT consists of (1) the altitude of the point, (2) its colatitude, (3) its longitude, (4) the number of propagation frequencies, (5) the array of propagation frequencies, (6) the sequential number of the point on the path (used for diagnostic printout only), and (7) a logical array which specifies the operational mode for the path.

The geomagnetic coordinates (geomagnetic colatitude and longitude, respectively) of the point are calculated from its geographic coordinates using

$$\theta_m = \arccos\left[\cos\theta_D\cos\theta_0 + \sin\theta_D\sin\theta_0\cos(\phi_D-\phi_0)\right] \tag{3-14}$$

$$\phi_m = \arctan\left[\frac{-\sin\theta_0\,\sin(\phi_D-\phi_0)}{\cos\theta_D\sin\theta_0\,\cos(\phi_D-\phi_0) - \sin\theta_D\cos\theta_0}\right] \tag{3-15}$$

where θ_D is the geographic colatitude of the dipole axis, ϕ_D is the geographic longitude of the dipole axis, θ_0 is the geographic colatitude of the point, and ϕ_0 is the geographic longitude of the point. The dipolar (α, β, ϕ) coordinates are then calculated from the geomagnetic coordinates using

$$\cos\alpha = \left(\frac{R_e}{R}\right)^2 \cos\theta_m \tag{3-16}$$

$$\sin\beta = \left(\frac{R_e}{R}\right)^{1/2} \sin\theta_m \tag{3-17}$$

$$\phi = \phi_m \tag{3-18}$$

where R_e is the radius of the earth [cm], and R is the radial distance [cm] to the point from the center of the earth.

Given the dipolar coordinates of the point, DATAPT proceeds to calculate the indices ($I_\alpha, I_\beta, I_\phi$) of the cell containing the point by searching through the arrays of grid coordinates read from the grid geometry record and determining the pairs of grid coordinates which bracket the coordinates of the point. DATAPT uses the convention that the index along a given axis equals the sequential number of the cell center with the largest coordinate which does not exceed the coordinate of the point on that axis. The geometry of the SCENARIO grid is complicated by the fact that the α coordinates along a field line are "staggered" -- that is, a specific α index corresponds to different α coordinates on different field lines (different β indices). DATAPT calculates four α indices for each point along its field line (β coordinate): one each for the two β indices above the point and for the two β indices below the point. (Currently, the α index of a point in the SCENARIO grid ranges between 0 and 11, and the β and ϕ indices range between 0 and 32.) A zero index indicates that the point lies below the lowest cell center on that axis, and the maximum value indicates that it lies above the highest cell center.

Denote the indices of the cell containing a point as I_α, I_β, and I_ϕ. DATAPT calculates the tube indices of the four tubes surrounding the point and the indices of the eight additional "next-nearest neighbor" tubes (for mode 1) using

$$N_{tube} = J_\beta + N_x*(J_\phi - 1) \qquad (3\text{-}19)$$

where N_x is the total number of tubes in the grid along the β axis (read from the header record). J_β ranges between $\max(I_\beta-1,1)$ and $\min(I_\beta+2,N_x)$ for mode 1, and between $\max(I_\beta,1)$ and $\min(I_\beta+1,N_x)$ for modes 2 and 3; whereas J_ϕ ranges between $\max(I_\phi-1,1)$ and $\min(I_\phi+2,N_y)$ for mode 1 and between $\max(I_\phi,1)$ and $\min(I_\phi+1,N_y)$ for modes 2 and 3. (The min and max functions insure that DATAPT does not attempt to retrieve data for tubes which do not exist.) Note that the four "corner" tubes with indices

$(I_\alpha-1,I_\phi-1)$, $(I_\alpha-1,I_\phi+2)$, $(I_\alpha+2,I_\phi-1)$, and $(I_\alpha+2,I_\phi+2)$ are not needed to calculate the density derivatives and are not stored. A schematic diagram of the relevant portion of the grid for a single DATAPT calculation is depicted in Figure 7. In order to reduce the amount of data transfer, DATAPT does not fetch the contents of an entire grid tube. Since we need data from only 4 cells for mode 1 (at 2 cell centers above the point and 2 cell centers below the point) or 2 cells for modes 2 and 3 (1 cell center above and below the point), DATAPT fetches data in units of these "subtubes." (Because of the staggering of the grid, it is important to remember that the α indices of the various subtubes will differ from one another, in general.)

DATAPT then checks the index of each of the 12 (or 4) neighboring tubes in the active/inactive tube map index. If the active/inactive tube index is zero, the tube is inactive, and DATAPT fetches ambient data for the the locations of the 4 (or 2) bracketing cell centers and stores them in the appropriate location in the local buffer. If the active/inactive tube index for the tube is non-zero, DATAPT fetches data for the bracketing cell centers and inserts them into the local buffer. From this point on, DATAPT makes no distinction between data from "active" or "ambient" cells.

DATAPT uses the four subtubes immediately adjacent to the point for spatial interpolation of SCENARIO data to the point. For each of the four tubes, we interpolate (log-linear) each datum between the cell centers with α coordinates bracketing that of the point. Then we interpolate in ρ to yield two values for each datum at the two ϕ coordinates bracketing the point, and finally, we interpolate in ϕ to yield the value of each datum interpolated to the coordinates of the point. In order to compute the density gradient, we calculate and store the logarithm of the electron density at each of the 8 cells surrounding the point and at the 24 'next-nearest' cell centers. We calculate the

first and second derivatives of $\log(N_e)$ in α along each of the four tubes immediately surrounding the point. (The logarithm of the mean density is used because log-linear interpolation of the density more accurately represents the denisty variation in space over the distances in question.) To approximate the derivatives along each tube, let f_i denote the values of the log density at the 4 points a_i along the α axis with $a_1 < a_2 < a_p < a_3 < a_4$, where a_p is the α coordinate of the point at which the derivative is to be calculated. (See Figure 7.) Owing to the "staggering" of the α coordinates, the a_i set will not, in general, be the same 4 values on the 4 tubes. Approximate the first derivatives at the three intermediate points halfway between a_1 and a_2, a_2 and a_3, and a_3 and a_4, respectively:

$$d_{21} = \frac{f_2-f_1}{a_2-a_1} \qquad \text{at } a_{21} = \frac{1}{2}(a_2+a_1) \tag{3-20}$$

$$d_{32} = \frac{f_3-f_2}{a_3-a_2} \qquad \text{at } a_{32} = \frac{1}{2}(a_3+a_2) \tag{3-21}$$

$$d_{43} = \frac{f_4-f_3}{a_4-a_3} \qquad \text{at } a_{43} = \frac{1}{2}(a_4+a_3) \tag{3-22}$$

Approximate the second derivatives at the 2 points near a_2 and a_3, respectively:

$$dd_{321} = \frac{d_{32}-d_{21}}{a_{32}-a_{21}} \quad \text{at } a_{321} = \frac{1}{2}(a_{32}+a_{21}) \tag{3-23}$$

$$dd_{432} = \frac{d_{43}-d_{32}}{a_{43}-a_{32}} \quad \text{at } a_{432} = \frac{1}{2}(a_{43}+a_{32}) \tag{3-24}$$

The value of the first derivative at the point $\alpha = a_p$ is then approximated by linear interpolation between the first differences at the two bracketing points:

$$\frac{\partial f}{\partial \alpha} \simeq d_{21} + \frac{d_{32}-d_{21}}{a_{32}-a_{21}} (a_p-a_{21}) = dd_{21} + dd_{321} (a_p-a_{21})$$

$$\text{if } a_p \leq a_{32} \tag{3-25}$$

$$\frac{\partial f}{\partial \alpha} \simeq d_{32} + \frac{d_{43}-d_{32}}{a_{43}-a_{32}} (a_p-a_{32}) = dd_{32} + dd_{432} (a_p-a_{32})$$

$$\text{if } a_p > a_{32} \tag{3-26}$$

In addition to these four values, the derivatives on the eight outer tubes are calculated using the two values bracketing the α coordinate of the point. These values are stored to be used later to calculate the mixed second derivatives in α and β, and in α and ϕ.

The value of the second derivative in α at $\alpha = a_p$ is approximated by linear interpolation between the second differences:

$$\frac{\partial^2 f}{\partial a^2} \simeq dd_{321} + \frac{dd_{432}-dd_{321}}{a_{432}-a_{321}} (a_p-a_{321}) \tag{3-27}$$

To calculate the derivatives at the point $(\alpha_p, \beta_p, \phi_p)$, we linearly interpolate each pair of values in β to yield two values at the ϕ coordinates bracketing the point. Then we interpolate in ϕ between these two values to yield the final approximation to the derivatives at the coordinates of the point.

Calculation of the derivatives in the β and ϕ directions is analogous to that in the α direction, but it is complicated by the fact that the grid is "staggered." Whereas all points with common β and ϕ indices have the same β and ϕ coordinates, the same is not true for the α indices and coordinates. A set of points with the same α and β indices, for example, does not constitute a "tube" along which all the points have

the same α and β coordinates. The simplest means to circumvent this difficulty is to interpolate linearly in α between the cell centers bracketing the α coordinate of the point along each (β, ϕ) tube to yield a grid of values for the function on the "α surface" containing the point. The derivatives in β can be calculated each of the two lines with ϕ coordinates bracketing that of the point. The two sets of values are then interpolated in ϕ to yield the approximate derivatives in β at the point. The derivatives in ϕ are obtained in the same manner by interpolation in β.

The mixed second derivatives in α and β, and in α and ϕ are calculated in exactly the same manner as the first derivative of log (N_e) using the derivatives in α at the twelve grid points calculated and stored above. The mixed second derivative in β and ϕ is caluclated using the six first derivatives in ϕ, plus the two additional differences obtained from the other four tubes. Differencing these eight values in β yields five estimates of $\partial^2 f/\partial\beta\partial\phi$. We then use the three values in the quadrant of the point to interpolate for the value at the point.

If the simulation times does not equal the grid dump time for the data in either of the data registers, interpolation in time of all the basic grid data is required. In this case, all the preceding DATAPT calculations are repeated for the second bracketing grid dump time. (It is the responsibility of the routine PROPEN to insure that the dump times of the data in the storage registers always bracket the simulation time.) Each pair of results is then interpolated (log-linear) to the simulation time.

The remainder of the DATAPT code is devoted to the calculation of several parameters which are derived as functions of the basic data whose calculation is described above and as functions of the location of the point, and to the transformation of the density derivatives from the curvilinear dipole coordinate system to a Cartesian system.

The mean electron-neutral momentum transfer collision frequency [per electron per second] is given by

$$\nu_{en} = 8.14\times10^{12}\ \rho_n\ T_i^{0.64} \qquad [sec^{-1}] \qquad (3\text{-}28)$$

where ρ_n is the neutral mass density [gm cm^{-3}] and T_i is the electron temperature [°K]. This formula is derived from Equation 5-31 of DNA-3827T[18] by assuming a uniform neutral atmosphere consisting of equal parts of monatomic nitrogen and monatomic oxygen (that is, a constant mean molecular weight of 15 gm $mole^{-1}$).

The root mean square [rms] electron density is given by

$$\langle N_e \rangle_{rms} = \sqrt{N_e^2 + \sigma_{N_e}^2} \qquad [cm^{-3}] \qquad (3\text{-}29)$$

where σ_{N_e} is the electron density standard deviation [cm^{-3}] and N_e is the mean electron density [cm^{-3}].

The mean electron-ion momentum transfer collision frequency per electron per second is given by

$$\nu_{ei} = 1.8\ \langle N_e \rangle_{rms}\ T_i^{-1.5}\ \ln\left(1.25\times10^{16}\ \frac{T_i^3}{f_c^2}\right) \qquad [sec^{-1}] \qquad (3\text{-}30)$$

where $\langle N_e \rangle_{rms}$ is the rms electron density [cm^{-3}], T_i is the local electron temperature [°K], and f_c is the signal carrier frequency [Hz]. (This equation was taken from page 5-1 of DNA-3499H[17].) Note that an array of electron-ion collision frequencies is calculated by DATAPT -- one for each carrier frequency in the simulation.

Collisions between ions and neutral molecules are ignored by PRPSIM because their contribution to the total transfer of momentum is negligible in comparision with collisions between electrons and neutral atoms at the frequencies and altitudes of interest here.

DATAPT sets the outer striation scale size parallel to the field vector to a constant value L_t = 1.5E+7 cm. This value insures that the ratio of the parallel scale size to the transverse scale is in the range 10—15.

Currently, the SCENARIO code assumes azimuthal symmetry about the field vector and generates only one transverse outer striation scale size. DATAPT assigns an equal value for the second transverse outer scale size, and sets the orientation of the axis of the greater scale size to zero.

DATAPT sets the isotropic inner striation scale size to a constant value ℓ = 1.0E+3 cm. This value gives a minimum outer to inner scale size ratio of approximately 1000.

The magnetic field vector is calculated by approximating the earth's field by that of a geocentric dipole moment of 8.1E+25 emu oriented along an axis through 78.6° north latitude and 69.8° west longitude (epoch 1950). The field strength is calculated as

$$|\vec{B}| = \frac{M_d}{R^3}\sqrt{1 + 3\cos^2\theta_m} \qquad \text{[Gauss]} \qquad (3\text{-}31)$$

where M_d is the dipole moment, R is the radial distance to the point from the center of the earth [cm], and θ_m is the geomagnetic colatitude of the point. By definition, the dipole field vector is directed along the -z axis.

To transform the components of the ion velocity, magnetic field, and electron density gradient from the field aligned coordinate system (α, β, ϕ) to the local tangent plane system, calculate the inclination (dip angle) and declination of the magnetic field vector:

$$DIP = \arctan\left(\frac{2\cos\theta_m}{\sin\theta_m}\right) \tag{3-32}$$

$$DEC = \arctan\left(\frac{\sin\theta_D \sin\theta_0 \sin(\phi_D-\phi_0)}{\cos\theta_D - \cos\theta_0\cos\theta_m}\right) \tag{3-33}$$

where θ_m is the geomagnetic colatitude of the point, θ_0 is the geographic colatitude of the point, ϕ_0 is the geographic longitude of the point, θ_D is the geographic colatitude of the dipole axis , and ϕ_D is the geographic longitude of the dipole axis. First, rotate the coordinate system clockwise about the ϕ axis through (π/2-DIP) to align the α-axis with the Z (vertical) axis; then, rotate the coordinate system counterclockwise about the Z-axis through (π/2+DEC) to align the X and Y-axes with east and north, respectively. Therefore, to transform the components of the ion velocity from field aligned coordinates to local tangent plane coordinates:

$$V_x = -V_\beta \sin DIP \sin DEC + V_\phi \cos DEC - V_\alpha \cos DIP \sin DEC \quad [cm\ sec^{-1}] \tag{3-34}$$

$$V_y = -V_\beta \sin DIP \cos DEC - V_\phi \sin DEC - V_\alpha \cos DIP \cos DEC \quad [cm\ sec^{-1}] \tag{3-35}$$

$$V_z = -V_\beta \cos DIP + V_\alpha \sin DIP \quad [cm\ sec^{-1}] \tag{3-36}$$

and similarly for the components of the magnetic field vector.

Next, we must transform the components of the mean electron density gradient and the second derivative from the curvilinear dipolar

coordinates to the tangent plane coordinate system. The gradient transforms as a vector, and the transformation is straightforward. First, we compute the linear components of the gradient along the Cartesian axes aligned along the α, β, and ϕ directions:

$$\frac{\partial f}{\partial u_\alpha} = \frac{1}{h_\alpha} \frac{\partial f}{\partial \alpha} \tag{3-37}$$

$$\frac{\partial f}{\partial u_\beta} = \frac{1}{h_\beta} \frac{\partial f}{\partial \beta} \tag{3-38}$$

$$\frac{\partial f}{\partial u_\phi} = \frac{1}{h_\phi} \frac{\partial f}{\partial \phi} \tag{3-39}$$

where h_α, h_β, and h_ϕ are the scale factors of the dipolar coordinate system in the α, β, and ϕ directions, respectively:

$$h_\alpha = R\sqrt{\frac{\rho^4 - \cos^2\theta_m}{1 + 3\cos^2\theta_m}} \qquad [\text{cm}] \tag{3-40}$$

$$h_\beta = \rho R\sqrt{\frac{\rho + \cos^2\theta_m - 1}{1 + 3\cos^2\theta_m}} \qquad [\text{cm}] \tag{3-41}$$

$$h_\phi = R\rho\sin\theta_m \qquad [\text{cm}] \tag{3-42}$$

where R is the radial distance to the point [cm] from the center of the earth, ρ is the ratio of that distance to the radius of the earth, and θ_m is the magnetic colatitude of the point from Equation 3-14. The components of the gradient are then transformed to the tangent plane system by

the two rotations defined in Equations 3-34, 3-36. Finally, the gradient of the log density is converted to the mean density gradient using

$$\text{grad}(N_e) = N_e \text{grad}(f) = N_e \text{grad}\left[\ln(N_e)\right] \qquad [\text{cm}^{-4}] \qquad (3\text{-}43)$$

where N_e is the interpolated local mean electron density.

The second derivative is more complicated because it is a second rank tensor and must be transformed accordingly. We must first select a fixed coordinate system in which we wish to calculate the components. The local tangent plane is not satisfactory because its orientation changes with a change in location. The LOS aligned system would seem to be the most logical choice because it is fixed and the components must ultimately be transformed to that system anyway. It is preferable, however, to define a Cartesian system with the z-axis aligned along the dipole axis, and the y-axis defined by the cross product of the rotation axis and the dipole axis. The coordinates of a point in that system are just

$$x = R\sin\theta_m\cos\phi \qquad [\text{cm}] \qquad (3\text{-}44)$$

$$y = R\sin\theta_m\sin\phi \qquad [\text{cm}] \qquad (3\text{-}45)$$

$$z = R\cos\theta_m \qquad [\text{cm}] \qquad (3\text{-}46)$$

where R is the radial distance [cm] to the point from the center of the earth, θ_m is the magnetic colatitude, and ϕ is the magnetic longitude. For a general transformation from curvilinear to Cartesian coordinates, the components of the gradient can be shown to be

$$\frac{\partial f}{\partial x_n} = \sum_j \frac{1}{h_j^2} \frac{\partial x_n}{\partial u_j} \frac{\partial f}{\partial u_j} \qquad (3\text{-}47)$$

By applying this operator to itself, we obtain a general expression for the components of the second derivative:

$$\frac{\partial^2 f}{\partial x_m \partial x_n} = \sum_j^3 \sum_k^3 \frac{1}{h_j^2} \frac{\partial x_m}{\partial u_j} \frac{\partial x_n}{\partial u_k} \frac{\partial f}{\partial u_k} \frac{\partial}{\partial u_j} \left(\frac{1}{h_k^2}\right)$$

$$+ \sum_j^3 \sum_k^3 \frac{1}{h_j^2} \frac{1}{h_k^2} \frac{\partial x_m}{\partial u_j} \frac{\partial x_n}{\partial u_k} \frac{\partial^2 f}{\partial u_j \partial u_k}$$

$$+ \frac{1}{2} \sum_j^3 \sum_k^3 \frac{1}{h_j^2} \frac{1}{h_k^2} \frac{\partial f}{\partial u_k} \left[\frac{\partial x_m}{\partial u_j} \frac{\partial^2 x_n}{\partial u_j \partial u_k} + \frac{\partial x_n}{\partial u_j} \frac{\partial^2 x_m}{\partial u_j \partial u_k}\right] \quad (3\text{-}48)$$

The derivation of the coordinate differentials $\partial x_n / \partial u_j$ is complicated by the fact that R and θ_m (and hence x, y, and z) cannot be expressed analytically as functions of α and β. That is, the inverses of Equations 3-16 and 3-17 do not exist in analytic form. We can, however, derive analytic expressions for the differentials if we introduce a third variable. For a given α and β, we may obtain the corresponding values for R and θ_m from the root of the quartic equation

$$\kappa^2 \zeta^4 + \zeta - 1 = 0 \qquad \text{with } 0 \leq \zeta \leq 1 \quad (3\text{-}49)$$

where

$$\kappa = \frac{\cos \alpha}{\sin^4 \beta} \quad (3\text{-}50)$$

then

$$R = \frac{R_e}{\sin^2 \beta} \zeta \quad (3\text{-}51)$$

and

$$\cos \theta_m = \kappa \zeta^2 \quad (3\text{-}52)$$

Equation 3-49 can be solved easily by a simple iterative technique. PRPSIM uses Newton's method with 6 iterations. For $\kappa \leq 10$, this is accurate to within 0.13%.

Although none of the parameters in question can be represented as analytic functions of α and β, they can all be represented as the products of analytic functions of α, β, and ζ. Let us represent the unknown function g as

$$q(\alpha,\beta) = u(\alpha)\ v(\beta)\ w(\zeta) \tag{3-53}$$

Then, because ζ is a function of κ alone, we may write

$$\frac{\partial g}{\partial \alpha} = v(\beta)w(\zeta)\ \frac{du}{d\alpha} + u(\alpha)v(\beta)\ \frac{dw}{d\zeta}\frac{d\zeta}{d\kappa}\frac{\partial \kappa}{\partial \alpha} \tag{3-54}$$

$$\frac{\partial g}{\partial \beta} = u(\alpha)w(\zeta)\ \frac{dv}{d\beta} + u(\alpha)v(\beta)\ \frac{dw}{d\zeta}\frac{d\zeta}{d\kappa}\frac{\partial \kappa}{\partial \beta} \tag{3-55}$$

where

$$\frac{\partial \kappa}{\partial \alpha} = -\frac{\sin\alpha}{\sin^4\beta} = -\kappa\tan\alpha \tag{3-56}$$

$$\frac{\partial \kappa}{\partial \beta} = -4\kappa\cot\beta \tag{3-57}$$

and from Equation 3-49 it is easily shown that

$$\frac{d\zeta}{d\kappa} = \frac{-2\zeta^3\sqrt{1-\zeta}}{4-3\zeta} \tag{3-58}$$

By employing this strategy, we obtain the expressions for the derivatives of the scale factors:

$$\frac{\partial}{\partial \alpha}\left(h_\alpha^{-2}\right) = -2\left\{\frac{(8-15\zeta+6\zeta^2)}{(4-3\zeta)^2} + \frac{1}{\cos\alpha\sin\alpha}\right\} h_\alpha^{-2} \tag{3-59}$$

$$\frac{\partial}{\partial\beta}\left(h_\alpha^{-2}\right) = -\,4\cot\beta\left\{\frac{2(8-15\zeta+6\zeta^2)}{(4-3\zeta)^2} - 1\right\} h_\alpha^{-2} \tag{3-60}$$

$$\frac{\partial}{\partial\phi}\left(h_\alpha^{-2}\right) = 0 \tag{3-61}$$

$$\frac{\partial}{\partial\alpha}\left(h_\beta^{-2}\right) = -\,12\tan\alpha\left\{\frac{(1-\zeta)(2-\zeta)}{(4-3\zeta)^2}\right\} h_\beta^{-2} \tag{3-62}$$

$$\frac{\partial}{\partial\beta}\left(h_\beta^{-2}\right) = -\,2\left\{24\,\frac{(1-\zeta)(2-\zeta)}{(4-3\zeta)^2}\cot\beta - \frac{(1+2\cos^2\beta)}{\cos\beta\,\sin\beta}\right\} h_\beta^{-2} \tag{3-63}$$

$$\frac{\partial}{\partial\phi}\left(h_\beta^{-2}\right) = 0 \tag{3-64}$$

$$\frac{\partial}{\partial\alpha}\left(h_\phi^{-2}\right) = -\,6\tan\alpha\left\{\frac{(1-\zeta)}{(4-3\zeta)}\right\} h_\phi^{-2} \tag{3-65}$$

$$\frac{\partial}{\partial\beta}\left(h_\phi^{-2}\right) = -\,4\cot\beta\left\{\frac{(2-3\zeta)}{(4-3\zeta)}\right\} h_\phi^{-2} \tag{3-66}$$

$$\frac{\partial}{\partial\phi}\left(h_\phi^{-2}\right) = 0 \tag{3-67}$$

For the coordinate differentials, we obtain

$$\frac{1}{x}\frac{\partial x}{\partial\alpha} = \frac{1}{y}\frac{\partial y}{\partial\alpha} = 3\tan\alpha\,\frac{(1-\zeta)}{(4-3\zeta)} \tag{3-68}$$

$$\frac{1}{z}\frac{\partial z}{\partial\alpha} = \tan\alpha\,\frac{(2-3\zeta)}{(4-3\zeta)} \tag{3-69}$$

$$\frac{1}{x}\frac{\partial x}{\partial\beta} = \frac{1}{y}\frac{\partial y}{\partial\beta} = 2\cot\beta\,\frac{(2-3\zeta)}{(4-3\zeta)} \tag{3-70}$$

$$\frac{1}{z}\frac{\partial z}{\partial\beta} = -\,6\cot\beta\,\frac{\zeta}{(4-3\zeta)} \tag{3-71}$$

$$\frac{\partial x}{\partial \phi} = - y \tag{3-72}$$

$$\frac{\partial y}{\partial \phi} = x \tag{3-73}$$

$$\frac{\partial z}{\partial \phi} = 0 \tag{3-74}$$

And for the second order coordinate differentials:

$$\frac{1}{x}\frac{\partial^2 x}{\partial \alpha^2} = \frac{1}{y}\frac{\partial^2 y}{\partial \alpha^2} = 3\{(1-\zeta) + \tan^2\alpha \frac{(28-75\zeta + 65\zeta^2 - 18\zeta^3)}{(4-3\zeta)^2}\}(4-3\zeta)^{-1} \tag{3-75}$$

$$\frac{1}{z}\frac{\partial^2 z}{\partial \alpha^2} = \{(2-3\zeta) + 6\tan^2\alpha \frac{(8-28\zeta + 29\zeta^2 - 9\zeta^3)}{(4-3\zeta)^2}\}(4-3\zeta)^{-1} \tag{3-76}$$

$$\frac{1}{x}\frac{\partial^2 x}{\partial \beta^2} = \frac{1}{y}\frac{\partial^2 y}{\partial \beta^2} = - 2\{(2-3\zeta) + 3\zeta\cot^2\beta \frac{(24-34\zeta + 9\zeta^2)}{(4-3\zeta)^2}\} (4-3\zeta)^{-1} \tag{3-77}$$

$$\frac{1}{z}\frac{\partial^2 z}{\partial \beta^2} = 6\zeta \{1 - \cot^2\beta \frac{(16-32\zeta + 9\zeta^2)}{(4-3\zeta)^2}\} (4-3\zeta)^{-1} \tag{3-78}$$

$$\frac{1}{x}\frac{\partial^2 x}{\partial \phi^2} = \frac{1}{y}\frac{\partial^2 y}{\partial^2 \phi} = - 1 \tag{3-79}$$

$$\frac{\partial^2 z}{\partial \phi^2} = 0 \tag{3-80}$$

$$\frac{1}{x}\frac{\partial^2 x}{\partial \alpha \partial \beta} = \frac{1}{y}\frac{\partial^2 y}{\partial \alpha \partial \beta} = 6\tan\alpha\cot\beta \{\frac{(1-\zeta)(8-22\zeta + 9\zeta^2)}{(4-3\zeta)^3}\} \tag{3-81}$$

$$\frac{1}{z}\frac{\partial^2 z}{\partial \alpha \partial \beta} = - 6\tan\alpha\cot\beta \{\frac{\zeta(16-26\zeta + 9\zeta^2)}{(4-3\zeta)^3}\} \tag{3-82}$$

$$\frac{\partial^2 x}{\partial\alpha\partial\phi} = -\frac{\partial y}{\partial\alpha} \tag{3-83}$$

$$\frac{\partial^2 y}{\partial\alpha\partial\phi} = \frac{\partial x}{\partial\alpha} \tag{3-84}$$

$$\frac{\partial^2 z}{\partial\alpha\partial\phi} = 0 \tag{3-85}$$

$$\frac{\partial^2 x}{\partial\beta\partial\phi} = -\frac{\partial y}{\partial\beta} \tag{3-86}$$

$$\frac{\partial^2 y}{\partial\beta\partial\phi} = \frac{\partial x}{\partial\beta} \tag{3-87}$$

$$\frac{\partial^2 z}{\partial\beta\partial\phi} = 0 \tag{3-88}$$

The second order coordinate differentials are, of course, symmetric with respect to the order of differentiation, i.e.,

$$\frac{\partial^2 x_n}{\partial u_j \partial u_k} = \frac{\partial^2 x_n}{\partial u_k \partial u_j} \tag{3-89}$$

The quantities defined in Equations 3-59 - 3-88 are then used in Equation 3-48 to calculate the components of the second derivative in the dipole aligned Cartesian system.

Next, we must rotate the second derivative into the tangent plane coordinate system. This is accomplished by a series of four rotations. The first two rotations rotate the coordinate axes from a dipole aligned system to a rotation axis aligned system. If the dipole axis points toward colatitude θ_D and east longitude ϕ_D, rotate the system clockwise about the y-axis through θ_D to align the z-axis with the rotation axis. Next, rotate the system clockwise about the z-axis

through ϕ_0 to align the x-axis with the Greenwich meridian. The next two rotations rotate the geocentric Cartesian axes into the tangent plane system. If the geographic colatitude and longitude of the site are θ_0 and ϕ_0, respectively, rotate the system counterclockwise about the z-axis through $\pi/2+\phi_0$ so that the x-axis points to the right, and the y-axis is directed away from the observer. Next rotate the system counterclockwise about the x-axis through θ_0 to align the z-axis with the vertical.

For a clockwise rotation of θ about the x-axis:

$$\frac{\partial^2 f}{\partial x'^2} = \frac{\partial^2 f}{\partial x^2} \tag{3-90}$$

$$\frac{\partial^2 f}{\partial y'^2} = \cos^2\theta \frac{\partial^2 f}{\partial y^2} - 2\cos\theta\sin\theta \frac{\partial^2 f}{dvdz} + \sin^2\theta \frac{\partial^2 f}{\partial z^2} \tag{3-91}$$

$$\frac{\partial^2 f}{\partial z'^2} = \sin^2\theta \frac{\partial^2 f}{\partial y^2} + 2\cos\theta\sin\theta \frac{\partial^2 f}{\partial y\,\partial z} + \cos^2\theta \frac{\partial^2 f}{\partial z^2} \tag{3-92}$$

$$\frac{\partial^2 f}{\partial x'\,\partial y'} = \cos\theta \frac{\partial^2 f}{\partial x\,\partial y} - \sin\theta \frac{\partial^2 f}{\partial z\,\partial x} \tag{3-93}$$

$$\frac{\partial^2 f}{\partial y'\,\partial z'} = \cos\theta\sin\theta \left(\frac{\partial^2 f}{\partial y^2} - \frac{\partial^2 f}{\partial z^2}\right) + (\cos^2\theta - \sin^2\theta) \frac{\partial^2 f}{\partial y\,\partial z} \tag{3-94}$$

$$\frac{\partial^2 f}{\partial z'\,\partial x'} = \sin\theta \frac{\partial^2 f}{\partial x\,\partial y} + \cos\theta \frac{\partial^2 f}{\partial z\,\partial x} \tag{3-95}$$

For a clockwise rotation of θ about the y-axis:

$$\frac{\partial^2 f}{\partial x'^2} = \cos^2\theta \frac{\partial^2 f}{\partial x^2} + 2\cos\theta\sin\theta \frac{\partial^2 f}{\partial z\,\partial x} + \sin^2\theta \frac{\partial^2 f}{\partial z^2} \tag{3-96}$$

$$\frac{\partial^2 f}{\partial y'^2} = \frac{\partial^2 f}{\partial y^2} \tag{3-97}$$

$$\frac{\partial^2 f}{\partial z'^2} = \sin^2\theta \frac{\partial^2 f}{\partial x^2} - 2\cos\theta\sin\theta \frac{\partial^2 f}{\partial z \partial x} + \cos^2\theta \frac{\partial^2 f}{\partial z^2} \quad (3\text{-}98)$$

$$\frac{\partial^2 f}{\partial x' \partial y'} = \cos\theta \frac{\partial^2 f}{\partial x \partial y} + \sin\theta \frac{\partial^2 f}{\partial y \partial z} \quad (3\text{-}99)$$

$$\frac{\partial^2 f}{\partial y' \partial z'} = - \sin\theta \frac{\partial^2 f}{\partial x \partial y} + \cos\theta \frac{\partial^2 f}{\partial y \partial z} \quad (3\text{-}100)$$

$$\frac{\partial^2 f}{\partial z' \partial x'} = \cos\theta\sin\theta \left(\frac{\partial^2 f}{\partial z^2} - \frac{\partial^2 f}{\partial x^2}\right) + (\cos^2\theta - \sin^2\theta) \frac{\partial^2 f}{\partial z \partial x} \quad (3\text{-}101)$$

And for a clockwise rotation of θ about the z-axis:

$$\frac{\partial^2 f}{\partial x'^2} = \cos^2\theta \frac{\partial^2 f}{\partial x^2} - 2\cos\theta\sin\theta \frac{\partial^2 f}{\partial x \partial y} + \sin^2\theta \frac{\partial^2 f}{\partial y^2} \quad (3\text{-}102)$$

$$\frac{\partial^2 f}{\partial y'^2} = \sin^2\theta \frac{\partial^2 f}{\partial x^2} + 2\cos\theta\sin\theta \frac{\partial^2 f}{\partial x \partial y} + \cos^2\theta \frac{\partial^2 f}{\partial y^2} \quad (3\text{-}103)$$

$$\frac{\partial 2f}{\partial z'^2} = \frac{\partial^2 f}{\partial z^2} \quad (3\text{-}104)$$

$$\frac{\partial^2 f}{\partial x' \partial y'} = \cos\theta\sin\theta \left(\frac{\partial^2 f}{\partial x^2} - \frac{\partial^2 f}{\partial y^2}\right) + (\cos^2\theta - \sin^2\theta) \frac{\partial^2 f}{\partial x \partial y} \quad (3\text{-}105)$$

$$\frac{\partial^2 f}{\partial y' \partial z'} = \cos\theta \frac{\partial^2 f}{\partial y \partial z} + \sin\theta \frac{\partial^2 f}{\partial z \partial x} \quad (3\text{-}106)$$

$$\frac{\partial^2 f}{\partial z' \partial x'} = - \sin\theta \frac{\partial^2 f}{\partial y \partial z} + \cos\theta \frac{\partial^2 f}{\partial z \partial x} \quad (3\text{-}107)$$

Finally, the components of the second derivative of the log density are converted to the components of the second derivative of the mean density itself:

$$\frac{\partial^2 N_e}{\partial x_j \partial x_k} = N_e \left[\frac{\partial^2 f}{\partial x_j \partial x_k} + \left(\frac{\partial f}{\partial x_j} \right) \left(\frac{\partial f}{\partial x_k} \right) \right] \qquad (3\text{-}108)$$

SECTION 4

LIST OF REFERENCES

1. Wittwer, L.A., Radio Wave Propagation in Structured Ionization for Satellite Applications, DNA-5304D, Defense Nuclear Agency, December 1979.

2. Wittwer, L.A., Radio Wave Propagation in Structured Ionization for Satellite Applications II, DNA-IR-82-02, Defense Nuclear Agency, August 1982.

3. Abramowitz, M. and Stegun, I.A. (editors), Handbook of Mathematical Functions, Dover Publications, Inc., New York, 1965.

4. Shkarofsky, I.P., "Generalized Appleton-Hartree Equation for any Degree of Ionization and Application to the Ionosphere", Proceedings of the IRE, Vol. 49, pp. 1857-1871, December 1961.

5. Davies, K., Ionospheric Radio Propagation, National Bureau of Standards Monograph 80, November 1965.

6. Wittwer, L.A., The Calculation of Signal Structure Properties in Turbulent Media, DNA/RAAE Technical Note, 6 June 1979.

7. Bogusch, R.L., and R.W. Hendrick, Effects of Propagation Disturbances on a Specific Satellite Communications Link, Volume II: Models of Propagation Disturbances, AFWL-TR-76-25, Vol. II, MRC-R-156, Mission Research Corporation, October 1976.

8. Wittwer, L.A., A Trans-Ionospheric Signal Specification for Satellite C3 Applications, DNA-5662D, Defense Nuclear Agency, December 1980.

9. Dana, R.A., Propagation of RF Signals through Structured Ionization -- Theory and Antenna Aperture Effects Applications, MRC-R-976, Mission Research Corp., January 1986.

10. Bogusch, R.L., Radar Propagation in Refractive Media: A New Computational Technique, MRC-R-119, Mission Research Corporation, February 1974.

11. Hildebrand, F.B., Methods of Applied Mathematics, Second Edition, Prentice Hall, 1965.

12. Stagat, R.W. and D.S. Sappenfield, SCENARIO: A Program for Satellite Signal Propagation Analysis Applications, AFWL-TR-78-137, MRC-R-404, Mission Research Corporation, July 1978.

13. Stagat, R.W., D.S. Sappenfield, and J.P. Incerti, The SCENARIO Code: Modifications in Version II and the Striation Convection Theory, AFWL-TR-80-124, MRC R-539, Mission Research Corporation, July 1980.

14. Landman, D.A., Ricchiazzi, P.J., White, W.W., SCENARIO User Manual, MRC-R-994, Mission Research Corporation, May 1986.

15. White, W., Standard Output Format for MICE/MELT and SCENARIO, MRC-N-718R, Mission Research Corporation, February 1986.

16. Dodson, R.E,. and Krueger, D.J., A Semi-Analytic Algorithm to Compute the Signal Time Delay Variance and the Frequency Selective Bandwidth, MRC-N-723, Mission Research Corporation, March 1986.

17. Knapp, W.S., and F.S. Schwartz, AIDS for the Study of Electromagnetic Blackout, DNA-2199H, Defense Nuclear Agency, February 1975.

18. Stoeckly, R.F., R.W. Stagat, and R.W. Kilb, Collisional Momentum and Energy Transfer Rates for Two-Fluid Nuclear Burst Simulations, DNA-3827T, Defense Nuclear Agency, July 1975.

DISTRIBUTION LIST

DNA-TR-87-162-V2

DEPARTMENT OF DEFENSE

US NUC CMD & CENTRAL SYST SUPPORT STAFF
ATTN: SAB H SEQUINE

DEFENSE ADVANCED RSCH PROJ AGENCY
ATTN: DR MANSFIELD

DEFENSE COMMUNICATIONS AGENCY
ATTN: A320

DEFENSE COMMUNICATIONS ENGINEER CENTER
ATTN: CODE R410

DEFENSE INTELLIGENCE AGENCY
ATTN: DC-6
ATTN: DIR
ATTN: DT-1B
ATTN: RTS-2B
ATTN: VP-TPO

DEFENSE NUCLEAR AGENCY
ATTN: DFSP G ULLRICH
ATTN: NANF
ATTN: NASF
ATTN: OPNA
3 CYS ATTN: RAAE
ATTN: RAAE A MARDIGUIAN
ATTN: RAAE G ULLRICH
ATTN: RAAE L SCHROCK
ATTN: RAAE M CRAWFORD
ATTN: RAAE P FLEMING
ATTN: RAAE S BERGGREN
ATTN: RAEE
4 CYS ATTN: TITL

DEFENSE NUCLEAR AGENCY
ATTN: TDNM
2 CYS ATTN: TDTT W SUMMA

DEFENSE TECHNICAL INFORMATION CENTER
2 CYS ATTN: DTIC/FDAB

JOINT DATA SYSTEM SUPPORT CTR
ATTN: C-312 R MASON

JOINT STRAT TGT PLANNING STAFF
ATTN: JK (ATTN: DNA REP)
ATTN: JKCS, STUKMILLER
ATTN: JPEM
ATTN: JPSS

NATIONAL SECURITY AGENCY
ATTN: B432 C GOEDEKE

STRATEGIC DEFENSE INITIATIVE ORGANIZATION
ATTN: EN
ATTN: EN LTC C JOHNSON
ATTN: PTN C GIESE
ATTN: PTP LTC SEIBERLING
ATTN: TN

THE JOINT STAFF
ATTN: J6

DEPARTMENT OF THE ARMY

ARMY LOGISTICS MANAGEMENT CTR
ATTN: DLSIE

U S ARMY ATMOSPHERIC SCIENCES LAB
ATTN: DR F NILES
ATTN: SLCAS-AE-E

U S ARMY COMMUNICATIONS R&D COMMAND
ATTN: AMSEL-RD-ESA

U S ARMY FOREIGN SCIENCE & TECH CTR
ATTN: DRXST-SD

U S ARMY NUCLEAR & CHEMICAL AGENCY
ATTN: MONA-NU

U S ARMY NUCLEAR EFFECTS LABORATORY
ATTN: ATAA-PL
ATTN: ATAA-TDC
ATTN: ATRC-WCC

U S ARMY STRATEGIC DEFENSE CMD
ATTN: DASD-H-SA R BRADSHAW
ATTN: DASD-H-SA/R SMITH
ATTN: DASD-H-SAV

USA SURVIVABILITY MANAGMENT OFFICE
ATTN: SLCSM-SE J BRAND

DEPARTMENT OF THE NAVY

COMMAND & CONTROL PROGRAMS
ATTN: OP 941

JOINT CRUISE MISSILES PROJECT OFC (PM-3)
ATTN: JCMG-707

NAVAL AIR SYSTEMS COMMAND
ATTN: PMA 271

NAVAL ELECTRONICS ENGRG ACTVY, PACIFIC
ATTN: CODE 250 D OBRYHIM

NAVAL RESEARCH LABORATORY
2 CYS ATTN: CODE 4100 H GURSKY
ATTN: CODE 4121.8 H HECKATHORN
ATTN: CODE 4183
ATTN: CODE 4720 J DAVIS
ATTN: CODE 4750 P RODRIGUEZ
ATTN: CODE 4780 B RIPIN
ATTN: CODE 4780 DR P BERNHARDT
ATTN: CODE 4780 J HUBA

NAVAL SURFACE WARFARE CENTER
ATTN: CODE H-21

NAVAL TECHNICAL INTELLIGENCE CTR
ATTN: DA44

NAVAL UNDERWATER SYSTEMS CENTER
ATTN: CODE 3411, J KATAN

OFC OF THE DEPUTY CHIEF OF NAVAL OPS
ATTN: OP 654
ATTN: OP 941D
ATTN: OP 981N

SPACE & NAVAL WARFARE SYSTEMS CMD
ATTN: CODE 3101 T HUGHES
ATTN: PD 50TD
ATTN: PD50TD1 G BRUNHART
ATTN: PME 106-4 S KEARNEY
ATTN: PME-106 F W DIEDERICH

THEATER NUCLEAR WARFARE PROGRAM OFC
ATTN: PMS-42331F D SMITH

DEPARTMENT OF THE AIR FORCE

AIR FORCE CTR FOR STUDIES & ANALYSIS
ATTN: AFCSA/SASC

AIR FORCE ELECTRONIC WARFARE CENTER
ATTN: LT M MCNEELY

AIR FORCE SPACE SYSTEMS DIVISION
ATTN: YA
2 CYS ATTN: YN

AIR UNIVERSITY LIBRARY
ATTN: AUL-LSE

HQ AWS, DET 3 (CSTC/WE)
ATTN: WE

SECRETARY OF AF/AQQS
RESEARCH, DEVELOPMENT & ACQ
ATTN: AF/RDQI

STRATEGIC AIR COMMAND/XRFS
ATTN: XRFS

WEAPONS LABORATORY
ATTN: NTCA
ATTN: NTN
ATTN: SUL

DEPARTMENT OF ENERGY

EG&G INC
ATTN: D WRIGHT

LOS ALAMOS NATIONAL LABORATORY
ATTN: D SAPPENFIELD
ATTN: D WINSKE

SANDIA NATIONAL LABORATORIES
ATTN: D HARTLEY 8300

SANDIA NATIONAL LABORATORIES
ATTN: A D THORNBROUGH 400
ATTN: CODE 9014 R BACKSTROM
ATTN: D DAHLGREN 6440
ATTN: ORG 9114 W D BROWN
ATTN: SPACE PROJECT DIV
ATTN: TECH LIB 3141

OTHER GOVERNMENT

CENTRAL INTELLIGENCE AGENCY
ATTN: OSWR/NED
ATTN: OSWR/SSD FOR L BERG

DEPARTMENT OF COMMERCE
ATTN: E MORRISON
ATTN: J HOFFMEYER
ATTN: W UTLAUT

U S DEPARTMENT OF STATE
ATTN: PM/TMP

DEPARTMENT OF DEFENSE CONTRACTORS

AEROSPACE CORP
ATTN: A LIGHTY
ATTN: B P PURCELL
ATTN: C CREWS
ATTN: C RICE
ATTN: M ROLENZ

ANALYTICAL SYSTEMS ENGINEERING CORP
ATTN: SECURITY

ATLANTIC RESEARCH SERVICES CORP
ATTN: R MCMILLAN

ATMOSPHERIC AND ENVIRONMENTAL RESEARCH INC
ATTN: M KO

AUSTIN RESEARCH ASSOCIATES
ATTN: J THOMPSON

AUTOMETRIC INCORPORATED
ATTN: C LUCAS

BDM INTERNATIONAL INC
ATTN: L JACOBS

BERKELEY RSCH ASSOCIATES, INC
ATTN: J WORKMAN
ATTN: S BRECHT

BOEING CO
ATTN: G HALL

CALIFORNIA RESEARCH & TECHNOLOGY, INC
ATTN: M ROSENBLATT

CHARLES STARK DRAPER LAB, INC
ATTN: A TETEWSKI

COMMUNICATIONS SATELLITE CORP
ATTN: G HYDE

CORNELL UNIVERSITY
ATTN: D FARLEY JR
ATTN: M KELLY

EOS TECHNOLOGIES, INC
ATTN: B GABBARD
ATTN: W LELEVIER

GENERAL RESEARCH CORP INC
ATTN: J EOLL

GRUMMAN AEROSPACE CORP
ATTN: J DIGLIO

HSS, INC
ATTN: D HANSEN

INSTITUTE FOR DEFENSE ANALYSES
ATTN: E BAUER
ATTN: H WOLFHARD

J S LEE ASSOCIATES INC
ATTN: DR J LEE

JAYCOR
ATTN: J SPERLING

JOHNS HOPKINS UNIVERSITY
ATTN: C MENG
ATTN: J D PHILLIPS
ATTN: R STOKES
ATTN: T EVANS

KAMAN SCIENCES CORP
ATTN: E CONRAD
ATTN: G DITTBERNER

KAMAN SCIENCES CORPORATION
ATTN: B GAMBILL
ATTN: DASIAC
ATTN: R RUTHERFORD

KAMAN SCIENCES CORPORATION
ATTN: DASIAC

LOCKHEED MISSILES & SPACE CO, INC
ATTN: J HENLEY
ATTN: J KUMER
ATTN: R SEARS

LOCKHEED MISSILES & SPACE CO, INC
ATTN: D KREJCI

LTV AEROSPACE & DEFENSE COMPANY
2 CYS ATTN: LIBRARY

M I T LINCOLN LAB
ATTN: D TOWLE L-230
ATTN: I KUPIEC L-100

MARTIN MARIETTA DENVER AEROSPACE
ATTN: H VON STRUVE III

MAXIM TECHNOLOGIES, INC
ATTN: B RIDGEWAY
ATTN: J SO

MCDONNELL DOUGLAS CORPORATION
ATTN: J GROSSMAN

METATECH CORPORATION
ATTN: R SCHAEFER
ATTN: W RADASKY

METEOR COMMUNICATIONS CORP
ATTN: R LEADER

MISSION RESEARCH CORP
ATTN: R ARMSTRONG
ATTN: W WHITE

MISSION RESEARCH CORP
ATTN: B R MILNER
ATTN: D ARCHER
2 CYS ATTN: D J KRUEGER
ATTN: D KNEPP
ATTN: D LANDMAN
ATTN: F FAJEN
2 CYS ATTN: F GUIGLIANO
ATTN: G MCCARTOR
ATTN: K COSNER
ATTN: M FIRESTONE
ATTN: R BIGONI
ATTN: R BOGUSCH
ATTN: R DANA
2 CYS ATTN: R E DODSON
ATTN: R HENDRICK
ATTN: S GUTSCHE
ATTN: TECH INFO CENTER
ATTN: TECH LIBRARY

MITRE CORPORATION
ATTN: M HORROCKS
ATTN: R C PESCI
ATTN: W FOSTER

NORTHWEST RESEARCH ASSOC, INC
ATTN: E FREMOUW

PACIFIC-SIERRA RESEARCH CORP
ATTN: E FIELD JR
ATTN: F THOMAS
ATTN: H BRODE

PHOTOMETRICS, INC
ATTN: I L KOFSKY

PHYSICAL RESEARCH INC
ATTN: W. SHIH

PHYSICAL RESEARCH INC
ATTN: H FITZ
ATTN: P LUNN

PHYSICAL RESEARCH, INC
ATTN: R DELIBERIS
ATTN: T STEPHENS

PHYSICAL RESEARCH, INC
ATTN: J DEVORE
ATTN: J THOMPSON
ATTN: W SCHLUETER

R & D ASSOCIATES
ATTN: C GREIFINGER
ATTN: F GILMORE
ATTN: G HOYT
ATTN: M GANTSWEG

RAND CORP
ATTN: C CRAIN
ATTN: E BEDROZIAN

RAND CORP
ATTN: B BENNETT

RJO ENTERPRISES/POET FAC
ATTN: A ALEXANDER
ATTN: W BURNS

SCIENCE APPLICATIONS INTL CORP
ATTN: C SMITH
ATTN: D HAMLIN
ATTN: D SACHS
ATTN: E STRAKER
ATTN: L LINSON

SCIENCE APPLICATIONS INTL CORP
ATTN: D TELAGE
ATTN: M CROSS

SRI INTERNATIONAL
ATTN: W CHESNUT
ATTN: W JAYE

STEWART RADIANCE LABORATORY
ATTN: R HUPPI

TELECOMMUNICATION SCIENCE ASSOCIATES
ATTN: R BUCKNER

TELEDYNE BROWN ENGINEERING
ATTN: J WOLFSBERGER, JR

TOYON RESEARCH CORP
ATTN: J ISE

TRW INC
ATTN: R PLEBUCH
ATTN: H CULVER

TRW SPACE & DEFENSE SYSTEMS
ATTN: D M LAYTON

USER SYSTEMS, INC
ATTN: S W MCCANDLESS, JR

UTAH STATE UNIVERSITY
ATTN: K BAKER
ATTN: L JENSEN

VISIDYNE, INC
ATTN: J CARPENTER

FOREIGN

FOA 2
ATTN: B SJOHOLM

FOA 3
ATTN: T KARLSSON